FACTORS AFFECTING THE LIFETIME OF THICK AIR PLASMA SPRAYED THERMAL BARRIER COATINGS

by

Michael Aaron Helminiak

BS, University of Pittsburgh, 2008

Submitted to the Graduate Faculty of

Swanson School of Engineering in partial fulfillment

of the requirements for the degree of

Master of Science

University of Pittsburgh

2010

UNIVERSITY OF PITTSBURGH

SWANSON SCHOOL OF ENGINEERING

This thesis was presented

by

Michael A. Helminiak

It was defended on

March 18th, 2010

and approved by

Fredrick S. Pettit, Professor Emeritus, Department of Mechanical Engineering and Materials Science

Brian M. Gleeson, Professor, Department of Mechanical Engineering and Materials Science

Nazik M. Yanar, Research Professor, Department of Mechanical Engineering and Materials Science

Thesis Advisor: Gerald H. Meier, Professor, Department of Mechanical Engineering and Materials Science

FACTORS AFFECTING THE LIFETIME OF THICK AIR PLASMA SPRAYED THERMAL BARRIER COATINGS

Michael A. Helminiak, M.S.

University of Pittsburgh, 2010

This research was directed at developing the fundamentals that will facilitate the fabrication of air plasma sprayed (APS) yttria-stabilized zirconia (YSZ) thermal barrier coatings (TBC) with controlled thickness and density combinations and bond coat optimization for maximum TBC durability. It includes research on the yttrium content and surface roughness of NiCoCrAlY bond coats deposited by argon-shrouded plasma spraying and on the microstructural control of APS topcoats to maximize the coating thicknesses that can be applied without spallation and to minimize the thermal conductivity of the TBC. The specimens used for this research were prepared by Praxair Surface Technologies and have been evaluated using cyclic oxidation and thermal shock tests. Important properties of the YSZ TBCs, such as resistance to sintering and phase transformation and the thermal conductivity were determined. Coefficients of thermal expansion were measured for the superalloy substrate materials.

The properties of high-purity, low-density (85%) APS TBCs on NiCoCrAlY bond coats were evaluated. The high purity resulted in topcoats which are highly resistant to sintering and transformation from the metastable tetragonal phase to the equilibrium mixture of monoclinic and cubic phases.

The thermal conductivity of the as-sprayed topcoats was measured to be less than 1 (W/m-K). The high sintering resistance means this low value will increase only slowly with high temperature exposure.

The porous topcoat microstructure also resulted in significant durability during thermal cycling. A 375μm thick APS coating was found to have a comparable furnace cyclic life to that of a standard 100μm EBPVD coating. The actual failure mechanisms of the APS coatings were found to depend on topcoat thickness and the nature of the thermal exposure. The failure times and mechanisms were found to depend strongly on the superalloy substrate used. This effect was found to be associated with the coefficient of thermal expansion (CTE) mismatch between the superalloy and topcoat.

The bond coat topography modifications implemented in this work did not have a significant effect on the cyclic behavior. However the yttrium content and distribution in the bond coat did have a significant effect on TBC lifetime.

TABLE OF CONTENTS

LIST OF TABLES

LIST OF FIGURES

PREFACE

A special thanks goes out to Praxair Surface Technologies for preparing all of the coatings used in this research and to Dr. Tom Taylor for all his advice and expertise called upon during the time of this research. I would also like to thank Dr. Nazik Yanar, for her collaboration and discussion of the results.

In this thesis, some of the specimens prepared are referred to as Phase I specimen and Phase II specimens. The Phase I specimens were prepare in September 2007 and the Phase II were prepared in July 2008.

1.0 INTRODUCTION

Hydrogen fuel technologies leading to FutureGen-type (i.e. near-zero emissions) power plants involve a transition from standard gas turbines operating with coal or natural-gas combustion to very high hydrogen fuels derived from syngas and syngas burned in nearly pure oxygen using steam to control temperatures (oxy-fuel systems). The transition will require materials technologies to accommodate expansion gases that are not only increasingly hotter but also contain higher concentrations of water vapor. The higher temperatures will require improved thermal barrier coatings (TBCs) for the structural materials.

The effectiveness of a thermal barrier coating can be scaled by looking at the effective thermal resistance, which is a ratio of the TBC thickness to the TBC thermal conductivity which is shown in Equation 1.

Equation 1

$$R_{therm} = \frac{h_{topcoat}}{\kappa_{topcoat}}$$

While there has been some progress in identifying oxides with lower thermal conductivities than conventionally-used yttria-stabilized zirconia (YSZ), these oxides do not have the balance of properties necessary for advanced systems. An alternative approach employed in this research is to improve the durability of air plasma sprayed TBCs so they can be

used at larger thicknesses. This requires improvement in bond coat properties as well as improved topcoats. It also requires a better idea of what properties in a TBC system affect the lifetime behavior.

A literature review was performed and several variables in the TBC system that can influence the lifetime were identified and were targeted in the experimental design. An investigation in to the lifetime behavior of TBC specimens with different topcoat thickness and different YSZ purity levels was targeted. The substrate superalloy was varied to determine whether it had an influence on lifetime and what kind of influence, mechanical or compositional, it had, if any. The roughness of the bond coat prior to TBC deposition was varied in attempt to induce a change in the lifetime performance. Likewise, a dense vertically cracked under-layer was added to the base of the TBC to determine whether or not a strain relieving layer could yield improved performance of the thicker topcoats.

2.0 BACKGROUND

Thermal Barrier Coatings (TBCs) are used primarily in turbine applications where high temperature stability is required (900°C-1100°C). At these temperatures the superalloys would degrade too quickly for practical application. More specifically, they are most often used in the hot sections of turbine engines (blades and vanes) and combustor liners [1]. TBCs have also been used to protect iron-based alloys and although the material systems are different, the principles behind the coatings are the same [2].

2.1 THERMAL BARRIER COATINGS: AN OVERVIEW

A thermal barrier coating system is comprised of three layers, the superalloy, the bond coat, and the ceramic topcoat. The superalloy provides the structural stability and mechanical strength for the engine component application and requires protection from the hot combustion gases during operation. It is designed to have enhanced high temperature creep resistance since creep is a major contributor to failure when operating at high temperatures. The alloy compositions required to achieve these properties however do not always provide adequate chemical protection from the combustion gases and fuel impurities.

The bond coat is a metallic coating that is applied directly over the superalloy. It protects the superalloy from oxidation and bonds the ceramic topcoat to the alloy substrate. It generally

has a similar coefficient of thermal expansion (CTE) to that of the substrate and will also be of similar chemical composition (not the same, but similar). Most bond coats used today have substantial levels of aluminum because alumina is a slow growing protective oxide that will provide the best oxidation protection for the underlying superalloy. The formation of the alumina scale is a major step during the thermal cycling of the system. This layer is known as the thermally grown oxide (TGO) and its thickness will increase with increased exposure time until a certain point when a majority of the aluminum in the bond coat is depleted [3]. Sometimes this layer will also include other oxides such as Al-Ni oxides and chromium oxides.

The final layer is the ceramic topcoat. There has been, and still is, a search for new materials for this layer. However yttria stabilized zirconia (YSZ) remains the dominant choice for this application. This material exhibits good high temperature phase stability, high toughness, low thermal conductivity, and an acceptable CTE that is similar to the other layers. The two main topcoat deposition techniques are air plasma spraying (APS) and electron beam physical vapor deposition (EBPVD). The strain tolerance of the APS topcoat results from the cracks and pores that are characteristic of its microstructure. When the topcoat is heated, the material expands to close the cracks and when it is cooled the voids reopen [4]. The main role of the topcoat is to protect the lower layers from the high temperatures by effectively producing a thermal gradient between the exposed top surface and the bond coat/topcoat interface. The topcoat does not protect the bond coat from oxidation (other than by lowering the temperature) because of its porosity and because of increased gas permeation and increased oxygen ion diffusion at high temperature [5].

2.2 TOPCOAT THICKNESS EFFECT

One way to accommodate higher operating temperatures would be to make the YSZ topcoats thicker, producing a larger effective temperature difference between interfaces. Consequently, because of these greater thermal gradients, there are also higher thermal stresses that occur within the material. In addition, the increased thickness of the coating will increase the elastic strain energy stored and hence, the energy release rate for crack propagation. For these reasons, thick topcoats have failed because of spalling, cracking, and chipping within the topcoat layer. Thinner coatings are less susceptible to these types of failures and are affected more so by thermal expansion mismatch between the various layers and by oxide formation at the bond coat/ topcoat interface. Therefore it has been suggested there is an optimum topcoat thickness between extremely thick (>1mm) and thin (<0.1mm) [6].

Two methods to accommodate the internal stresses are to either introduce vertical cracks within the topcoat or to grade the porosity of the topcoats. The vertical cracks provide strain relief within the topcoat and temporarily relieve the stress buildup during cooling and heating. These types of controlled cracks are common in EBPVD topcoats due to the columnar growth mechanisms during deposition [7]. Praxair Surface Technologies (PST) has developed a dense, thermally-sprayed topcoat with controlled vertical crack segmentation that provides very high thermal shock resistance [8].The second mechanism utilizes a gradient in porosity which reflects a gradient in elastic properties that can accommodate the high temperatures at the top surface and the mismatch stresses at the bond coat/topcoat interface. These types of coatings are relatively new and are in the experimental phase [6].

2.3 TOPCOAT POROSITY

The density and porosity of thermally sprayed ceramic topcoats can be adjusted by altering the spraying conditions during deposition. Spraying parameters such as particle size, angle of impact, particle velocity, and substrate temperature can all have dramatic effects on the morphology of the as-sprayed topcoat [9]. Different types of pores and cracks form within the topcoat during the spraying and cycling of the coatings. When the melted particles of YSZ hit the substrate, they rapidly solidify which can cause interlamellar pores to form (pores lying parallel to the surface of the substrate). These pores help reduce the through-thickness thermal conductivity of the coating, which is beneficial. However, they also can act as sites for crack nucleation and delamination. Similarly, the large quenching stresses usually cannot be retained within the individual splats as residual stresses and so the splats shrink and form micro-cracks that help relieve these internal stresses. The micro-cracks provide a small degree of in-plane compliance, allowing the coating to accommodate the thermal expansion stresses during heating and cooling. Another type of pore, the globular pore, is a result of a lack of filling, stacking inconsistencies and coverage issues during the spraying process. These pores are generally undesirable because they can be initiation sites for failure. Finally, in air plasma sprayed coatings, the controlled presence of vertical cracks can increase the in-plane compliance of the coating. In general practice, these cracks usually do not form during the spraying process, but instead result from thermal stresses associated with the difference in coefficients of expansion during heating and cooling [9]. In the PST vertically segmented Zircoat™, segmentation is controlled by the thermal spray parameters [8].

In general, by increasing the porosity of the YSZ topcoat, the density, and thus thermal conductivity, of the material can be minimized [10]. However, during thermal cycling, the

porosity can change because of particle sintering at high enough temperatures. Thermal diffusivity tends to increase as a result of increasing thermal cycling up to a point after which the delta in thermal diffusivity tapers off [11]. Along with an increase in thermal conductivity, the elastic modulus also increases and the strain tolerance during heating and cooling also decreases because of the decrease in concentration of strain-relief pores as the result of sintering.

The lifetimes of TBC's are related to their resistance to spallation and crack formation during the thermal cycling process where residual stresses are built up in the material [12]. In air plasma sprayed coatings there is a compressive residual stress at the topcoat-bond coat interface. Continuing away from this interface, the residual stress decreases as the surface is approached. When the TBC is cycled at high temperatures, these compressive stresses tend to increase because of thermal expansion mismatch and sintering effects. It has been seen that lower porosity materials have higher compressive residual stresses than high porosity materials [12]. However, as mentioned above, the type of porosity and distribution of pores can also affect the lifetime of the coatings.

2.4 YSZ TOPCOAT PHASE BEHAVIOR

The phase diagram for YSZ is shown in Figure 1.

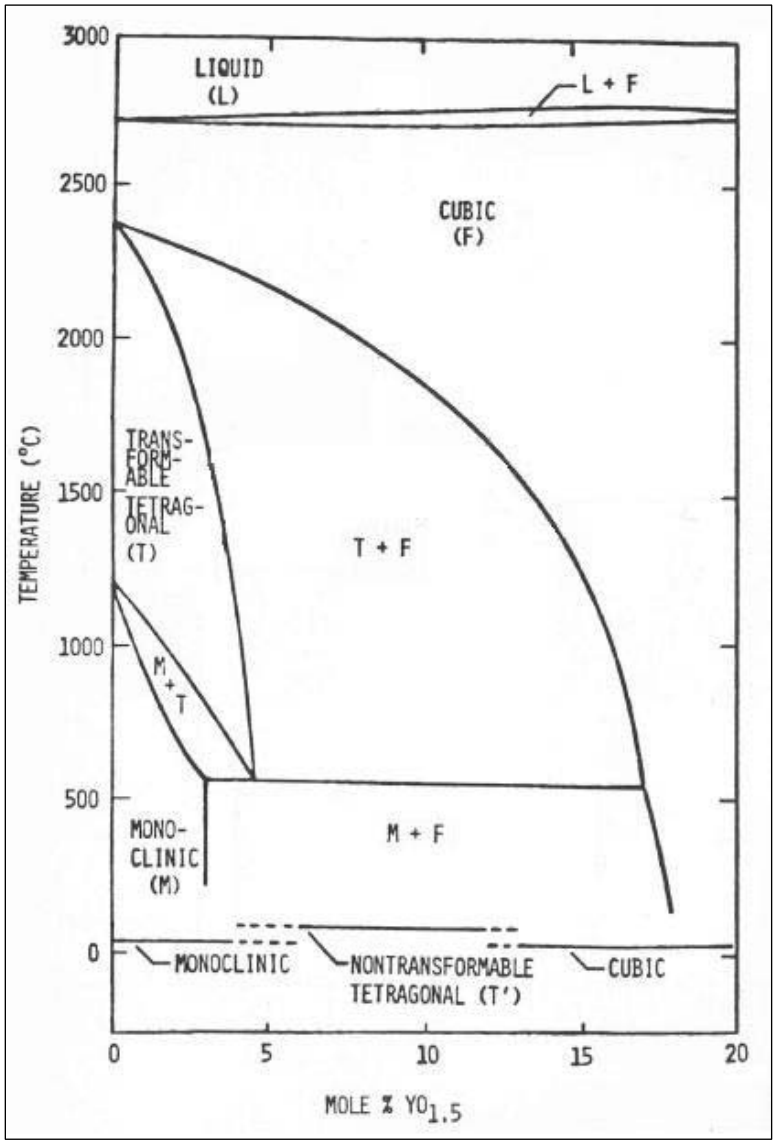

Figure 1 - Phase diagram for YSZ at zirconia rich end.[13]

The four primary phases in this portion of the diagram are the cubic (*f*), tetragonal (*t*), monoclinic (*m*) and liquid phases. For a solid, high density 7wt% Y_2O_3 - ZrO_2 ceramic (roughly equivalent to a 7mol% $YO_{0.5}$ coating in Figure 1), which is the composition of choice for most APS TBC coatings, the equilibrium phase transformations from extremely high temperatures (T > 2700C) to room temperature proceed as follows [4]. The first solid to form upon cooling is the *f*-phase. Further equilibrium cooling shifts the alloy from the *f*-phase region into the *f* –*t* two phase region where a yttria-rich *f*-phase and a yttria-deficient *t*-phase co-exist. With slow cooling past the eutectoid temperature of 580ºC, the *t*-phase YSZ present transforms into the *m*-phase and *f*-phase producing an alloy with a mixture of *f* – *m* phases. Furthermore, the $t \rightarrow m$ phase transformation is accompanied by a 3% volume expansion. This transformation is a diffusion-less Martensitic shear transformation and it can be utilized as a strengthening mechanism in many ceramic products [4]. More specifically, through careful processing steps and heat treatments, fine particles of the transformable *t*-phase can be retained at room temperature within the matrix of the ceramic component. Then, if a crack forms or propagates near these particles in the matrix, the increased stress field at the crack tip causes the *t*-phase to shear transform into the monoclinic phase which, as mentioned above, is accompanied by a volume expansion. The volume expansion induces a compressive stress near the crack tip counteracting the tensile stress present at the crack tip, hindering its ability to propagate further. This strengthening mechanism is utilized in solid YSZ ceramics and is also believed to affect thermally sprayed TBC performance as well [4].

The description given above for solid fully dense YSZ differs significantly from what occurs in TBCs because of the kinetic restraints imposed by the processing conditions. YSZ TBCs are, in most all applications, made by either air plasma spraying (APS) or electron beam

physical vapor deposition (EBPVD). During deposition of a 7wt% YSZ topcoat via APS, the yttria stabilized zirconia powder is melted in the plasma jet stream. Ideally, before impact with the bond coat surface, the liquid droplets have a uniform composition of 7wt% yttria and are completely in the liquid phase. When the droplet impacts the bond coat surface it freezes almost immediately, preventing the equilibrium phases, *m* and *f* phases, from forming. When the coating is finished, the starting microstructure present is a metastable yttrium-rich 7wt% YSZ tetragonal phase. This is a non-equilibrium phase and because of the high yttria content, it cannot transform martensitically into the monoclinic phase. This phase is represented by the dashed lines on the phase diagram where alloys between 6 and 11 mol% yttria can form the non-transformable tetragonal phase.

Although there is little to no transformable tetragonal phase in the as sprayed coatings, some can form through thermal cycling and extended exposure at high temperatures. At high temperature (T > 1200°C) the non-transformable tetragonal YSZ is located in the two phase cubic-tetragonal region on the phase diagram. The transformation of the high-yttria metastable tetragonal phase (*t'*) into the low-yttria tetragonal phase (*t*) and high-yttria cubic phase (*f*) phase is a diffusion controlled reaction. At high enough temperatures and long enough times, the reaction can produce significant amounts of *t*-YSZ which upon cooling will transform to the monoclinic phase accompanied by the volume expansion [14]. The effects of this transformation in APS coatings are of some debate as to whether they are beneficial or detrimental to the coating performance. The benefits of said transformation suggest that volume expansion can produce a fine microcrack network that can dissipate the energy associated with the extension of large cracks in these coatings [15]. Also, there is some limited evidence that the presence of *m*-phase in the intragranular regions of the coatings can improve the overall thermal shock

performance [16]. The detrimental effects of the volume phase transformation and volume expansion suggest that these large volume contractions and expansions that occur on heating and cooling can cause the coating to “crumble” and eventually fail [15].

Regardless of whether the effects of such transformation are detrimental or beneficial, both viewpoints would agree that too much of the *t*-phase or *m*-phase in the TBC coatings is undesired property as such a coating would fail quite rapidly. So it remains that control over the different phase quantities in the APS coatings is desirable.

2.5 TOPCOAT PURITY

The powder used for TBC always contains impurities. Typical impurities in zirconia and yttria powders are titania, silica, and alumina. The effects of these impurities on microstructural behavior and TBC lifetime behavior have been studied in previous works [17-22]. Miller *et al* studied the effect of varying the silica content of a 7wt% YSZ plasma sprayed coating in a burner rig test [21]. The results are shown in Figure 2.

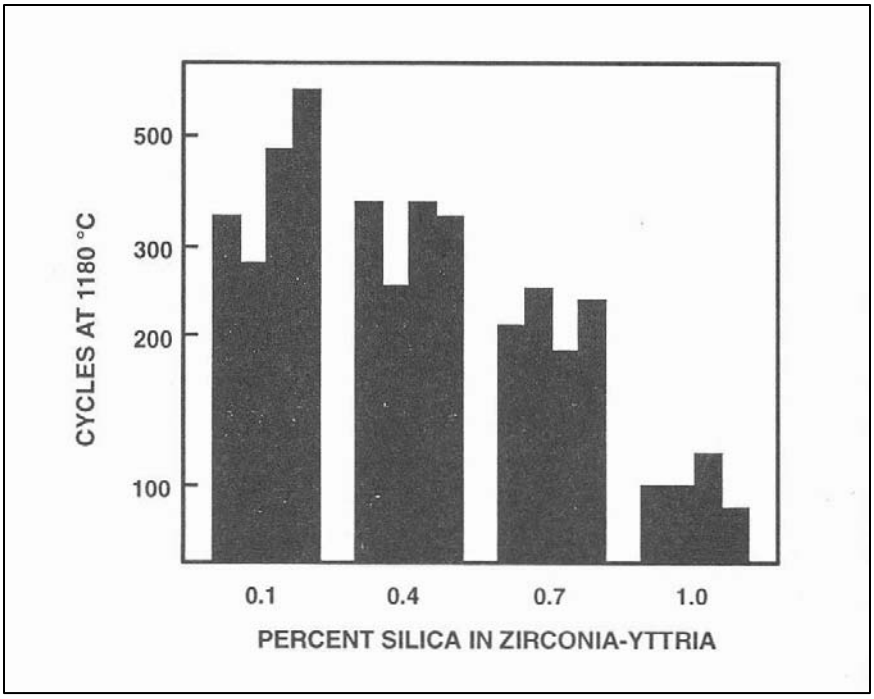

Figure 2 - Burner rig life versus percent silica[21].

This plot indicates that as the silica content in the coating increases, the lifetime of the TBC system decreases. The differences in the coating lifetime was simply attributed to the increased silica contents [22]. Another study by Vaßen et al examined the sintering behavior of plasma sprayed TBCs with varying impurity contents of alumina, silica, and titania [20]. They performed high temperature anneals of free standing coatings at 1200°C and measured the changes in length as a function of time and calculated the mean shrinkage rates. A plot of the mean shrinkage rate as a function of impurity content is shown in Figure 3.

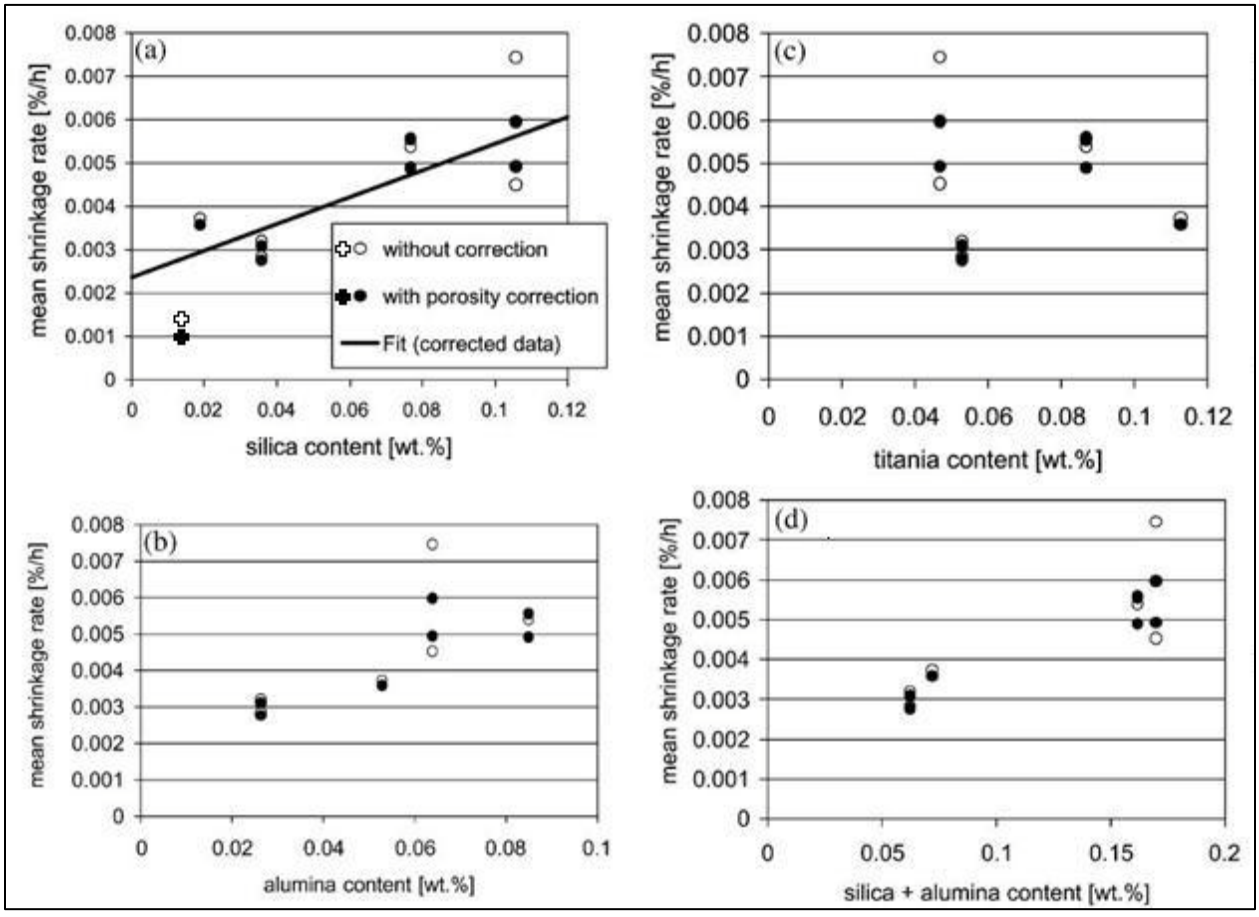

Figure 3 - Influence of: a.) silica; b.) alumina; c.) titania; and d.) silica & alumina content on the mean shrinkage at 1200°C within the first 60hr [20].

From their findings they concluded that both alumina and silica contributed to the shrinkage of the coatings. Paul *et al* [17] found very similar results in their work and they hypothesize that the sintering of these coatings causes splats to bond chemically and small pores to heal which causes the stiffness and elastic modulus of the coating to increase. Eaton and Novak [19] also reported that in increase in SiO_2 content of plasma sprayed TBCs from 0.2wt% to 4.0wt% caused a five fold increase in the percent shrinkage after 24hrs at 2600ºF as seen in the right hand plot in Figure 4 from their work.

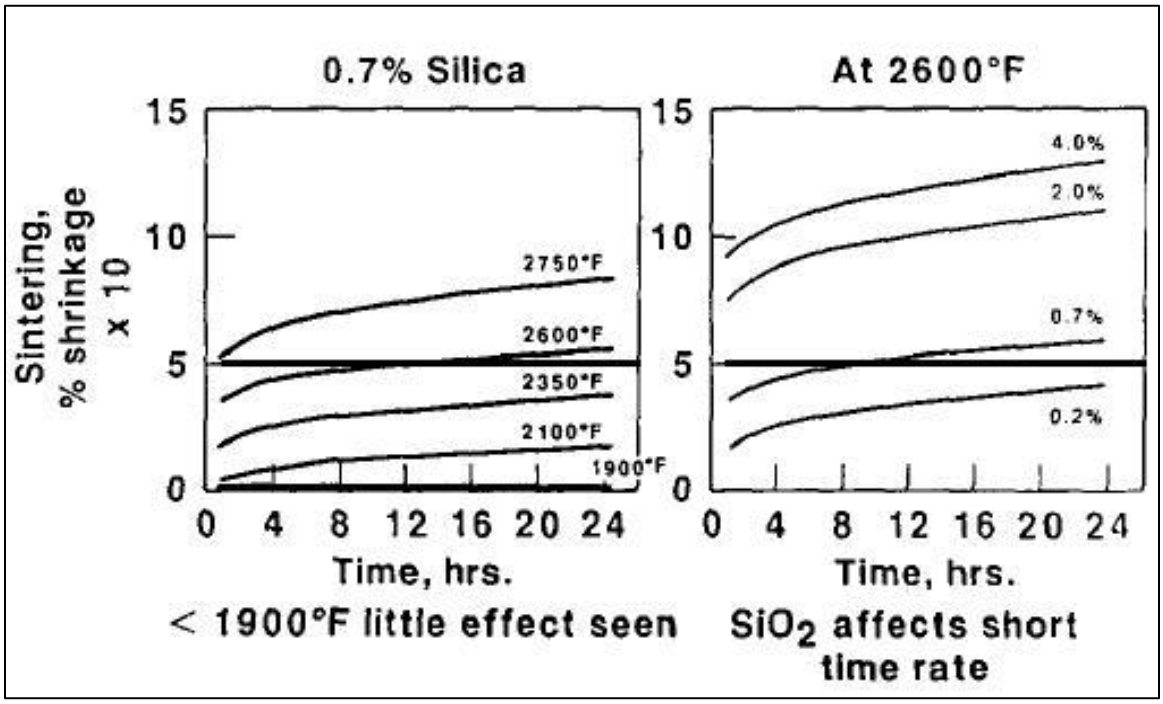

Figure 4 - The effect of time, temperature, and impurity level on shrinkage [19].

This plot also indicates that SiO_2 content affects the short term sintering behavior of the plasma sprayed coatings, where the the 4.0wt% coatings show rapid shrinkage after this short amount of time. They too propose the SiO_2 impurities (and other impurities like NaO, CaO, and

Al_2O_3) cause rapid bridging between splats, which then stiffens the entire coating [19]. As the elastic modulus of the topcoat increases, the strain tolerance decreases and the coating becomes much more brittle. Along with a decrease in toughness, the accelerated healing of microcracks and splat pores in the coatings caused by these impurities also causes the through thickness thermal conductivity to increase. This is undesired as the function of the TBC is to provide thermal protection which is negated by increasing the thermal conductivity of the protecting layer. Paul *et al* observed this rise in conductivity as the level of alumina and silica increased, which can be observed in Figure 5. Note the almost identical values of thermal conductivity at the start of the test for all three specimens.

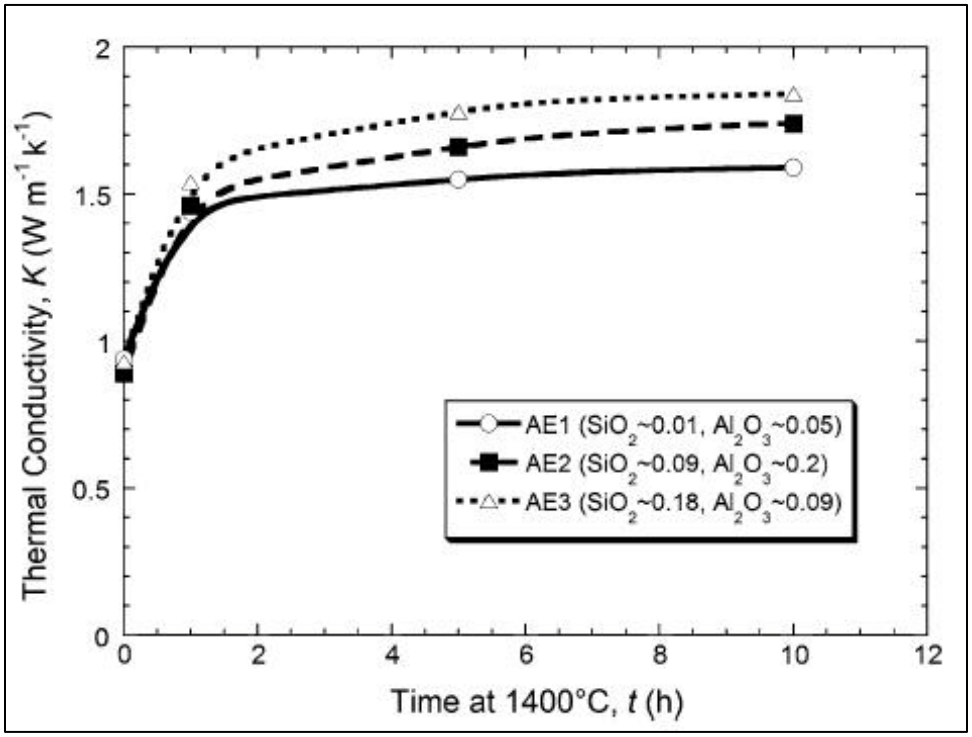

Figure 5 - Through thickness thermal conductivity as a function of time spent at 1400°C [17].

2.6 BOND COAT ROUGHNESS EFFECT

In general, surfaces with high roughness are preferred with plasma-sprayed YSZ topcoat layers. The rough surface allows for better mechanical attachment of the topcoat [4]. However, this increased roughness can cause inhomogeneous TGO formation during oxidation. In particular, local areas where the bond coat protrudes into the topcoat tend to form thicker TGO layers. In these regions, because of their curvature, the aluminum can diffuse to the topcoat interface and deplete the bond coat at a faster rate than in the smooth areas, therefore allowing the TGO to grow faster causing inhomogeneous scale thickening [6]. As the TGO thickens, the thermal expansion mismatch between the three layers (TGO-BC-TC) becomes more significant and cracks can begin to nucleate. As a result, the regions where the TGO is relatively thick can serve as failure nucleation regions [23]. In these regions, the rapid depletion of aluminum can also lead to the formation of other oxides involving chromium, nickel, or cobalt that can weaken the interface between the TGO and the topcoat. Therefore, it is evident that a smooth bond coat surface will not provide adequate mechanical attachment while an extremely rough interface can lead to the formation of an abnormally thick TGO layer and transient oxide formations that can later serve as failure initiation sites. Also, if the bond coat surface is too rough, voids can form during the spraying of the topcoat which weakens the interface.

Traegar et al [24] performed a study where, by changing the powder particle size, the roughness of the bond coat was varied between R_a=5.5μm and R_a=9.8μm. They cycled these specimens in a burner rig and their results are shown in Table 1.

Table 1 - R_a and R_z values, BC temperature and cycles to failure for three samples with different roughness values of the BC-ceramic interface [24].

#	R_a (µm)	R_z (µm)	$T_{bond\ coat}$ (K)	$1000/T_{bond\ coat}$ (K^{-1})	Cycles to Failure
1	5.6	34.8	1035	0.7645	1033
2	5.8	34.0	1036	0.7639	1672
3	9.9	54.9	1030	0.7675	2704

From these results and from FEA simulations they propose that by increasing the roughness of the bond coat, the initial compressive and tensile stress states in the YSZ between the hills and valleys of the bond coat, respectively, are larger. So when the stress state in these regions is reversed by the growing TGO layer, it will take more cycles (a thicker TGO) to reverse the larger stress fields to allow for crack propagation [24].

Smialek too compared the cyclic lifetime behavior of TBCs with different bond coat finishes. In his work Smialek [25] intentionally introduced groove patterns and rib patterns to the surface of disc PWA 1484 substrates and then sprayed them with 8YSZ coatings and cycled them both in 1 hour cycles and 100 hour cycles. Results are shown in Figure 6.

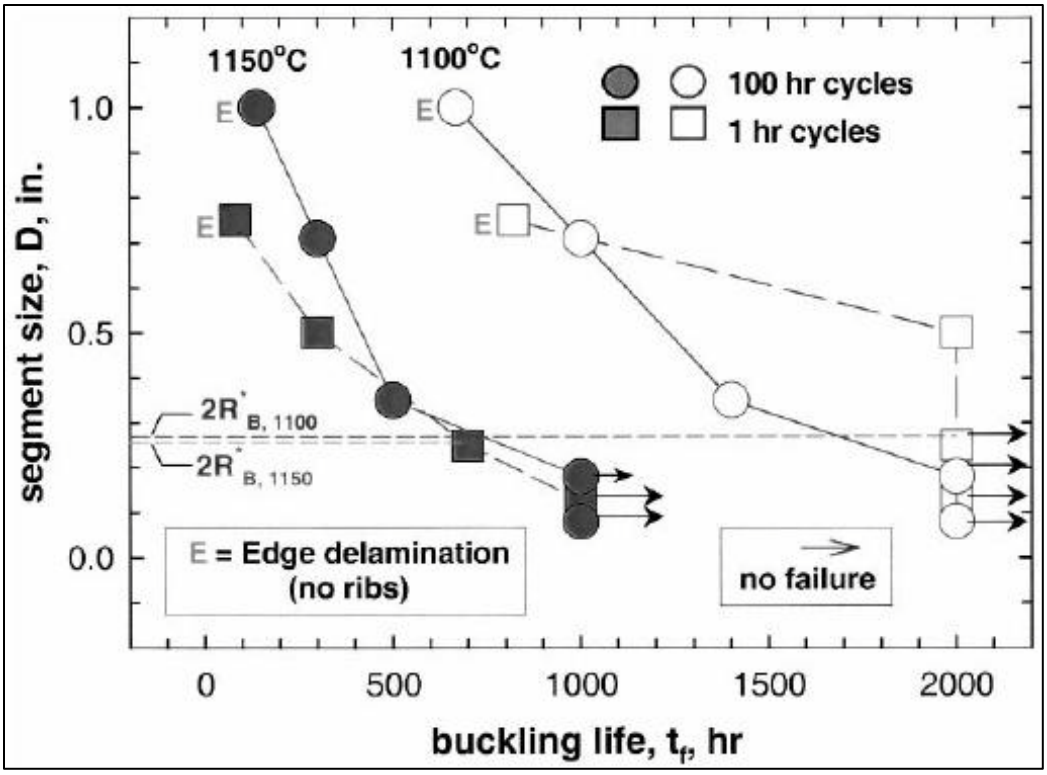

Figure 6 - Effect of segment size and test temperature on buckling life for segmented TBCs in interrupted and cyclic exposures (Points labeled "E" refer to edge delaminations of non-segmented backside or control samples; arrows indicate no failure at end of test) [25].

The ribs, or grooves, provide a mechanical barrier to delamination and from the plot above, the closer the ribs are together, the longer the lifetime of the coatings. The explanation is that the critical stress needed for delamination of the YSZ between these ribs is inversely proportional to the spacing between the ribs, thus smaller spacings require a larger stress for delamination [25]. This idea of precisely tailoring the surface of the bond coat is a new approach to increasing TBC lifetime and has accompanied with it some major questions (i.e. how will this ribbing affect the aerodynamics or oxidation resistance of the engine component) however, it nonetheless indicates the importance of bond coat topography on TBC lifetime.

2.7 BOND COAT YTTRIUM CONTENT EFFECT

For most APS TBC systems, M-CrAlY bond coats are used because of the protective slow growing alumina scales they form during high temperature exposure [26]. The protectiveness, growth rate, and adherence of the alumina TGO is controlled by the composition and microstructure of the bond coat and the composition of the substrate, as mentioned above. Small additions of yttrium and other elements such as Zr, Re, Hf, are often added to induce certain "reactive element effects" within the alloy such as increasing the adherence and slow growth of the alumina scale. One such possible effect is that these elements act as "sulfur-getters," preventing sulfur from segregating to the metal scale interface by tying up the excess sulfur in the bulk of the alloy/bond coat. They can also suppress outward growth of alumina by migrating and segregating on the scale's grain boundaries. By suppressing the outward diffusion of aluminum (and inward diffusion of vacancies), void coalescence at the scale metal interface can be prevented [27].

However, too much yttrium has been shown to be detrimental to TBC performance [27-29]. Over doping has been shown to cause yttria stringers to form in the alumina scale at grain boundaries which act as fast-transport diffusion paths for inward oxygen diffusion. This can cause rapid aluminum depletion in the bond coat and the formation of Ni-Al-Cr spinel oxides to form, weakening the adherence of the TBC system.

Thus it seems a compositional limit exists in achieving the beneficial aspects of the reactive element effect. Review of the literature indicates this beneficial limit is somewhere between 0.1-1.0wt% Y in the bond coat [27-29]. Achieving such narrow composition range is possible with the manufacturing techniques used today, however there have still been issues with sporadic coating behavior between coatings with nominally identical starting compositions [30].

Variation in lifetime has been attributed to the various processing steps during the manufacturing of these coatings that cause variations in the coating microstructure and elemental distribution. Such processing steps include deposition technique (VPS, APS, Ar-Shrouded APS etc…) deposition parameters (i.e. torch stand-off, torch power, powder feed rate etc…), heat treatment conditions (i.e. oxygen partial pressure in vacuum, temperature of anneal, length of heat treatment), and surface finishing processes [27, 30]. Work by Subanovic et al [30] has shown that a high oxygen partial pressure during the deposition of NiCoCrAlY+Hf coatings by VPS can cause the reactive elements to be tied up in the bulk of the material as oxides, which inhibits their reactive element benefits from taking effect. Similarly, they also showed that a low oxygen partial pressure resulted in the over doping of yttrium and hafnium leading to rapid scale growth. They also pointed out the importance of the temperature of the heat treatment. At high treatment temperatures the yttrium and hafnium are very mobile in the alloy and can quickly diffuse to the surface where they form oxides that eventually result as stringers and fast diffusion paths in the alumina TGO. By lowering the temperature, the yttrium is less mobile and alumina precipitates can form at the surface promoting the formation of a more protective scale when exposed to more oxidizing conditions [30]. Gil et al. reported similar behavior with NiCoCrAl-0.3Y and NiCoCrAl-0.6Y coatings [27].

2.8 SUBSTRATE SELECTION EFFECT

The superalloy substrate has been shown to affect the lifetime behavior of TBCs in two direct ways: through compositional effects and the through thermal expansion misfit effects. Compositional effects arise from interdiffusion between the bond coat and the substrate material.

In this study, the bond coatings used are NiCoCrAlY bond coats which are alumina formers. As the alumina scale forms during high temperature exposure, the aluminum in the bulk of the coatings diffuses up to the surface where it is incorporated in the scale. Likewise, when at high temperatures, the aluminum can also diffuse down into the substrate given the appropriate thermodynamic conditions. Such conditions require a chemical potential gradient to exist which is established by the composition difference between the bond coat and superalloy. In the case where a gradient does exist with the underlying alloy, the aluminum will be depleted faster than in the case with just the scale formation because of the second "sink" the aluminum is "consumed" by. Once the aluminum content drops below a critical level, alumina is no longer the stable oxide and so nickel and chromium oxides can begin to grow. These oxides are not as adherent as the alumina and can spall off more easily [31-32].

Similar to the aluminum depletion by diffusion into the substrate alloy, elements in the substrate material can diffuse up into the bond coat. Elements such as tantalum (Ta), niobium (Nb), sulfur (S), and yttrium (Y) can diffuse through the bond coat and affect the growth rate and adherence of the oxide and thus affect the overall TBC lifetime [1, 33]. Pint et al. showed this by coating two different René N5 substrates, one with and the other without yttrium, with a PtAl bond coat and a YSZ TBC and thermally cycling the specimens until failure. The specimens with yttrium in the substrate had longer lifetimes as shown in Figure 7 [31].

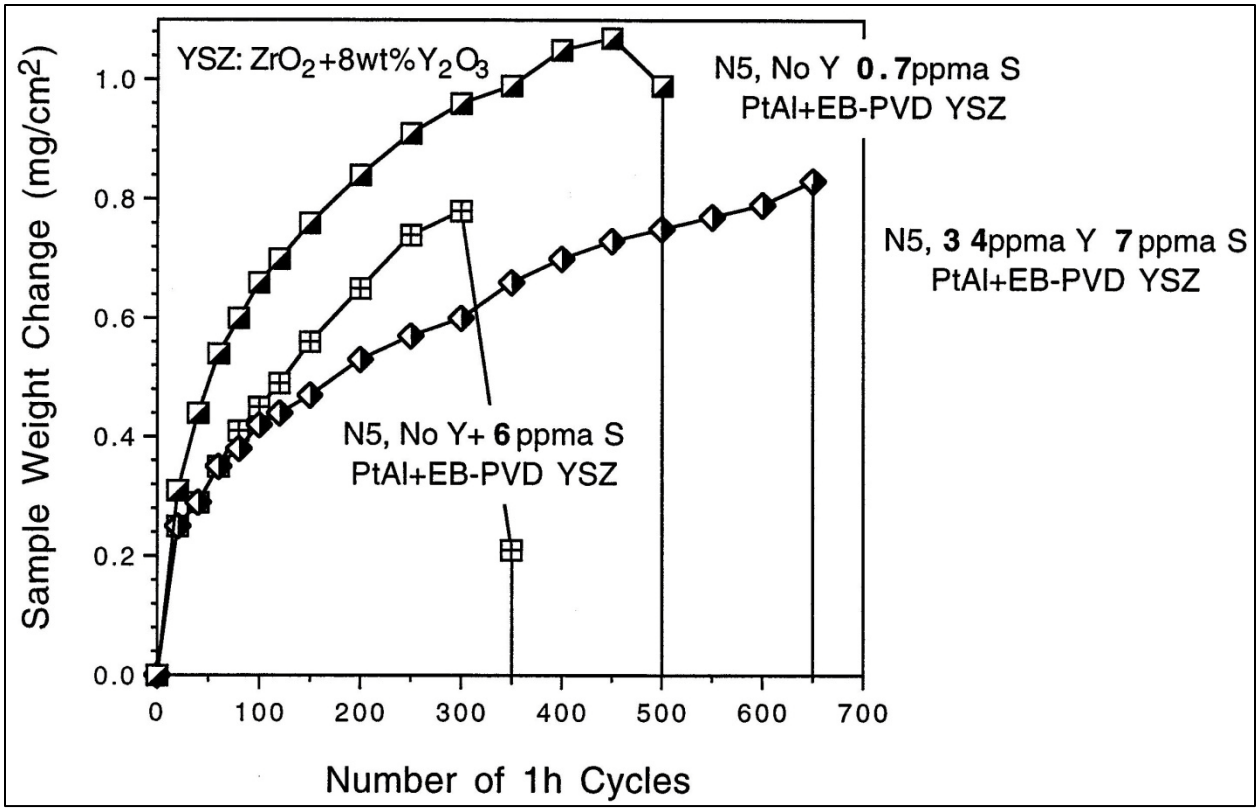

Figure 7 - Weight change of Pt aluminde/EB-PVD TBC coated René N5 during 1 hr cycles at 1150°C. Both desulfurization and the addition of Y to the underlying substrate improved coating lifetime [31].

The yttrium from the Rene N5 was believed to induce the reactive element effect described in Section 2.7. Lifetime was also improved through desulfurization of the substrate. At high enough levels, sulfur can weaken the cohesive strength of the scale metal interface causing spallation [1, 31].

Thermal expansion differences between the different component layers in a TBC will give rise to stresses at these interfaces and by minimizing the thermal expansion mismatch, the stresses will be reduced which should increase TBC lifetime [34]. Previously, the effect of substrate selection on TBC performance reported by Stecura showed, in furnace and burner rig

testing, that by changing the base substrate metal to alloys with lower thermal expansion coefficients, that the lifetime of the coatings could be increased [35]. Wu et al. argue however, that coating lifetime is not directly proportional to coefficient of thermal expansion (CTE) mismatch but instead more solely dependent on bond coat oxidation with the CTE mismatch acting as a conjugate part of the failure mechanism [36]. Regardless of whether the CTE mismatch is a dominant or conjugate failure mechanism, a review of the literature indicates that it is nonetheless detrimental to the coating lifetime and should be minimized.

3.0 EXPERIMENTAL

3.1 COATING FABRICATION

3.1.1 First Generation Specimens

Initially 60 2.5 cm diameter buttons of IN 718 were coated with a NiCoCrAlY bond coat by argon-shrouded plasma spraying at Praxair Surface Technologies (PST), vacuum heat treated for 4 h at 1080˚C, and coated with APS-TBCs (85% dense YSZ) of three thicknesses. 15, 30, and 45 mil (375, 700, and 1,125μm). Table 2 presents the compositions of the substrate, bond coat and topcoat. The YSZ powder used was of very high purity, particularly with regard to alumina and silica impurities.

Table 2 - Compositions of Substrate, Bond Coat, and Topcoat

Composition of Materials (wt%)															
Layer	**Material**	**Ni**	**Co**	**Cr**	**Al**	**W**	**Mo**	**Fe**	**Mn**	**Si**	**Ta**	**Nb**	**Ti**	**C**	**Re**
Superalloy	**IN-718**	**52.5**	**1**	**17.5**	**1**	**-**	**3**	**Bal**	**0.35**	**0.35**	**-**	**5**	**0.3**	**0.08**	**-**
Superalloy	**HA-188**	**10**	**Bal**	**20**	**-**	**15**	**-**	**3**	**1.5**	**0.4**	**-**	**-**	**-**	**0.1**	**-**
Superalloy	**Rene N5**	**Bal**	**7.5**	**7.5**	**6.3**	**6.4**	**1.4**	**-**	**-**	**-**	**7.1**	**-**	**-**	**0.05**	**2.8**
Superalloy	**MarM-509**	**10**	**Bal**	**23**	**-**	**7**	**-**	**-**	**-**	**-**	**-**	**3.5**	**0.2**	**0.6**	**-**
Bond Coat	**NiCoCrAlY**	**Ni**	**Co**	**Cr**	**Al**	**Y**									
		Base	**22**	**16**	**13**	**0.5**	**-**	**-**		**-**		**-**	**-**	**-**	**-**
YSZ TBC		**ZrO_2**	**Y_2O_3**	**Al_2O_3**	**CaO**	**Fe_2O_3**	**HfO_2**	**MgO**		**SiO_2**		**All Other**			
	High Purity	**Base**	**7.736**	**0. 011**	**0.003**	**0.007**	**1.69**	**<0.001**		**0.013**		**0.157**			
	Conventional Purity	**Base**	**7.5**	**0.1**	**-**	**0.033**	**1.6**	**0.005**		**0.3**		**0.443**			

Figure 8 presents the surface morphology of the bond coat prior to topcoat deposition. The surface roughness was characterized with a Talysurf stylus machine at 15 random locations yielding an Ra = 11.1±1.1µm. Figure 9-11 present cross-sections of the as-deposited coatings of each thickness.

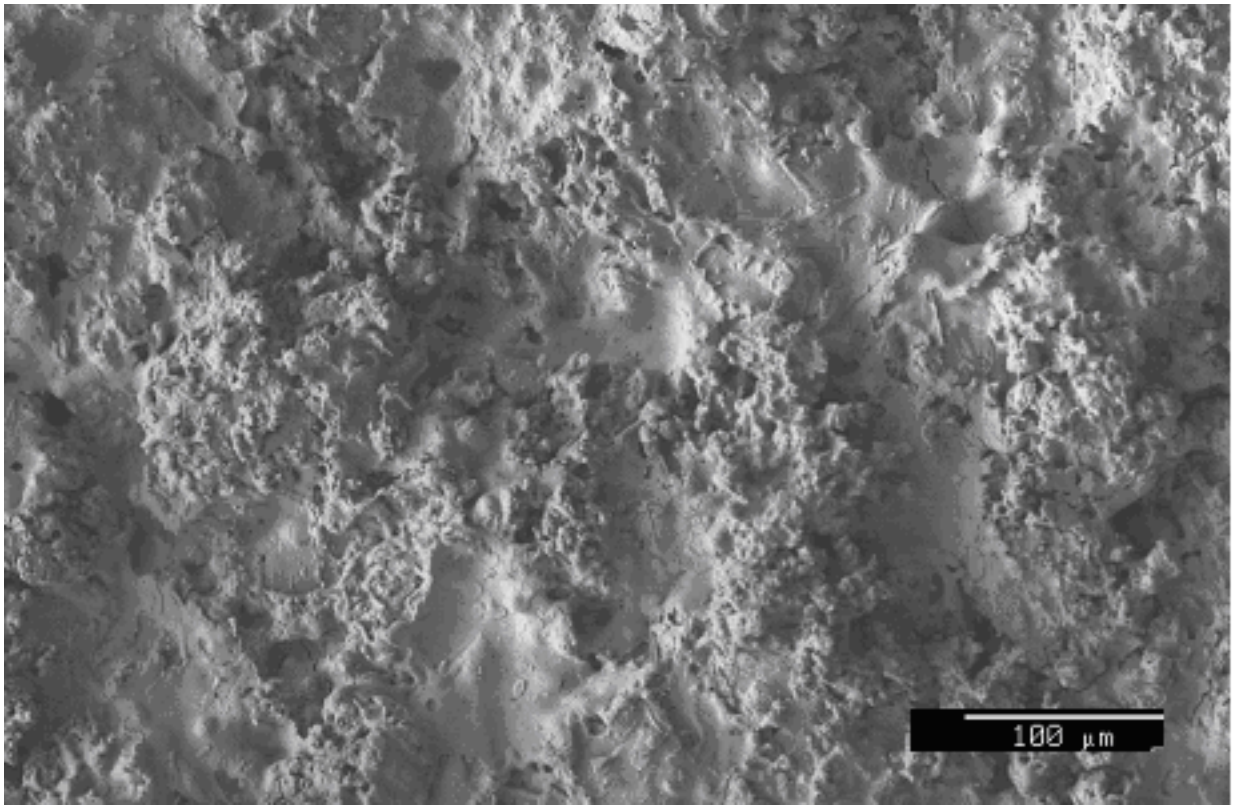

Figure 8 - Surface morphology of the NiCoCrAlY bond coat prior to topcoat deposition. (Ra = 11.1±1.1µm)

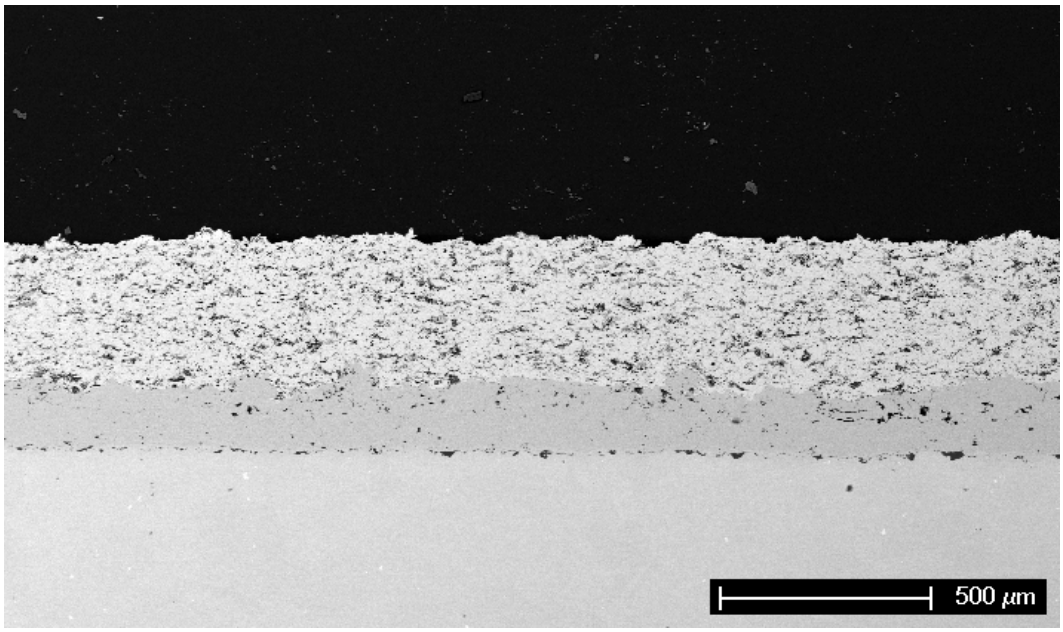

Figure 9 - Cross-section of as-deposited 15 mil TBC.

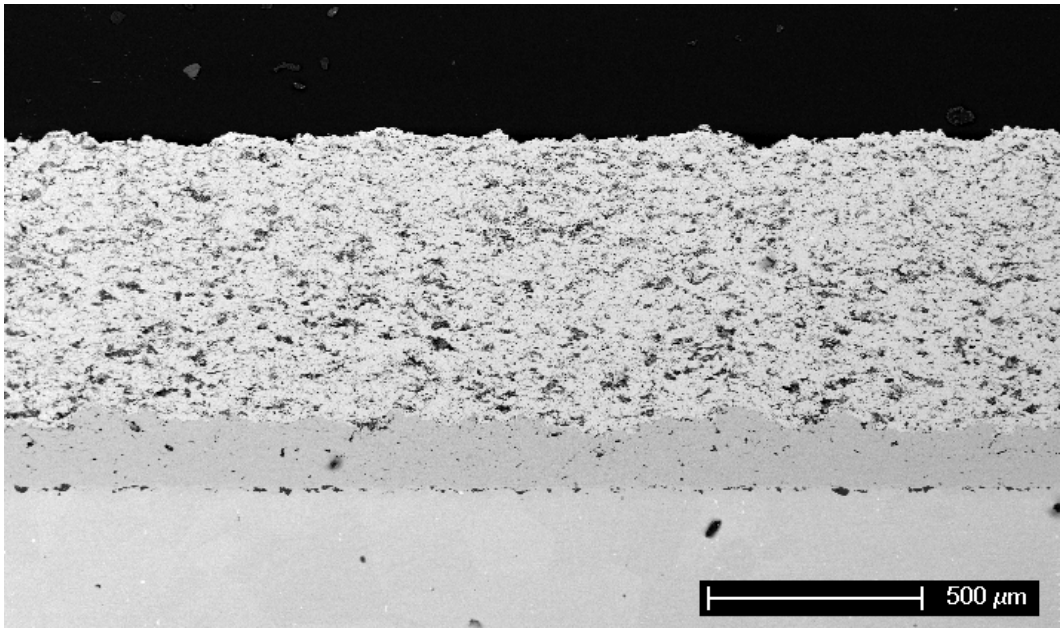

Figure 10 - Cross-section of as-deposited 30 mil TBC.

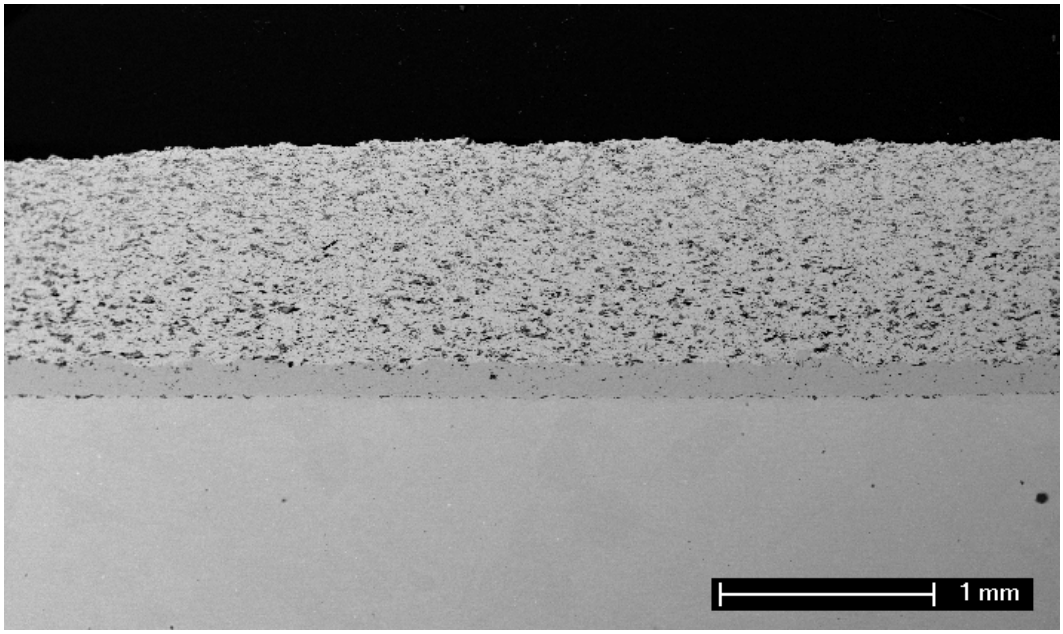

Figure 11 - Cross-section of as-deposited 45 mil TBC.

3.1.2 Second Generation Specimens

Based on the experimental results from the First Generation Specimens a second group of specimens was prepared to evaluate the effects of specific variables. The same high-purity YSZ was used to prepare the majority of these specimens. Topcoats were prepared in two thicknesses, 15 and 45mils. Specific variables addressed were:

1. Effect of Superalloy Substrates Selection: René N5, HA 188, and IN718 substrates were used (See Table 2 for compositions.)
2. Topcoat Purity: one set of specimens was prepared using YSZ of conventional purity and MarM509 substrates.

3. Use of Dense Vertically Crack (DVC) inner layers in the topcoat. Two sets of specimens were prepared with a DVC inner layer under the porous topcoat. In one set the deposition conditions were changed continuously to produce the two layers. In the second the deposition was interrupted between preparation of the two layers.

4. Modification of the bond coat topography. Bond coats were prepared from a mixture of two particle sizes of the NiCoCrAlY powder to give a single layer bond coat. Afterwards, the specimens were vibratory finished for various times.

Additional experiments involved measurement of the thermal conductivity of as-sprayed topcoats and measurement of the coefficient of thermal expansion (CTE) of all the superalloys studied. Both the thermal conductivities and the thermal expansion measurements were performed at the Thermophysical Properties Research Laboratory (TPRL). The thermal conductivity was measured by the laser flash technique and the thermal expansion coefficients were measured with a dual push rod dilatometer in a stagnant helium atmosphere with a 2°C/minute heating rate.

3.2 EVALUATION OF COATING PROPERTIES

The cohesive strength of TBCs of each thickness was measured using the bondcap method of ASTM C 633 at Praxiar Surface Technology (PST) facilities. The coatings were epoxy glued to mating pull caps and tested in a Tinius-Olsen tensile machine using a crosshead speed of 0.1 cm/min. The fracture surfaces were evaluated by SEM.

3.3 HIGH TEMPERATURE EXPOSURES

3.3.1 Sintering and Phase Transformation Experiments

The resistance of the topcoats to sintering and phase transformation was evaluated using free standing high purity 45 mil YSZ coatings which were prepared by depositing the YSZ on aluminum panels and then carefully removing them. The free standing coatings were exposed for 100 hours at temperatures of 1200, 1300, 1400, and 1500˚C (three specimens at each temperature). The densities were measured using ASTM B-328, including oil infiltration. One specimen from each temperature was examined by x-ray diffraction (XRD) to determine the extent of transformation to the monoclinic phase. This portion of the work was done at PST's facilities in Indianapolis, IN.

3.3.2 Thermal Cycling Experiments: Furnace Cycle Tests (FCT)

The thermal cyclic durability of the TBCs was evaluated by cycling three specimens of each thickness in a bottom loading furnace Figure 12. The specimens were heated to 1100ºC over a period of ten minutes, held there 45 minutes, and then forced-air cooled for another ten minutes. This cycle was repeated until 50% or more of the topcoat had spalled off or appeared to be delaminated.

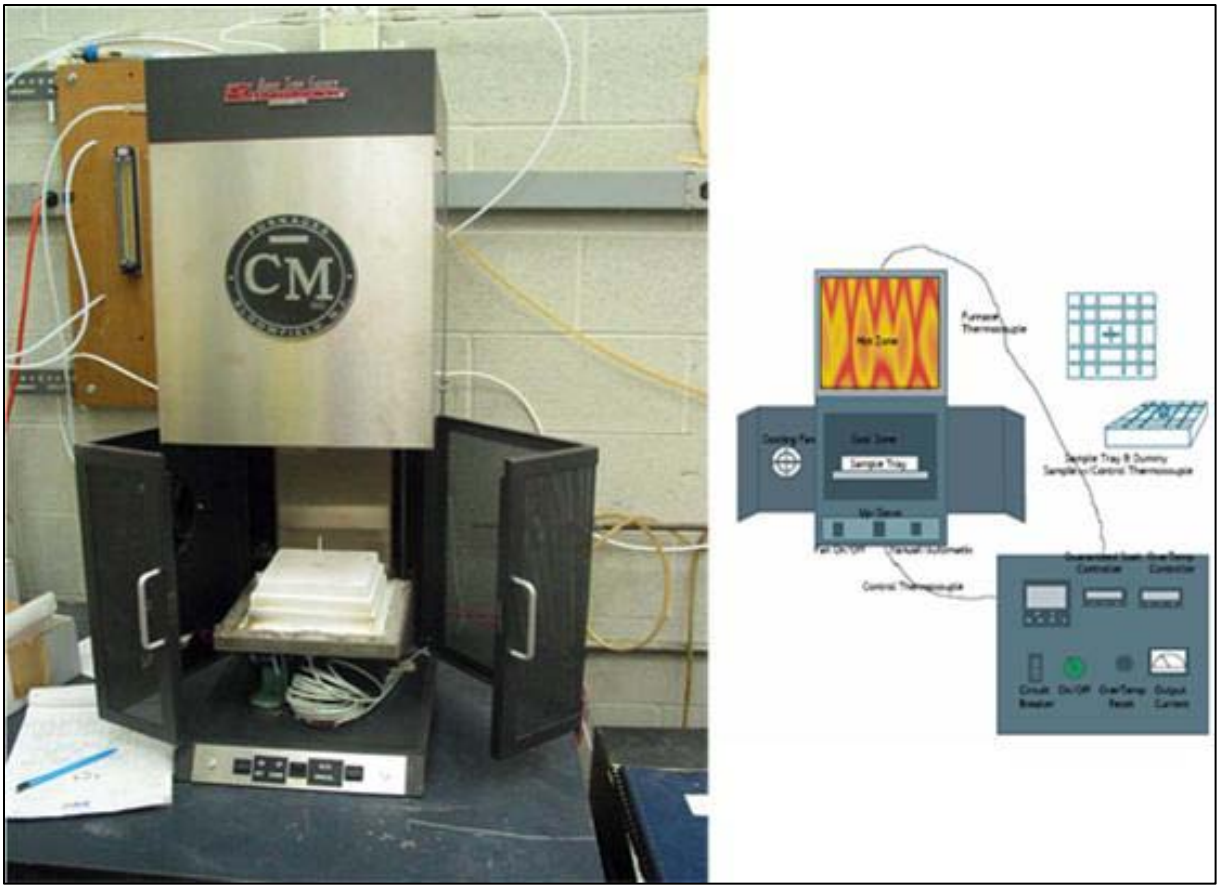

Figure 12 – Bottom loading furnace for furnace cycling tests (FCT).

An average lifetime for each of the three TBC thicknesses was estimated using the data from cycle to failure tests. Then interrupted lifetime tests were performed for three 30 mils samples corresponding to 25%, 50%, and 75% of the lifetime (40, 80, 120 cycles respectively). Also, a 15 mil specimen and a 45 mil specimen were cycled to 50% of their lifetime (100 and 10 cycles respectively). These tests were run at the University of Pittsburgh by the author.

3.3.3 Thermal Cycling Experiments: Jet Engine Thermal Simulation (JETS)

A more simulative durability (JETS) test, which is modeled after the operating conditions in a turbine, was performed by technicians at PST. In this test, disk specimens with the three TBC thicknesses were tack welded onto a large rotating ring Figure 13.

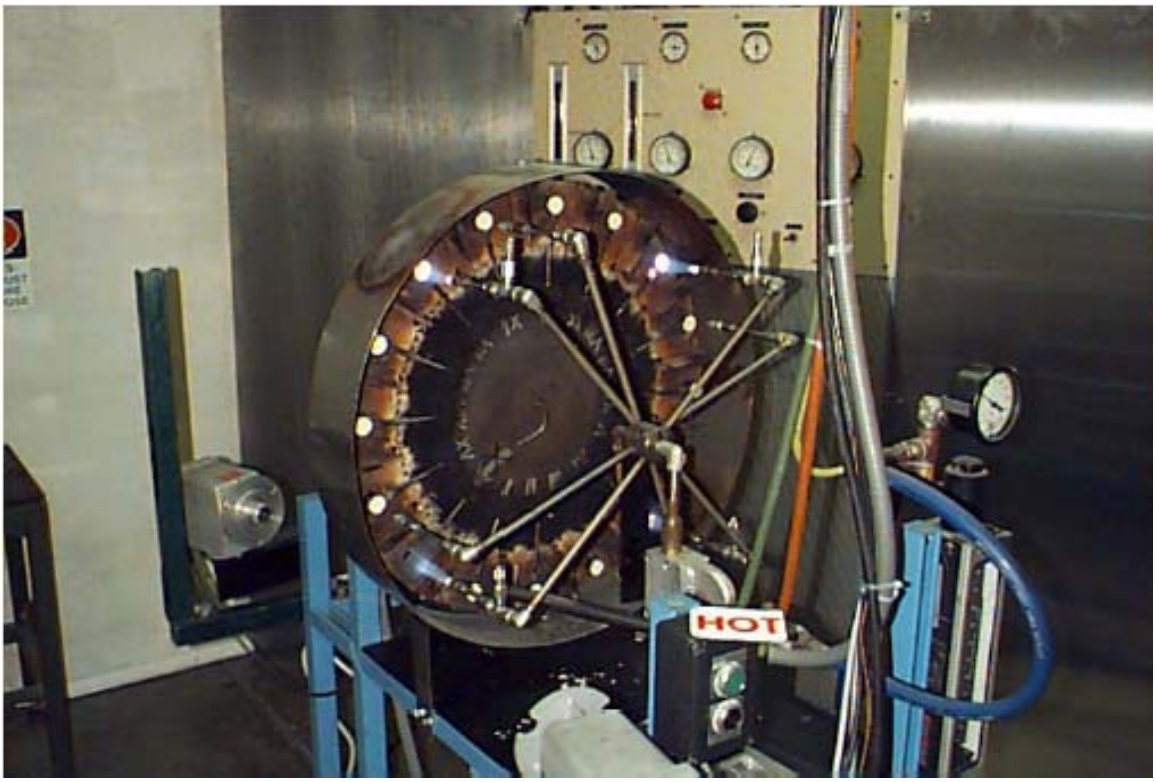

Figure 13 - Praxair JETS testing rig.

The specimens were then rotated through a series of different exposure conditions. In the first condition, the sample is rotated under a oxy-propylene flame for 20 seconds which heats the surface to approximately 1400ºC. The specimen is then rotated under a nozzle that forced-gas cools the YSZ surface for another 20 seconds with compressed nitrogen. After this, the specimen

is rotated to positions where it undergoes ambient air cooling for two periods of 20 seconds each. This procedure is repeated for 2000 cycles max or until failure occurs. The damage was monitored by a 10X optical pyrometer that measured and recorded the back face temperature. In the event some of the YSZ spalled off, the temperature of the back face would spike up and so an accurate number of cycles to spallation could be determined.

3.3.4 Thermal Cycling Experiments: Extended Duration Thermal Cycling

Extended duration testing is aimed at inducing bond coat related failure in the APS TBCs. This is done by minimizing the number of the heating and cooling sequences the samples experience while still providing sufficient hot exposure time. The as-coated specimens were placed in a bottom loading furnace, heated to 1100°C over a period of 10 minutes, held at this temperature for 60 hours, and then force air cooled for 10 minutes. This cycle was repeated until spallation of 50% of the topcoat occurred. As with the other furnace cycling experiments, these tests were performed at the University of Pittsburgh by the author.

3.4 POST-TESTING ANALYSIS

The fracture surfaces of specimens from these exposure tests were analyzed using SEM techniques to determine the composition and morphology of the material at the surface. Cross-sections of the specimens were examined using SEM. This work was performed by the author.

4.0 RESULTS AND DISCUSSION

4.1 FIRST GENERATION SPECIMENS

4.1.1 Cohesive Strength Tests

The cohesive strength of the as-deposited topcoats is presented in Figure 14. The cohesive strength decreased with increasing YSZ thickness. It is speculated that this is the result of increasing residual stress in the underlying layers as additional coating is built up during the spraying process. Observation of the fracture surfaces by SEM showed qualitatively that the average position of the fracture plane moved closer to the bond coat/YSZ interface as the topcoat thickness was reduced.

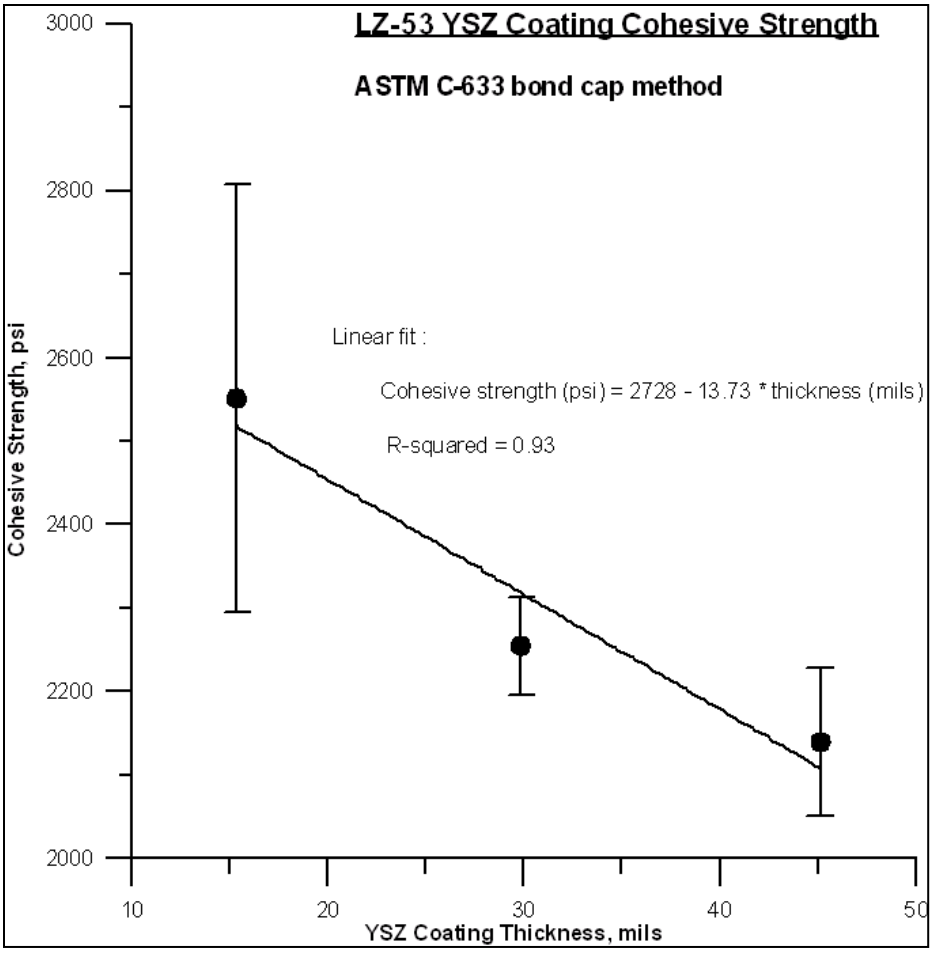

Figure 14 - Cohesive bond strength of as-deposited topcoats as a function of thickness.

4.1.2 Sintering and Phase Transformation Behavior

The effect of 100 hour exposures at various temperatures on YSZ density is shown in Figure 15.

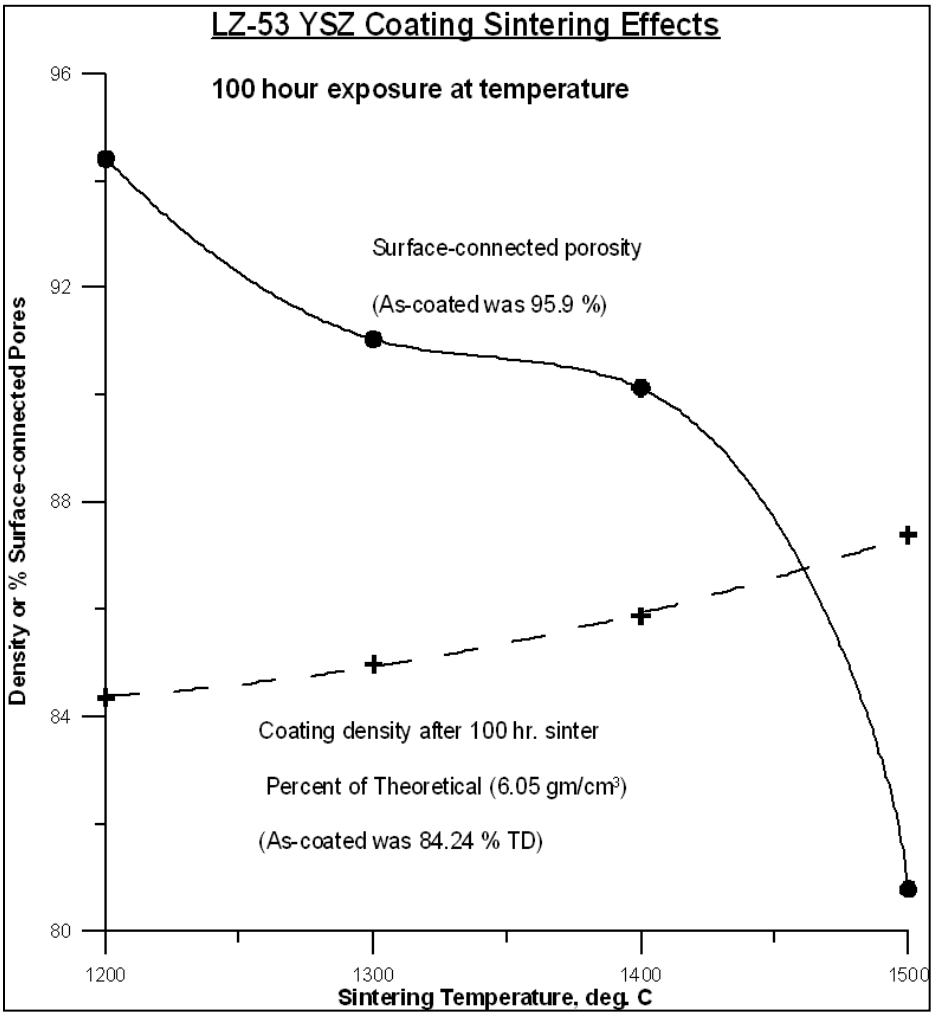

Figure 15 - Topcoat density (dashed line) and percent surface-connected porosity (solid line) after 100 hours exposure as a function of exposure temperature.

The exposures at 1200˚C and 1300˚C, the highest temperature likely to be encountered in most applications, resulted in negligible increases in density. It should be noted that the starting

density for these coatings, prior to the thermal anneal was 84.24% theoretical density. Exposures at 1400˚C and 1500˚C resulted in small increases in density. The surface connected porosity decreased slowly and systematically up to 1400˚C but dropped sharply at 1500˚C. The high resistance to sintering exhibited by these TBCs is attributed to the very high purity YSZ powder used in this study. Coatings prepared from YSZ of conventional purity would be expected to undergo significant sintering at temperatures as low as 1000˚C [20].

The sintering data at 1200˚C may be compared with those of Vaβen et al [20] who studied the sintering of APS-TBCs of differing purity including SiO_2 contents between 0.036 and 0.106 wt%. The findings of that study included:

1. There was no influence of TiO_2 on sintering rate.
2. Sintering rate increased with increasing SiO_2 content.
3. Sintering rate increased with increasing Al_2O_3 content.

An interesting point is that when the plot of sintering rate versus SiO_2 content was extrapolated to zero SiO_2 content the intercept gave a significant rate. It was concluded from this that there is not a significant benefit of going to high-purity TBCs. However, the 1200˚C sintering rates estimated for the high-purity coatings in the present study fall far below the extrapolated line in Vaßen's paper [20]. Since the dilatometer results in Vaßen et al are linear with time the total densification was divided by 100 to yield a sintering rate of Rate = 0.0012 %/h. This point placed on Figure 3a (shown as crosses) at a SiO_2 content of 0.013 wt% is well below the extrapolated value at about 0.0028%/h. Thus, it seems the shrinkage data do not extrapolate linearly at low SiO_2 content. It has been proposed by Eaton and Novak that silicate phases can form and could contribute to liquid phase sintering and/or promote rapid bridging between splats [19]. One possibility is that the ultra-pure powder in the present coatings has

SiO_2 (and Al_2O_3) content below the solubility limit so no new phases can form between adjacent splats. This result is significant because both the thermal conductivity and elastic modulus of the topcoat will increase as sintering proceeds. However, at this time, there is no experimental data available for a direct comparison between the behaviors of the high purity YSZ and the conventional purity with similar as-deposited density.

In the present study the transformation of the high purity topcoats from the metastable tetragonal structure to monoclinic was investigated by XRD using the procedure outlined in [4]. The as-sprayed coating is non-equilibrium tetragonal of 7wt% YSZ. At equilibrium it should consist of very low Y monoclinic and high Y tetragonal / cubic phases. The exposures for 100 hours at 1200˚C, 1300˚C, and 1400˚C resulted in no observable monoclinic phase. Only a small amount of monoclinic phase (≈0.6%) was formed even at 1500˚C. Typical lower purity YSZ has been found to form over 19% monoclinic phase in 100 hours at 1400˚C [37]. It is believed this phase stability is also the result of the high purity. It is speculated that the transformation may be accelerated in lower purity YSZ by enhanced diffusion of yttrium at grain boundaries, probably aided by the silicon impurity.

4.1.3 Thermal Cycling Behavior

4.1.3.1 Furnace Cycling Tests

The results from the bottom-loading furnace (FCT) testing are displayed in Table 3.

Table 3 - Number of cycles to failure in FCT.

Number of Cycles to Failure @ 1100^{o}C (9 specimens total, 3 per thickness)			
	Spec #1	**Spec #2**	**Spec #3 (Edges Ground)**
15 mils of APS TC	180	220	220
30 mils of APS TC	140	160	140
45 mils of APS TC	20	40	40

A general trend seen in the data indicates that a longer lifetime is associated with thinner topcoats. The spread in the individual data for each thickness is minimal indicating good reproducibility of the failure times. Also, there is a large difference in the lifetimes of the thick 45-mils specimens and the two thinner 15 and 30 mil specimens. This is illustrated in Figure 16 in which the reciprocal of the number of cycles to failure is plotted versus topcoat thickness.

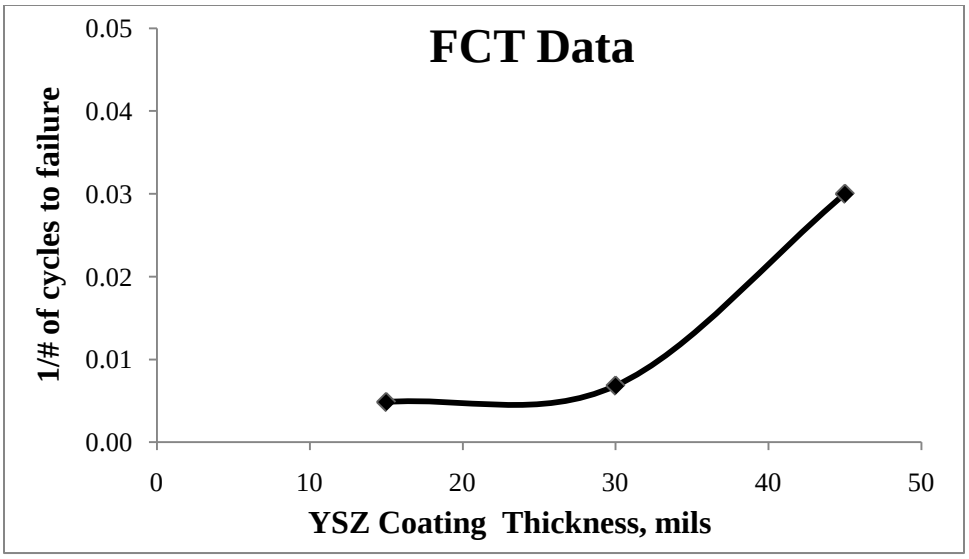

Figure 16 - Reciprocal of the number cycles to failure in the 1100˚C FCT as a function of YSZ thickness.

Figure 17- 19 are the fracture surfaces of the three thicknesses of the topcoats at both high and low magnifications in backscattered mode (15, 30 and 45 mils respectively).

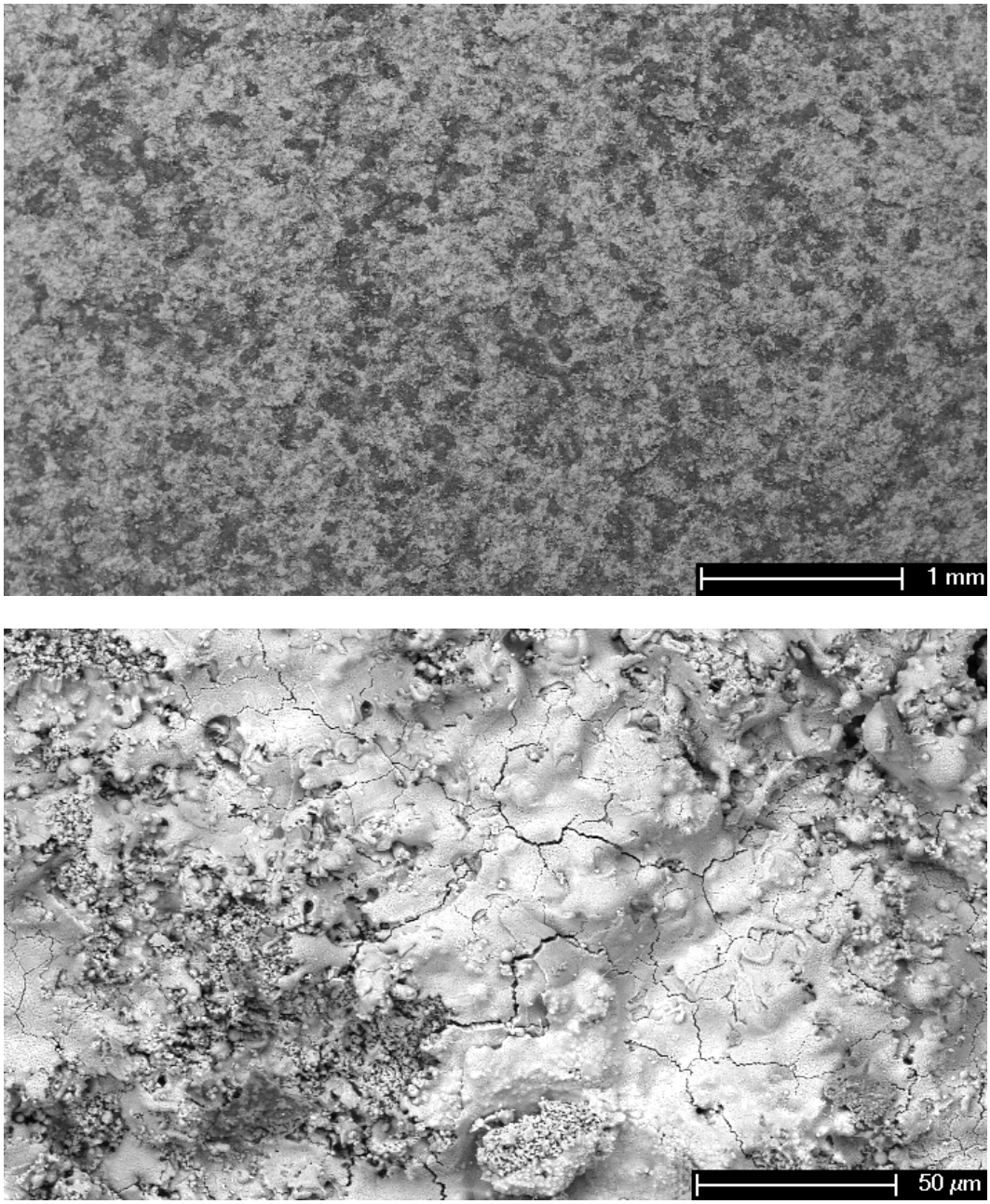

Figure 17 - Fracture surface (at low (top) and high (bottom) magnification) of a 15 mil TBC after failure in the 1100˚C FCT.

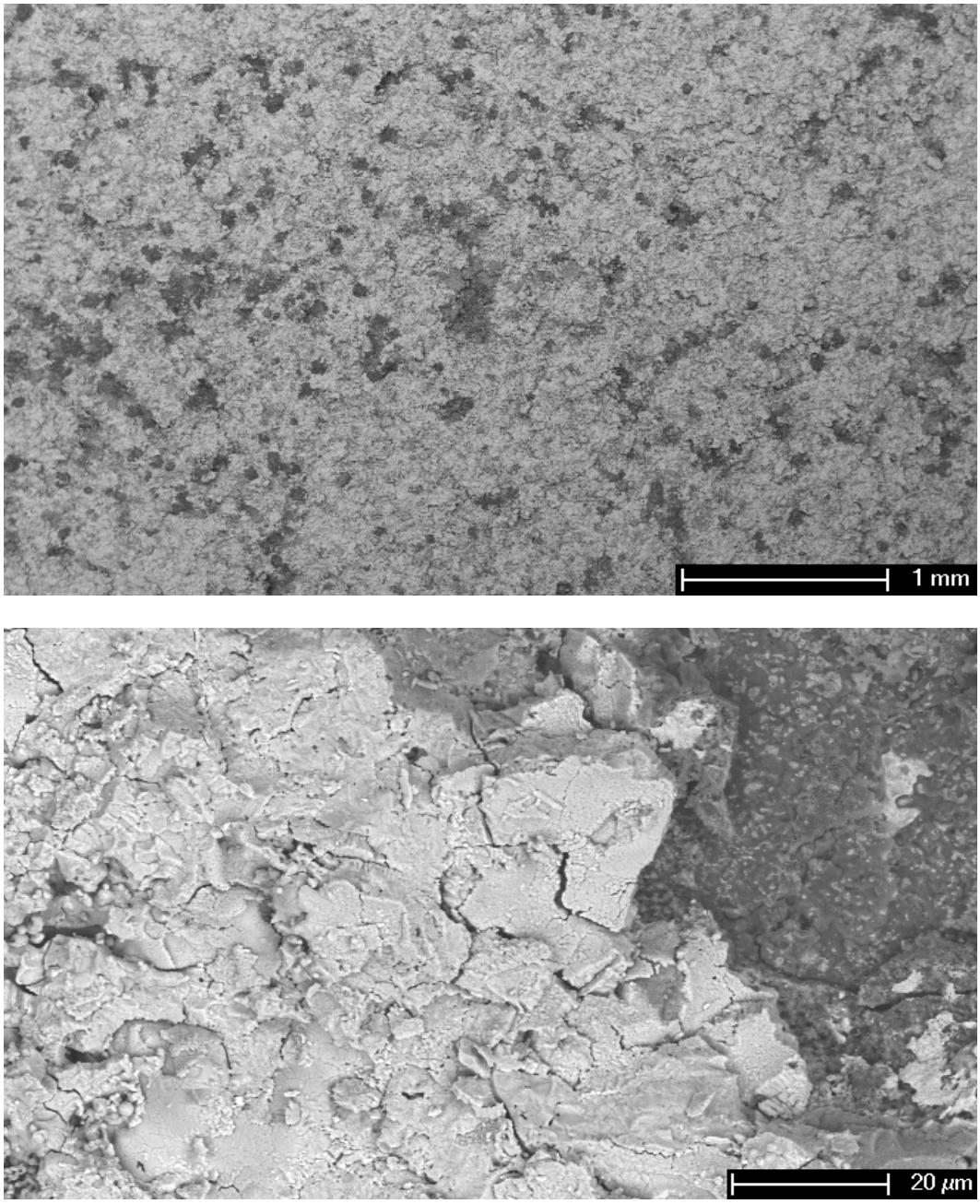

Figure 18 - Fracture surface (at low (top) and high (bottom) magnification) of a 30 mil TBC after failure in the 1100˚C FCT.

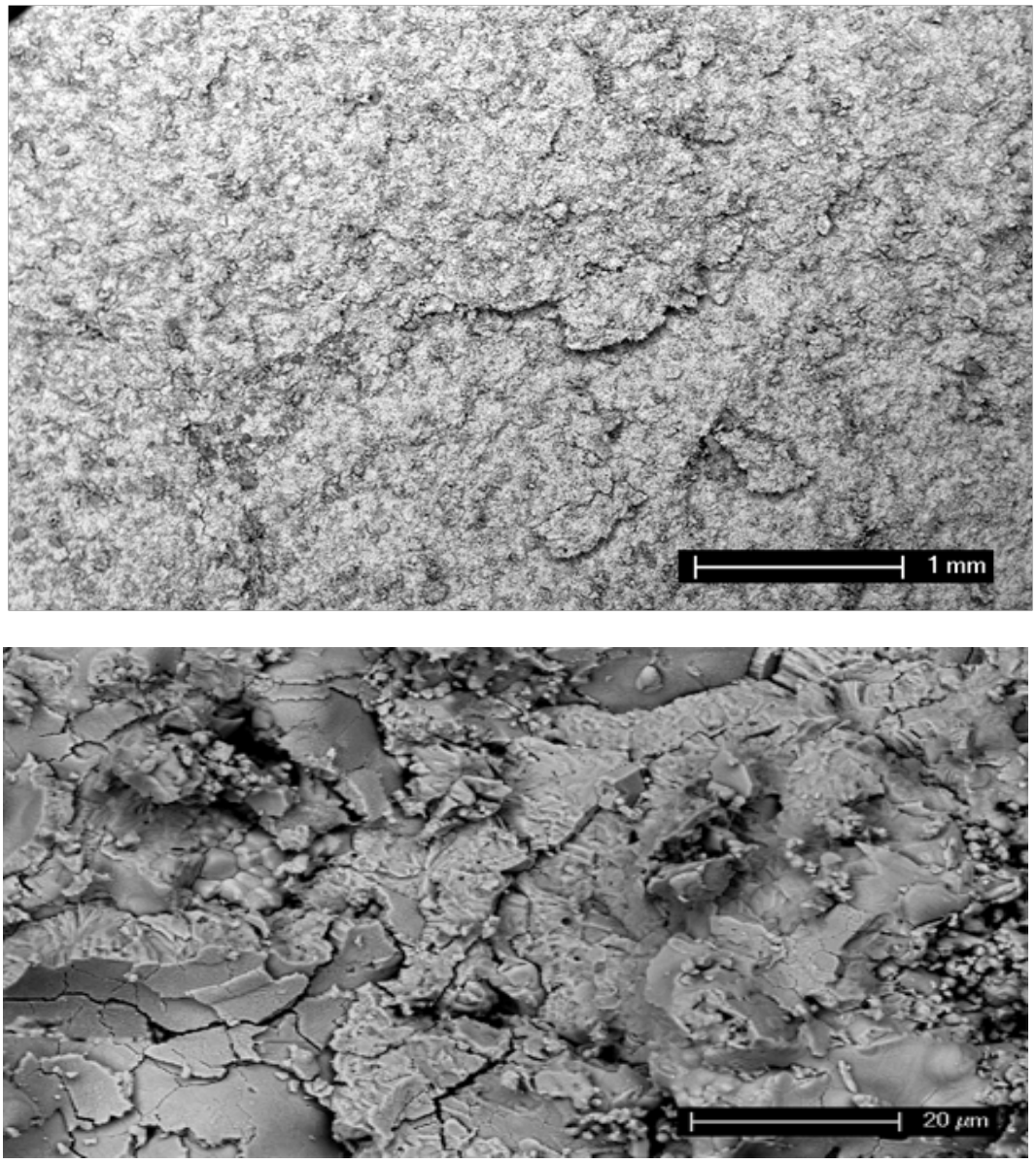

Figure 19 – Fracture surface (at low (top) and high (bottom) magnification) of a 45 mil TBC after failure in the 1100˚C FCT.

The dark black regions are the TGO and the lighter white regions are the YSZ topcoat. Upon analysis, the fracture surface of the thick 45 mil coating appeared to be comprised entirely of YSZ topcoat whereas the two thinner coatings both show more TGO at the fracture surface

along with regions of YSZ. The fracture in the YSZ propagated mainly by cracks along splat boundaries which linked up by propagation through dense YSZ. The cross-sections of the fractured specimens in Figure 20- 22 show the same trends observed on the fracture surfaces.

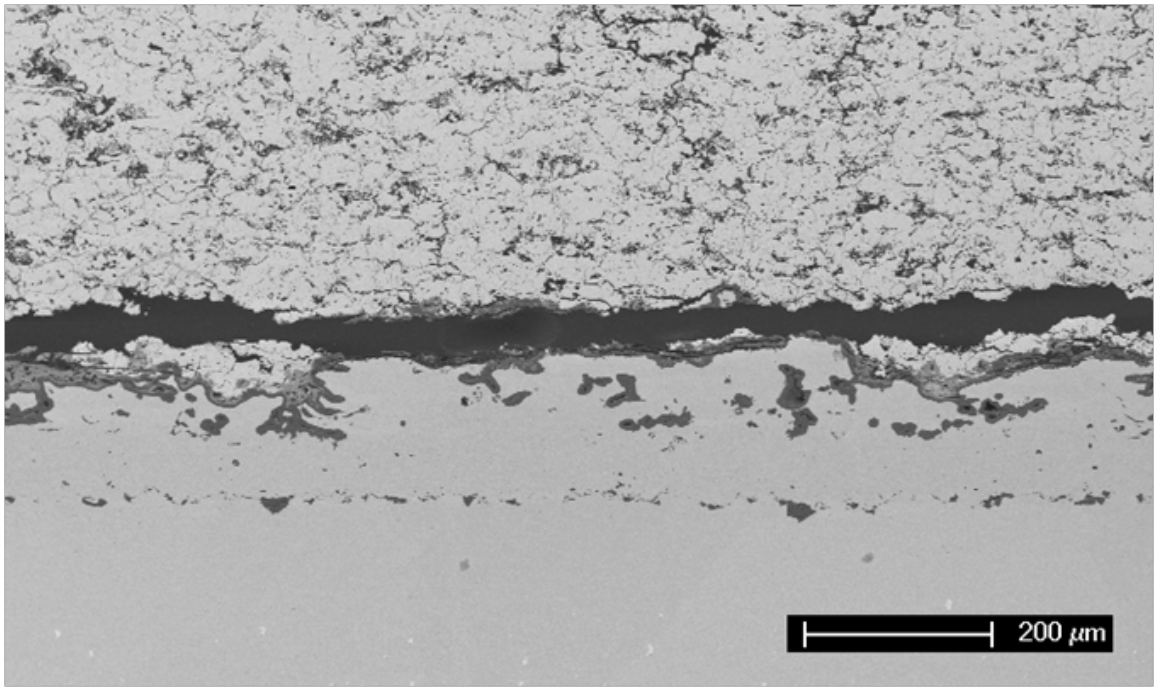

Figure 20 - Cross-section of 15 mil coating after failure.

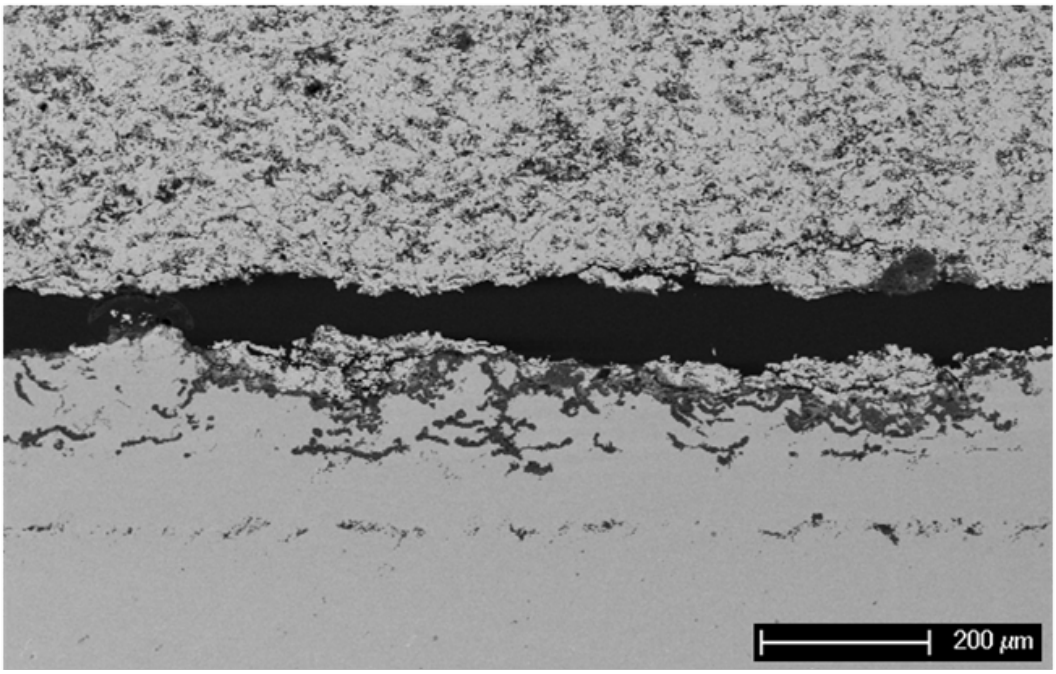

Figure 21 - Cross-section of 30 mil coating after failure.

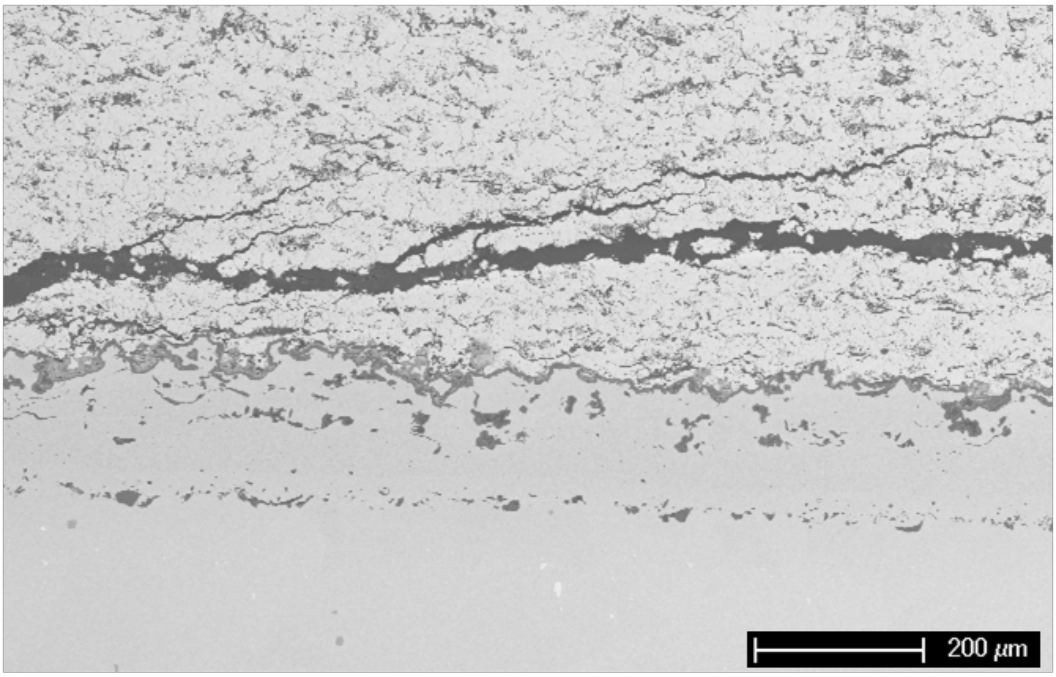

Figure 22 - Cross-section of 45 mil coating after failure.

From the cross-sections and fracture surface micrographs there appears to be two different fracture mechanisms occurring with these specimens. The first, fracture mechanism one, occurred with the thick 45mil TBCs. It is characterized by failure associated with cracking and spallation of the TBC well within the YSZ topcoat and away from the bond coat topcoat interface. Fracture mechanism one usually leads to failure after a relatively short number of cycles, so short that the effects of bond coat oxidation have not yet become important (20-40 cycles). Both Figure 19 and Figure 22 show that the fracture surface is entirely composed of YSZ.

Fracture mechanism two is associated with the thinner 30mil and 15mil TBCs. Here failure occurs at or very near the topcoat – TGO interface and it is associated with bond coat oxidation affects. This fracture mechanism occurs after an increased number of cycles (140-220) which allows for bond coat oxidation to occur.

Figure 23 shows extensive β-phase depletion in the bond coat as a result of TGO formation and interdiffusion with the substrate. Depending upon the porosity of the bond coat and composition of the substrate, the beta-phase can become completely depleted anywhere from 150 to 200 cycles based on the samples we have tested.

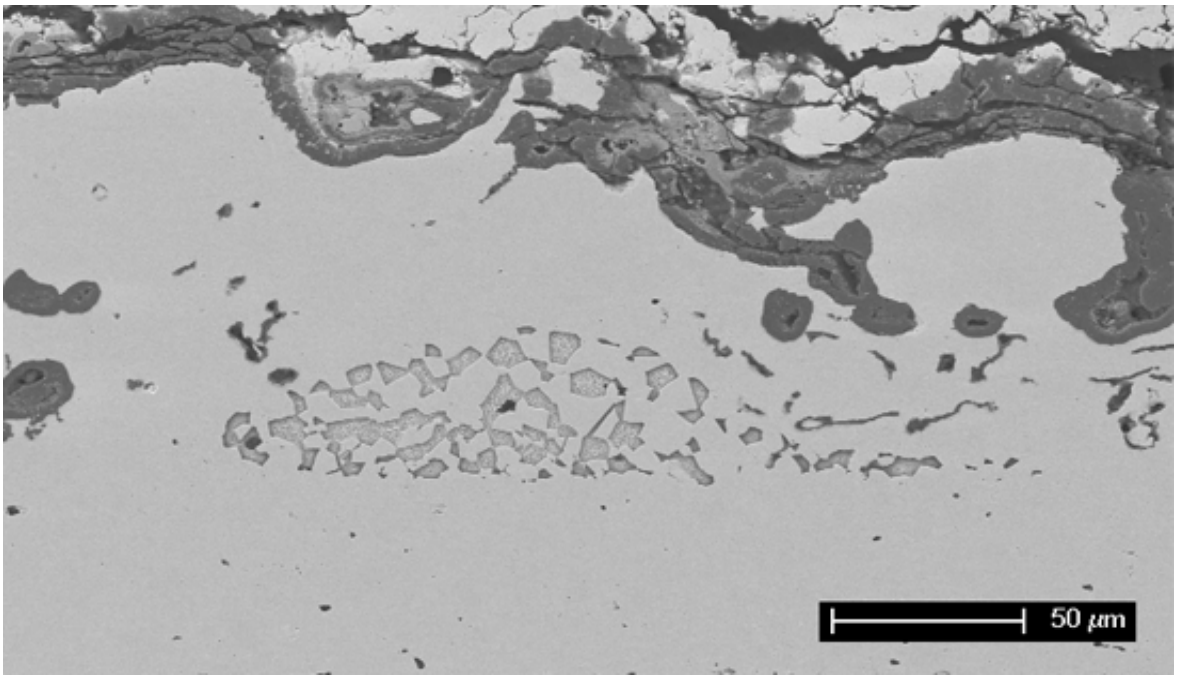

Figure 23 - Cross-section of 30 mil coating after failure (140 cycles) showing β-phase depletion from the BC.

Table 4 shows the numbers of cycles that were used for the interrupted lifetime tests and Figure 24-26 show cross-sections of the 30 mil specimen exposed for three different times (25%, 50%, and 75% of life, respectively).

Table 4 - Summary of specimens exposed to various fractions of life.

Percent Lifetime at 1100°C (5 Specimens Total)			
Thickness	**~25%**	**~50%**	**~75%**
15 mils of APS TBC	-	100	-
30 mils of APS TBC	40	80	120
45 mils of APS TBC	-	10	-

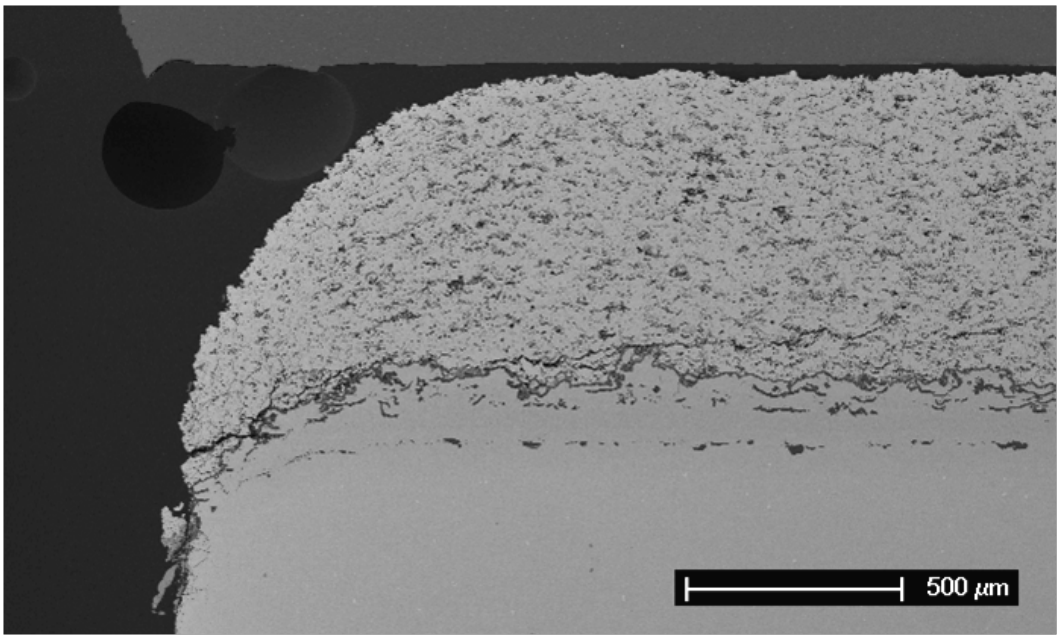

Figure 24 - Cross-section of 30 mil coating exposed to 25% of lifetime (40 cycles).

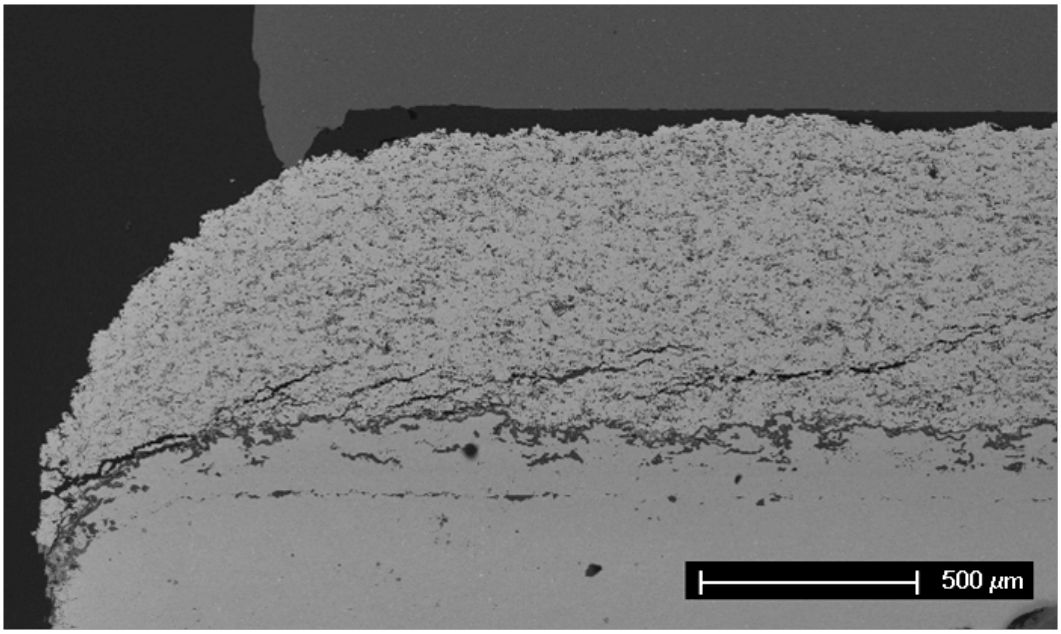

Figure 25 - Cross-section of 30 mil coating exposed to 50% of lifetime (80 cycles).

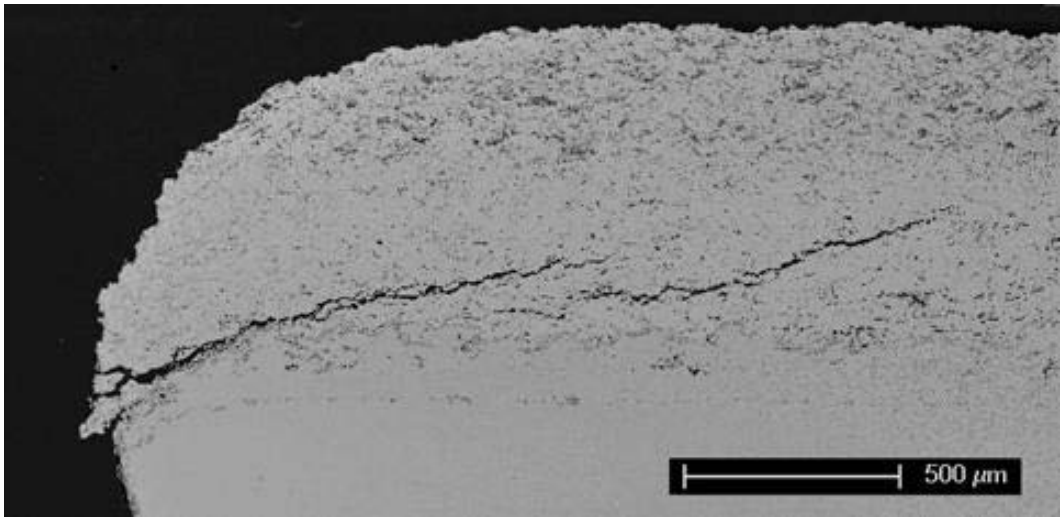

Figure 26 - Cross-section of 30 mil coating exposed to 75% of lifetime (120 cycles).

These micrographs reveal that, as exposure time increases, the amount of edge cracking also increases. However, these cracks did not cause failure in the 30 mil specimens. This is supported by reexamining the 30mil cross sections. Looking at the completely failed 30mil TBCs in Figure 18 and Figure 21, failure occurred near the TGO-topcoat interface. Whereas, the edge cracks seen in the Figure 24 -26 are above and run at angles non-parallel to this interface. If these cracks were to have been the cause of failure, it might be expected that only portions or chips of the topcoat would come off, however the experimental results show complete topcoat spallation. This edge cracking trend was also apparent in the 15 and 45 mil specimens as seem in Figure 27 and Figure 28.

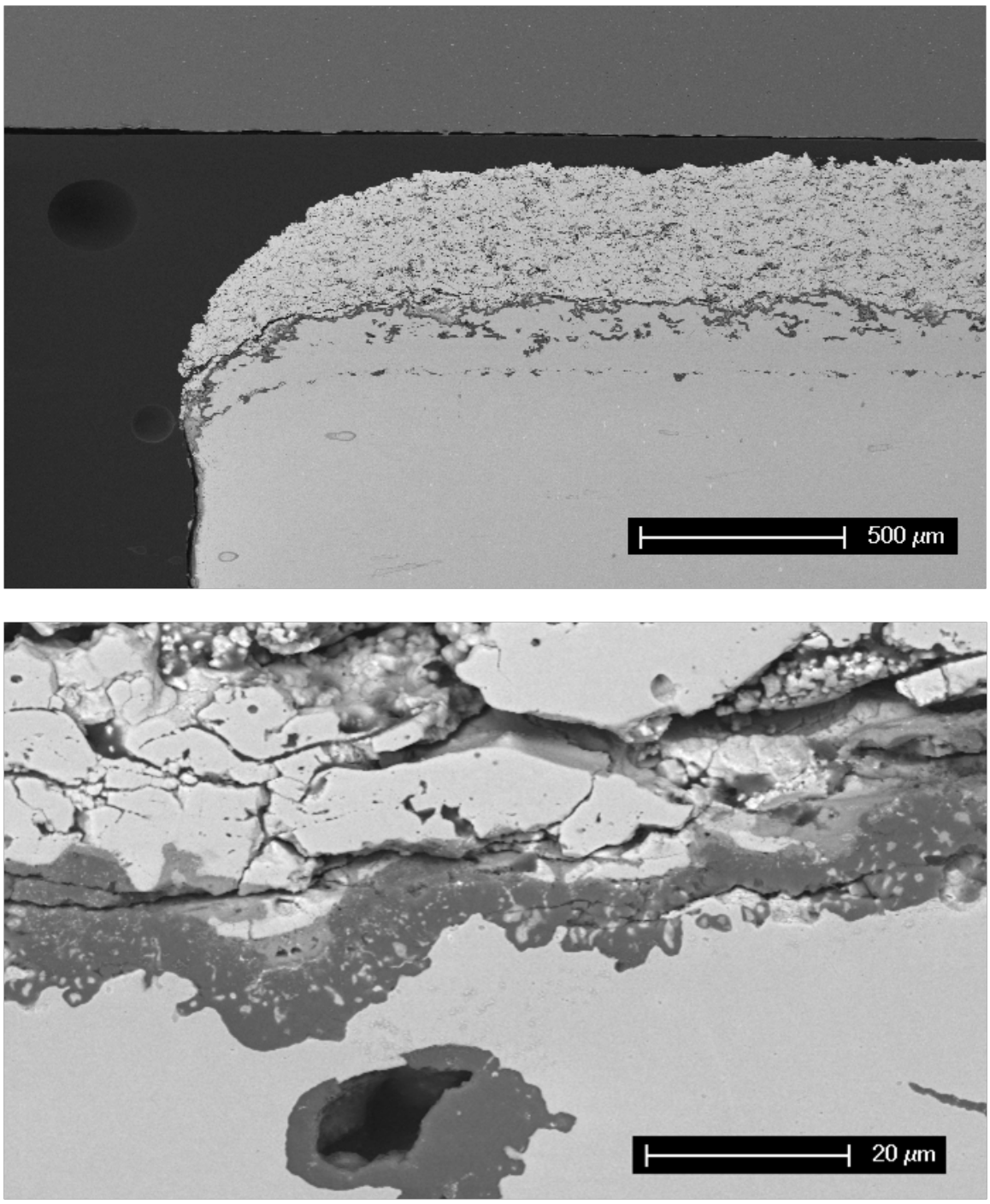

Figure 27 - Cross-section of 15 mil coating exposed to 50% of lifetime (100 cycles).

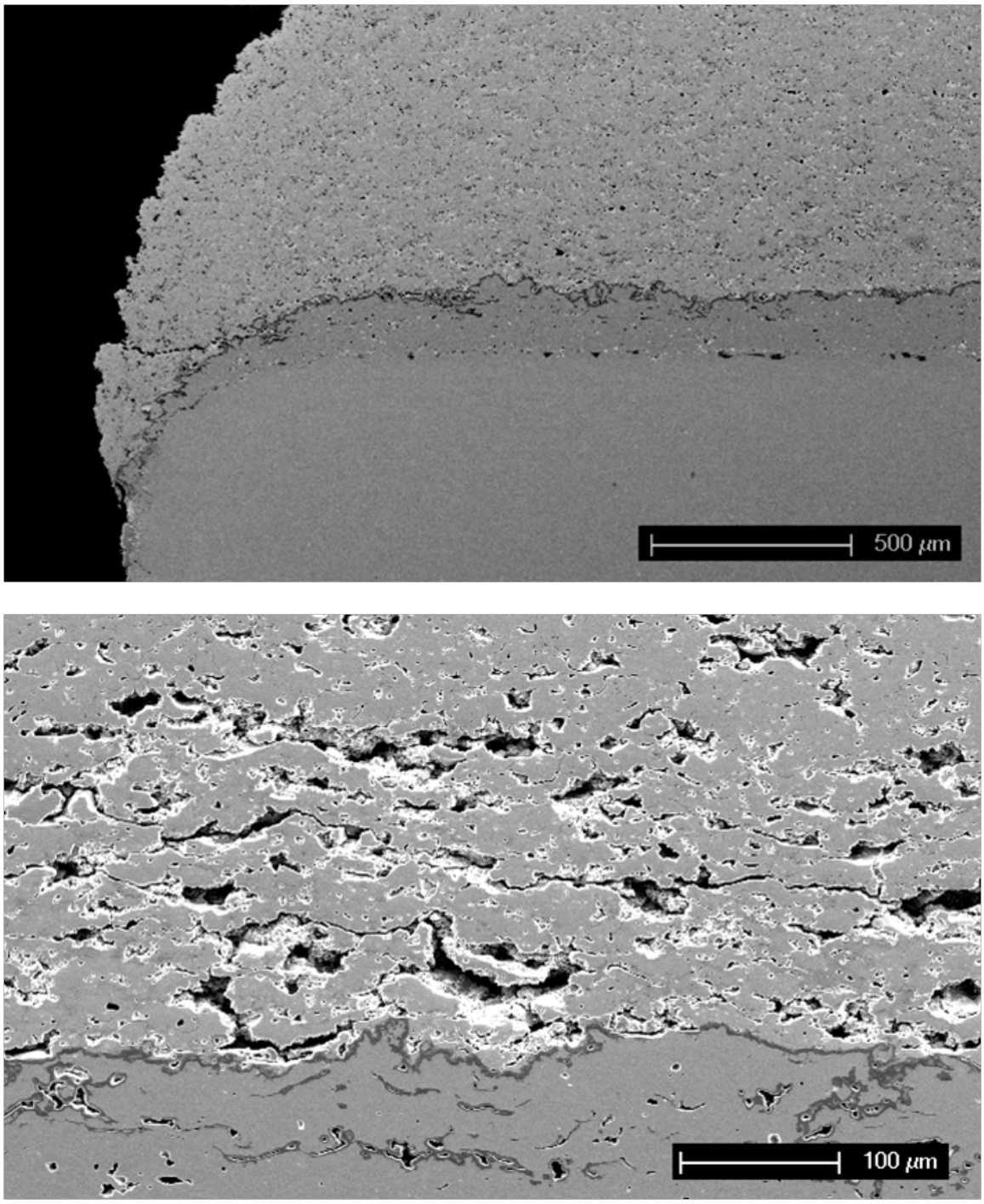

Figure 28 - Cross-section of 45 mil coating exposed to 50% of lifetime (10 cycles).

The data in Table 3 may be compared with failure times for EBPVD TBCs exposed under identical FCT conditions [7]. A 100μm (4 mil) thick EBPVD TBC on the same composition bond coat with a grit blast surface (R_a=5-10μm) fails in approximately 100 cycles. Therefore, the low density APS-TBCs in the current study have comparable lives (≈150 cycles) at a topcoat thickness of 750μm and longer lives (≈210 cycles) at a thickness of 375μm compared to the much thinner EBPVD coating. It should be noted that optimizing the bond coat surface finish for the EBPVD coating by polishing to R_a=0.3μm increases the average life to approximately 1000 cycles [7].

4.1.3.2 JETS Testing

During the JETS testing, surface temperature readings were taken during one complete cycle. The typical time dependent thermal profile of the top surface during one cycle for the 30 mil specimen is depicted in Figure 29.

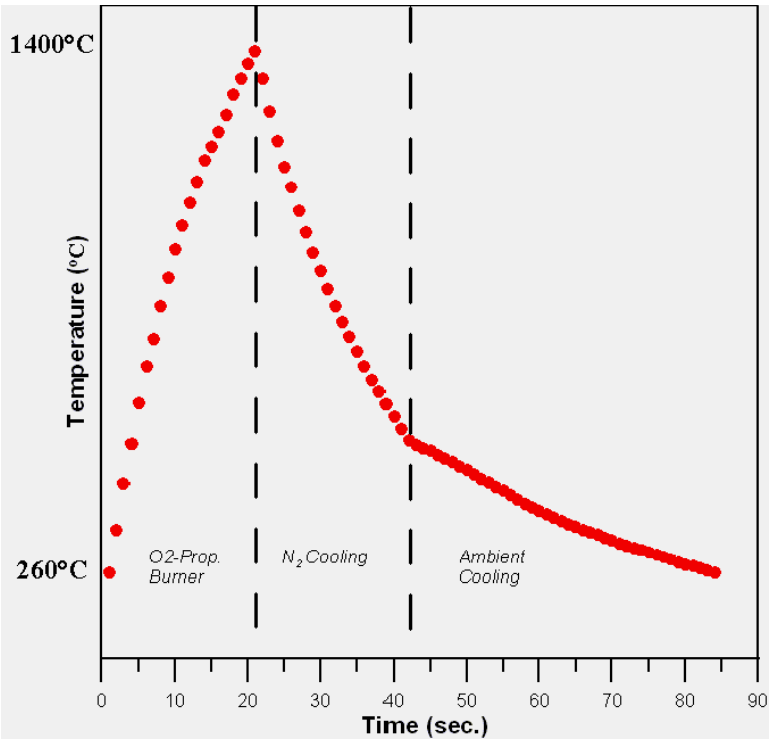

Figure 29 - JETS testing time dependent thermal profile for typical sample.

Also during the testing, the maximum front YSZ and back alloy substrate surface temperatures were recorded at the end of the 20 second heating period for the three different thickness topcoats which can be seen in Figure 30a. The increased YSZ surface temperature as the coating thickness increases is caused by the increased distance in the YSZ through which the heat must be conducted in order to reach the substrate, where it is conducted away more rapidly.

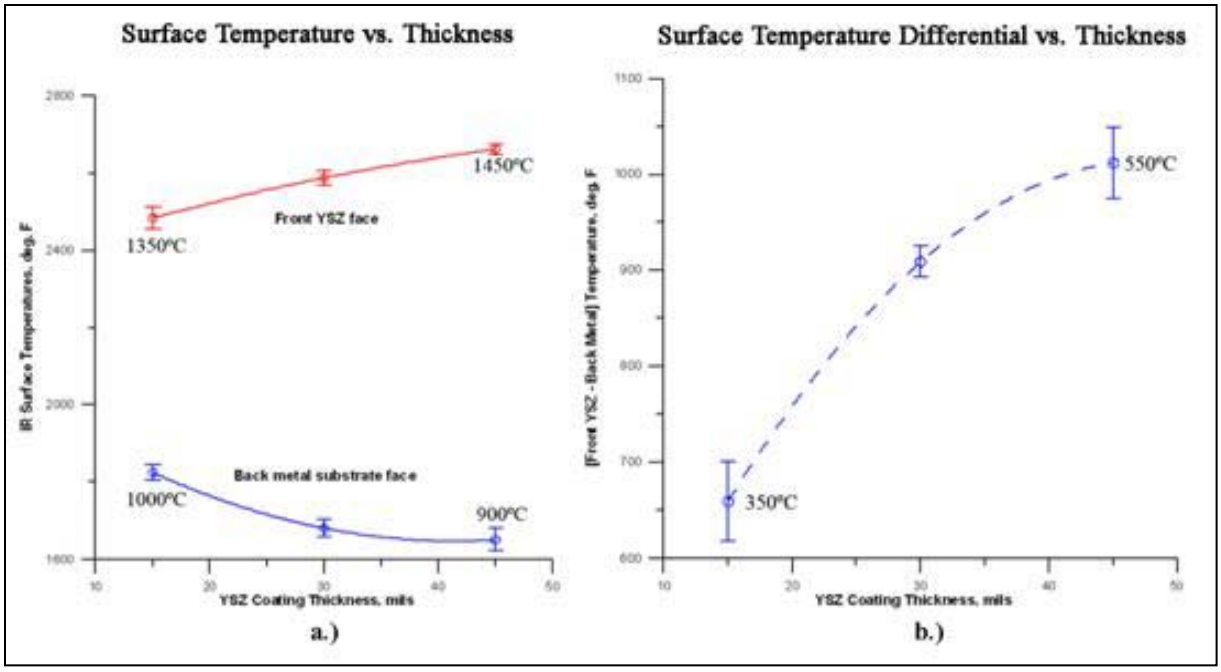

Figure 30 - Temperature plots from JETS testing: a.) average temperatures at the front and back surfaces of the JETS buttons after a 20 second heating stage, b.) average temperature difference across the JETS buttons as a function of topcoat thickness.

Figure 30b is a plot of the temperature difference between the front and back face of the buttons as a function of YSZ coating thickness. This plot shows that the thicker coatings provide increased thermal protection.

In JETS testing, two observations were made relative to the failure process. After the full test, the outside edges of the specimens were examined with a 30X microscope, measuring and summing up any separation cracks between the YSZ and the bond coat. The total length of the cracks was divided by the specimen circumference and expressed as a percent. The YSZ layer was usually fully intact and still bonded to the specimen. In some cases, the YSZ layer had spalled off in sections or as a complete disk. Separation cracks between the YSZ and bond coat

could also initiate and grow within the central section of the button's area during the test. This can be observed from the full 2000 cycle plot of the front (YSZ surface) and back (metal substrate) temperatures in Figure 31.

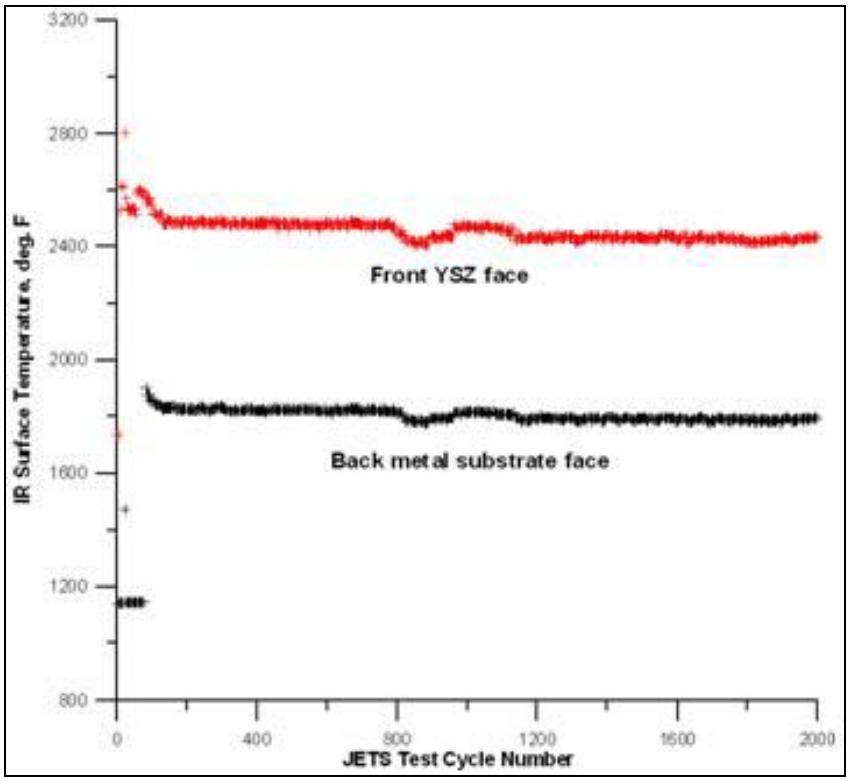

Figure 31 - Front and back face temperature shown for a 15mil TBC on IN718 substrate

When an internal separation occurs, the temperature diverges more than the difference produced simply by the low thermal conductivity of the YSZ. Internal separation cracks cause gaps in the YSZ that produce step changes in the two temperatures if the crack occurs suddenly.

This internal failure time can be pinpointed to within a few test cycles. When complete spallation occurs, the front and back temperatures become equal. The edge cracking observed for the phase I specimens during the JETS tests are summarized in Table 5.

Table 5 - Summary of JETS failures.

JETS Testing Results (6 Specimens Total)		
	Percent Failure	
	Specimen 1	**Specimen 2**
15 mils of APS TBC	0	4
30 mils of APS TBC	71	88
45 mils of APS TBC	100	100

These results are plotted in Figure 32 as a function of the YSZ thickness. The shape of the fit line and the data points indicates that the amount of failure within the specimens steadily increases as coating thickness increases.

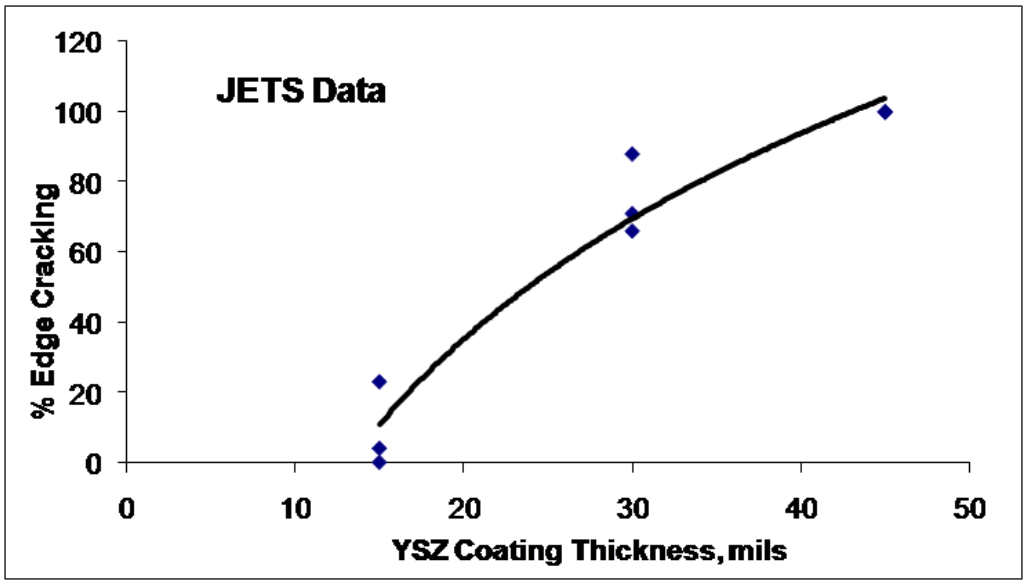

Figure 32 - Percent edge cracking after 2000 cycles in the JETS test.

The 45mil specimens failed by the spallation of portions of the YSZ topcoat which left a dimpled morphology at the fracture surface as seen in Figure 33.

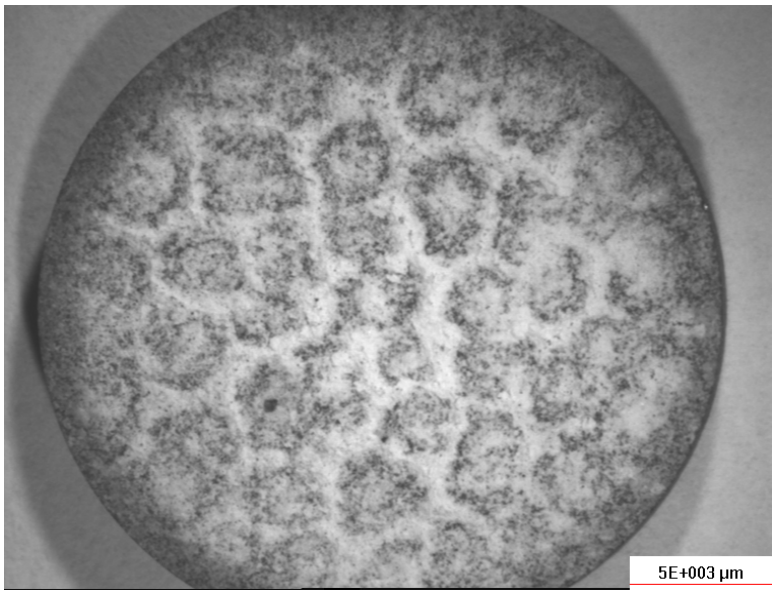

Figure 33 - Fracture surface of 45mil JETS tested specimen.

Still more information is gained by closely examining Figure 33. The darker rim around the edge of the button shows the edge crack fully surrounding the button early in the test. The dark tint is caused by carbon deposited by the impinging flame, which has decorated the extent of the inward growth of the edge crack. The inward growth varied from about 1000 to 3000μm at different locations around the circumference. Finally the YSZ layer completely spalled near the end of the test on final cool-down, since no carbon deposit is seen in the central area of the button.

Each of the two 45 mil specimens examined contained roughly 40 dimples each. The individual dimples had a raised outer YSZ edge, a flat YSZ/TGO inner ring, and occasionally a raised center YSZ peak as seen in Figure 34.

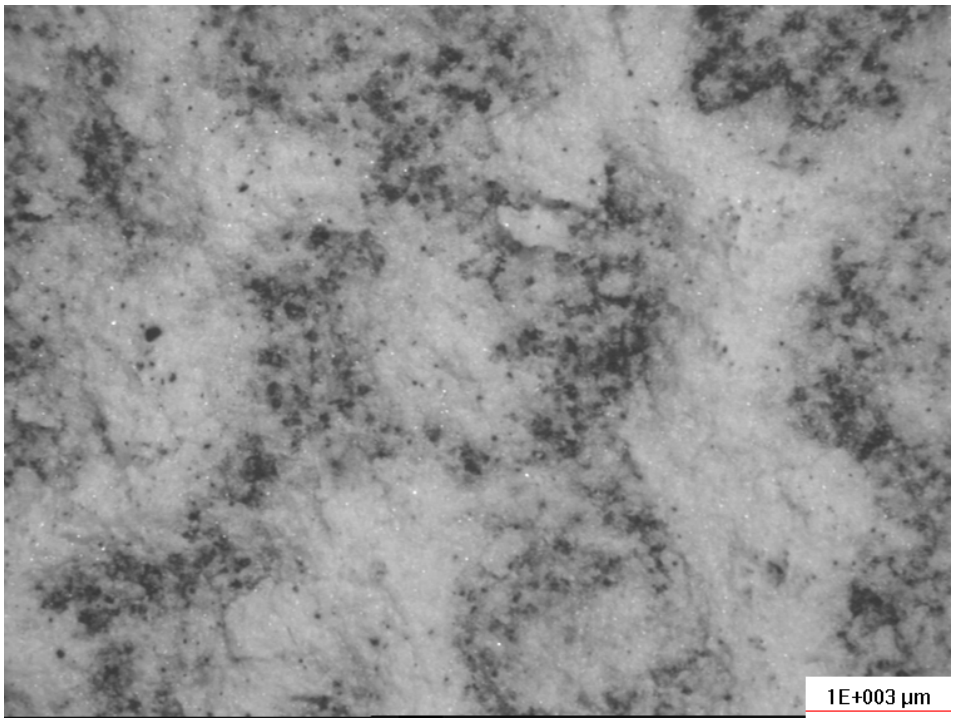

Figure 34 - Structure of a dimple on the 45mil fracture surface. Raised outer ring with lower flat internal ring and a raised center peak.

The average diameter of the dimples was 3.3mm with a standard deviation of 0.5mm. Given this statistic, the average number of dimples across the diameter of a single button is approximately 7-8 dimples. SEM analysis of the fracture surface revealed that fracture occurred mostly within the YSZ topcoat because there was relatively little TGO at the fracture surface. This can be observed in the backscattered micrograph in Figure 35. The fracture path appeared to be mixed between intersplat fracture and intrasplat fracture as seen in Figure 36.

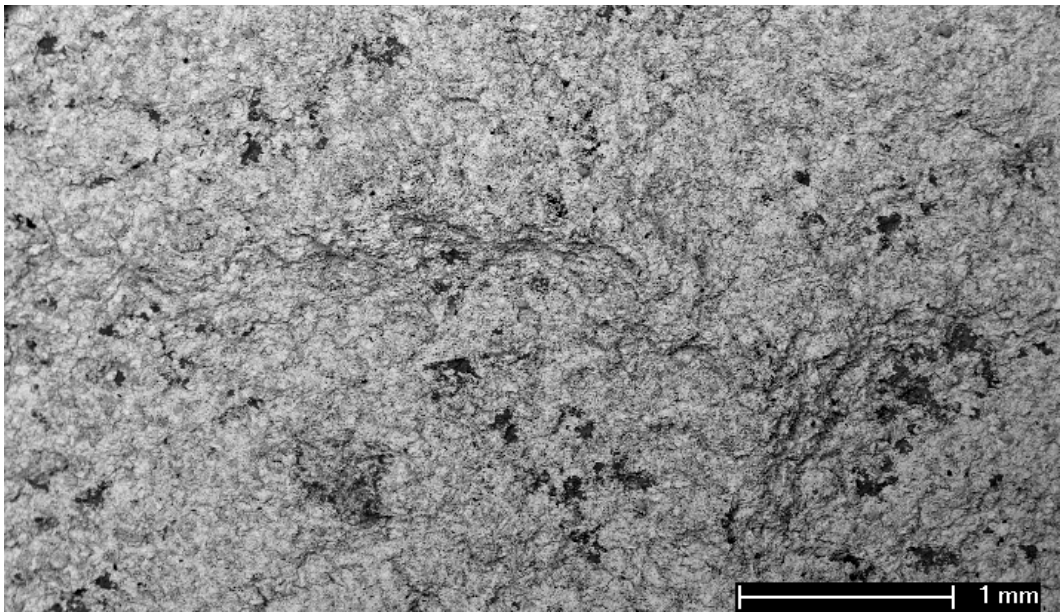

Figure 35 - Fracture surface of the 45miml JETS sample. White is YSZ topcoat and dark regions are TGO.

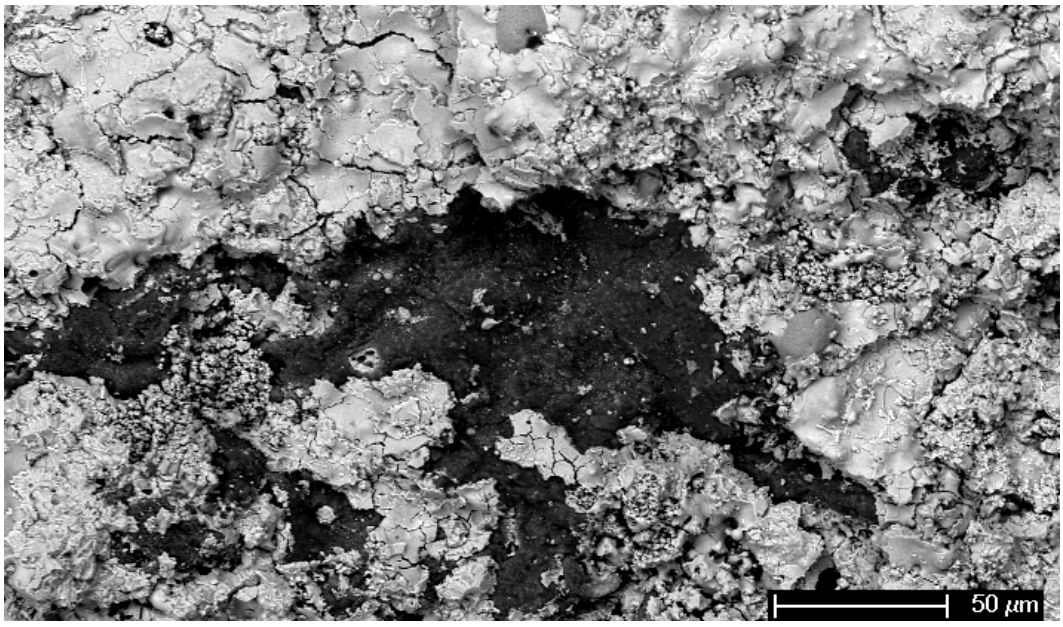

Figure 36 - Fracture surface of 45mil JETS Sample. Dark region is TGO and White is YSZ.

Surface analysis of the 15 mil and 30 mil specimens revealed little information other than the observation that the topcoats remained completely intact. The only notable observation was that the 30 mil specimens had some visible surface cracking near the edges of the button.

A cross-section of the 45 mil specimen again showed that the surface was primarily covered with YSZ topcoat. The thickness of this remaining layer was approximately 40-50μm (Figure 37) on average but there were isolated regions of exposed TGO (Figure 38) and others with a YSZ thickness up to 150 μm (Figure 39). The thick regions depict the elevated edges of the dimples found on the fracture surface (Figure 34).

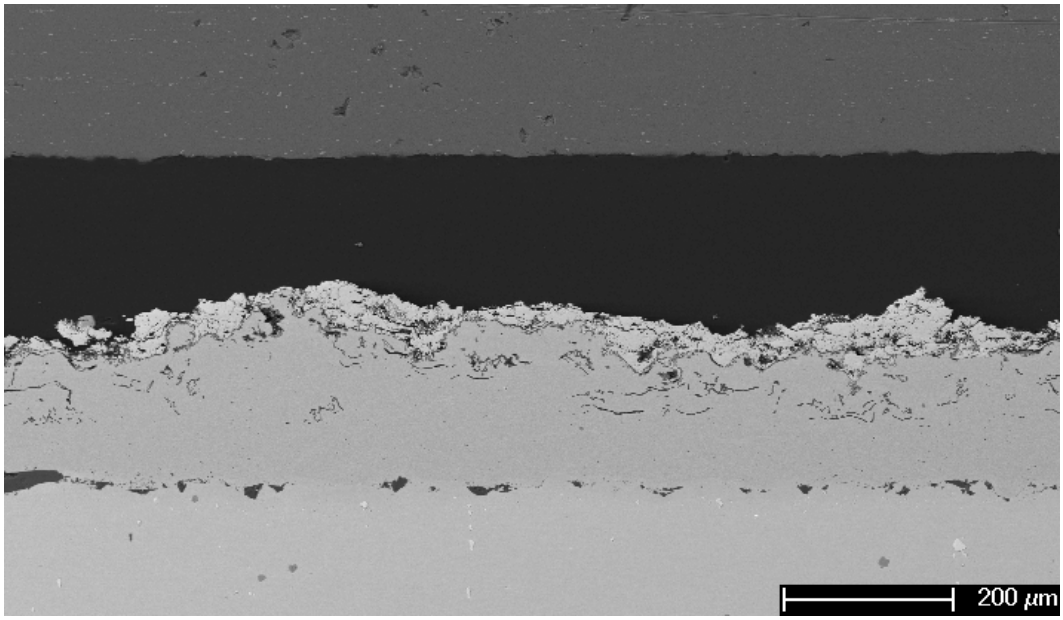

Figure 37 - Typical amount of YSZ covering the fracture surface of the 45mil JETS sample.

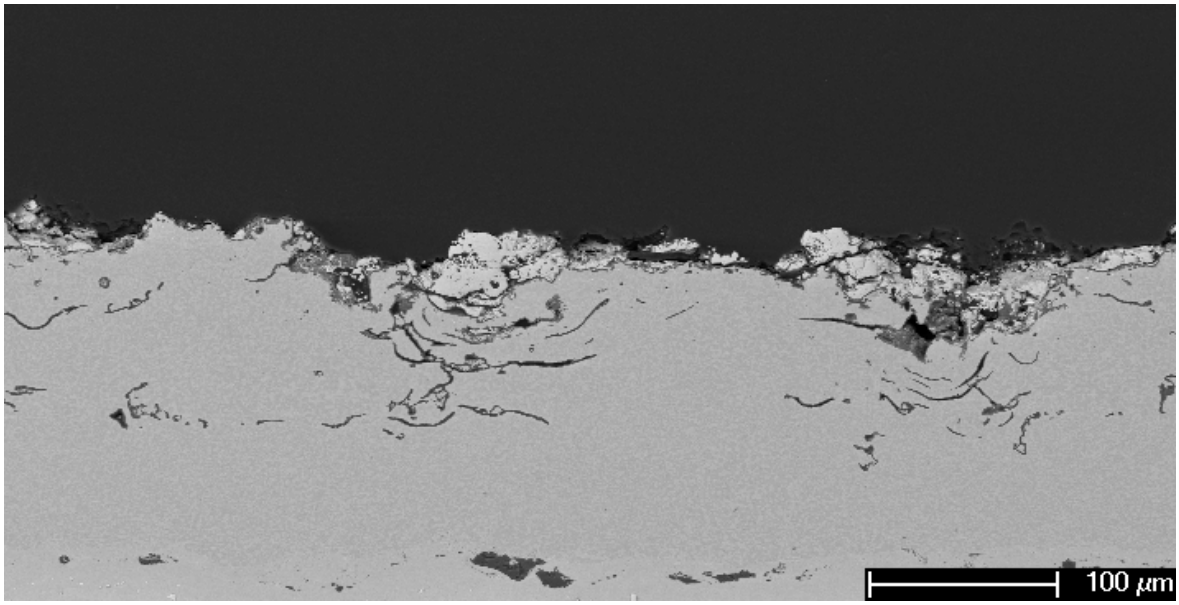

Figure 38 - Area of exposed TGO on the 45mil fracture surface.

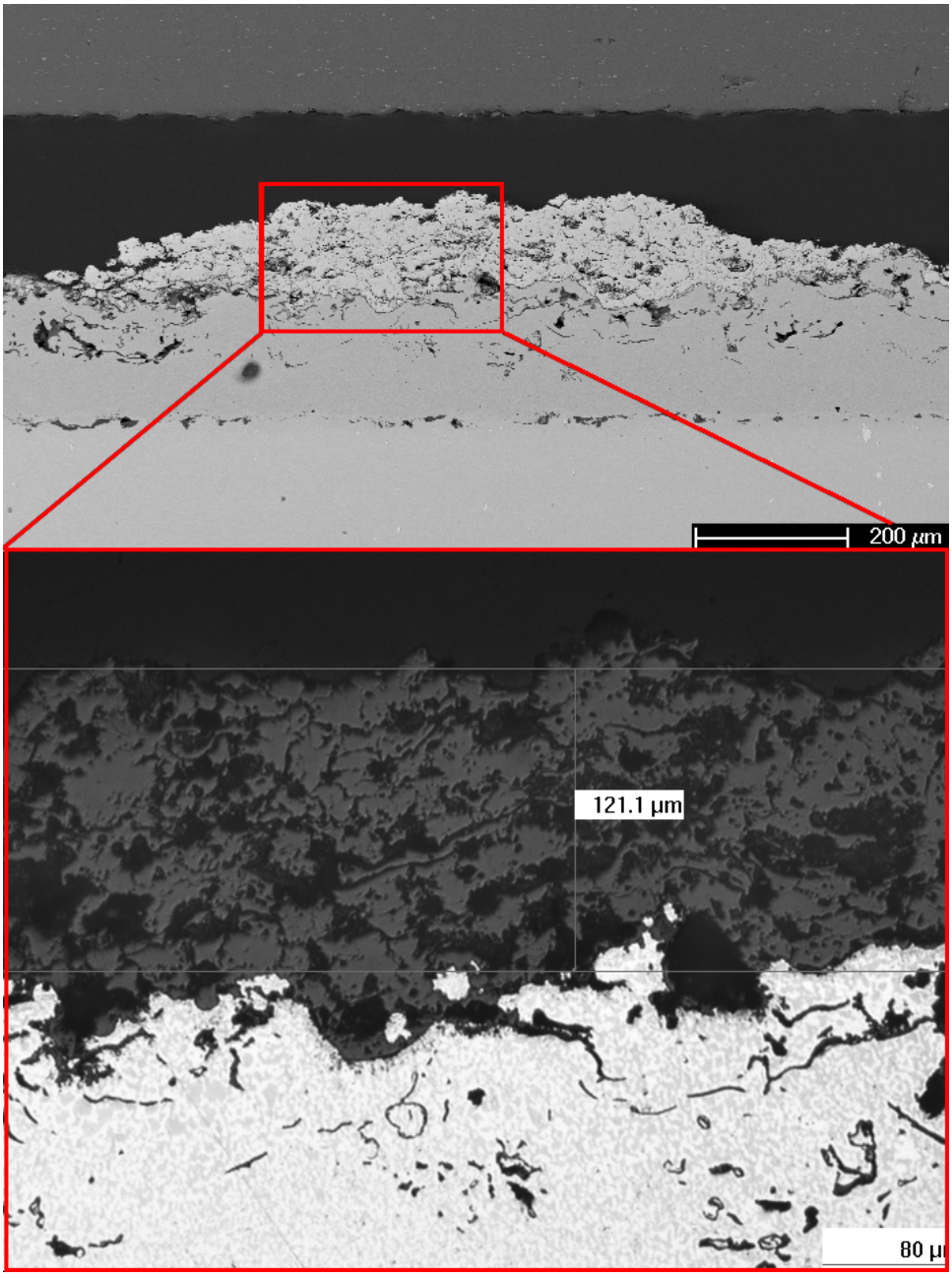

Figure 39 - Micrograph of the remaining YSZ on the 45mil JETS sample. The maximum thickness of this region was approx 120µm.

Cross-sections of the 30 mil specimen showed both horizontal and vertical cracking in the topcoat. The horizontal cracks were found connected to the edges and also found isolated in

the bulk of the specimen. They were located both at the bond coat interface and above the bond coat interface; however, a majority of the cracking was in the region above the interface. The vertical cracks, which are defined as cracks which extend from the surface of the topcoat down to the bond coat interface (or within 100-150µm), were located in the interior of the specimen and primarily positioned above horizontal cracks. Examples of the mentioned observations are presented in Figure 40 - 43.

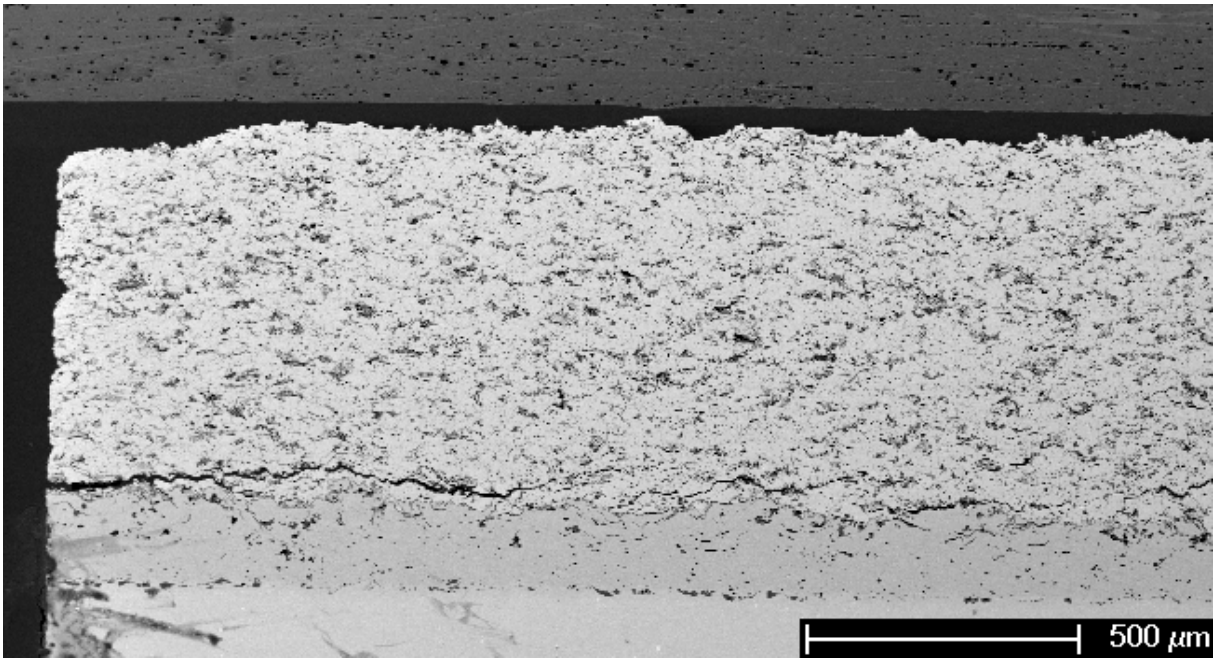

Figure 40 - Edge crack found in the 30mil sample.

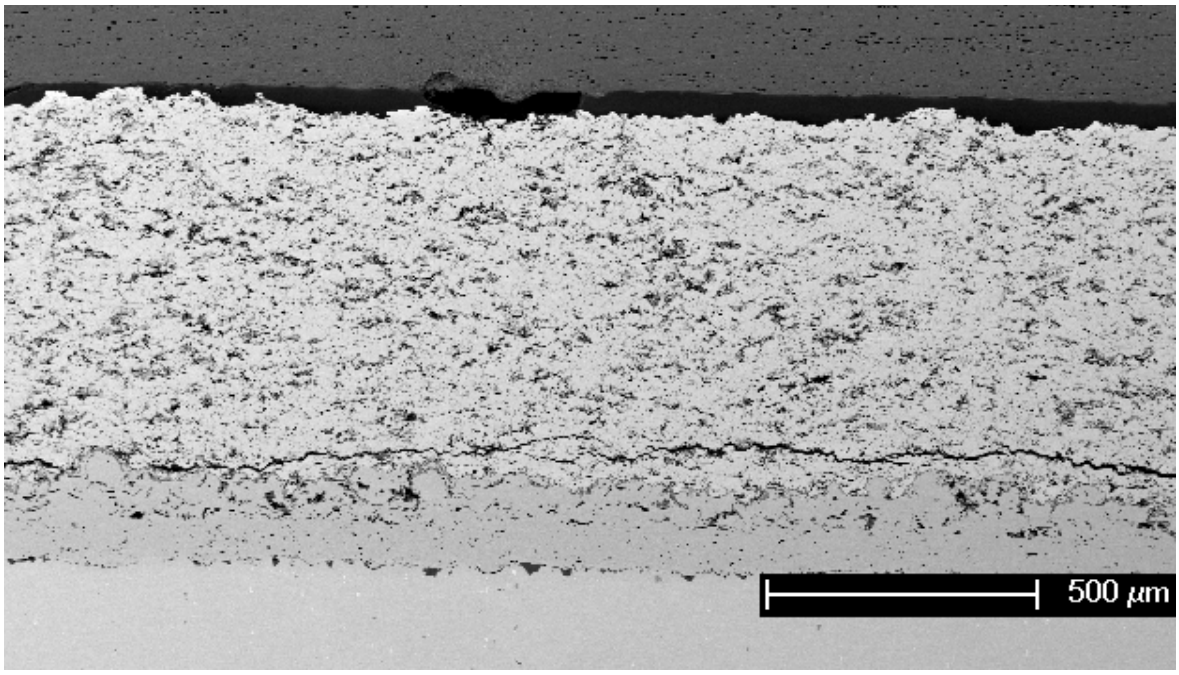

Figure 41 - Internal horizontal crack in 30mil sample.

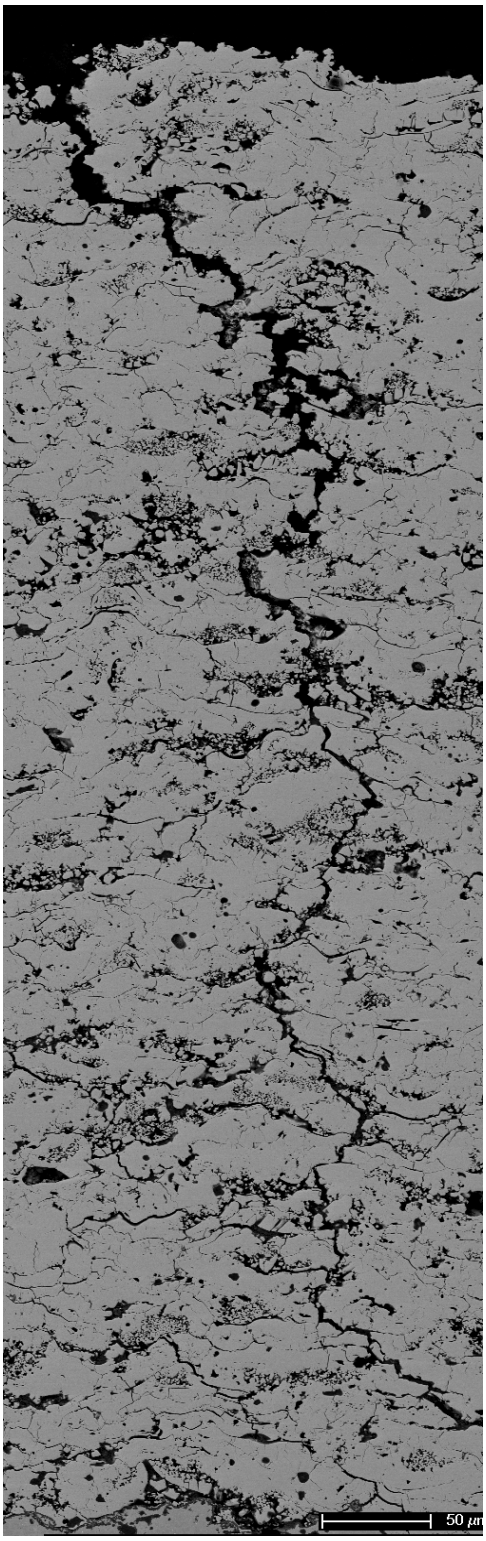

Figure 42 - Vertical crack found in 30 mil sample.

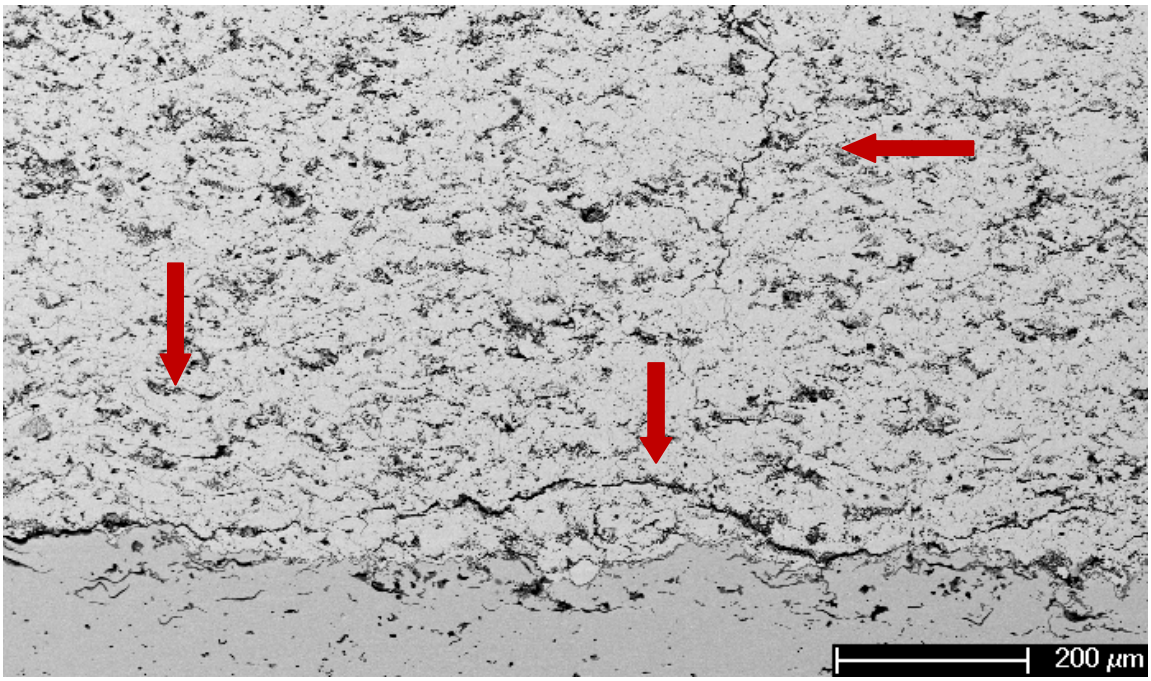

Figure 43 - Vertical crack in 30mil sample located above a horizontal crack. Also note the cracking occurring both above and at the bond coat interface.

Within the cross-section of the 30 mil specimen, there was a total of 8 vertical cracks that were found. As mentioned above, most of the vertical cracks appeared to be linking up with horizontal cracks located lower in the topcoat near the bond coat interface. Some of these crack intersections appeared to be perpendicular in nature, where the vertical crack and the horizontal crack intersect at a right angle, as seen in Figure 44. However, a majority of the cracks appeared to be intersecting at varying angles and directions as seen in Figure 45.

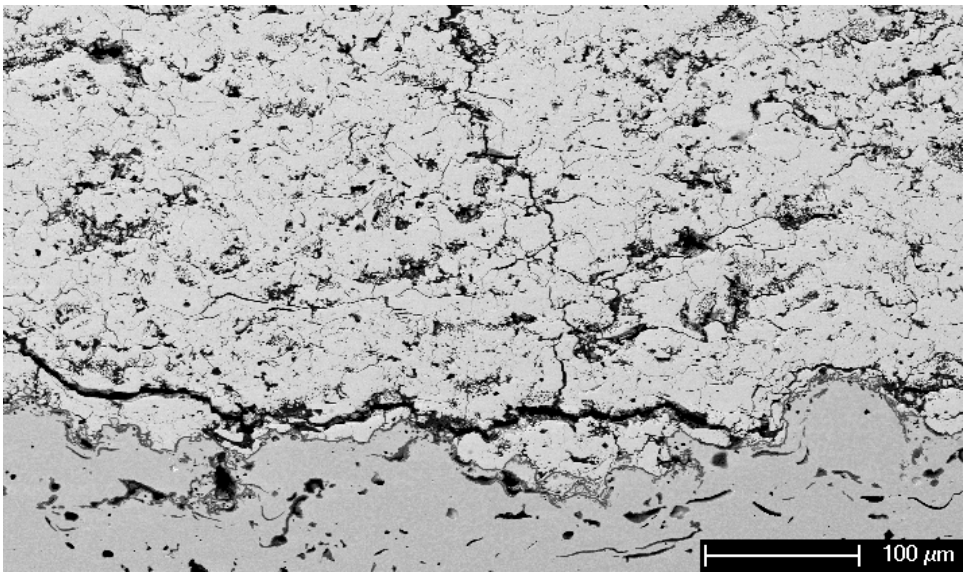

Figure 44 - Perpendicular intersection of a horizontal and vertical crack.

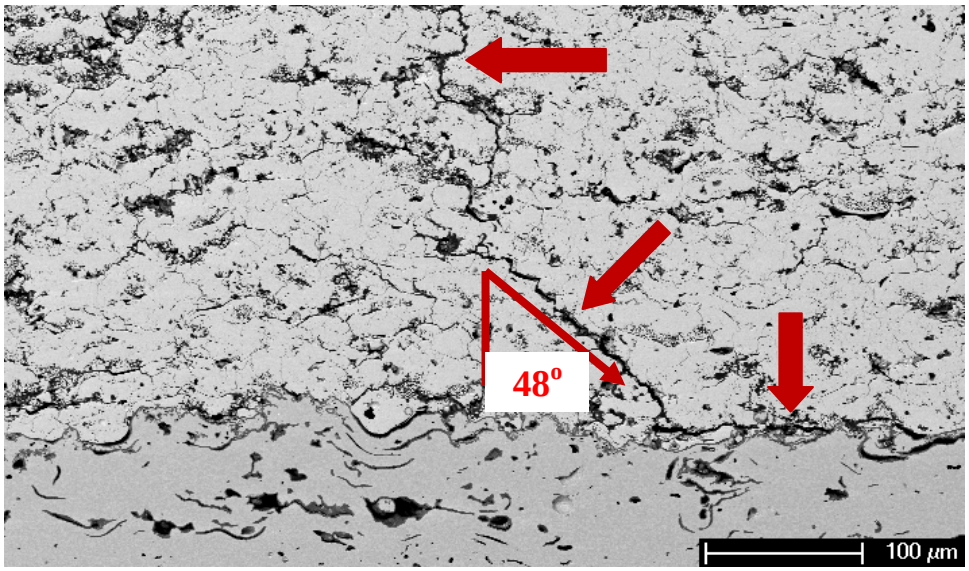

Figure 45 - Horizontal crack linking up with a vertical crack at a 48 degree angle in 30mil sample.

Here, the vertical crack extends from the surface and at a distance of 100μm from the bond coat interface it deflects at a 48 degree angle from the normal and then intersects with a horizontal crack that runs parallel to the interface. Considering this cracking behavior, it seems that if the 30 mil specimen would have been cycled in the JETS test setup until failure, the fracture surface might resemble that of the 45-mil specimen which had the cellular failure structure.

Analysis of the 15 mil cross-section revealed few horizontal cracks in the microstructure and no observable vertical cracks of any sort. The horizontal cracking was primarily edge related with isolated regions within the bulk of the specimen where small cracks were found. These two structures are seen in Figure 46 and Figure 47, respectively.

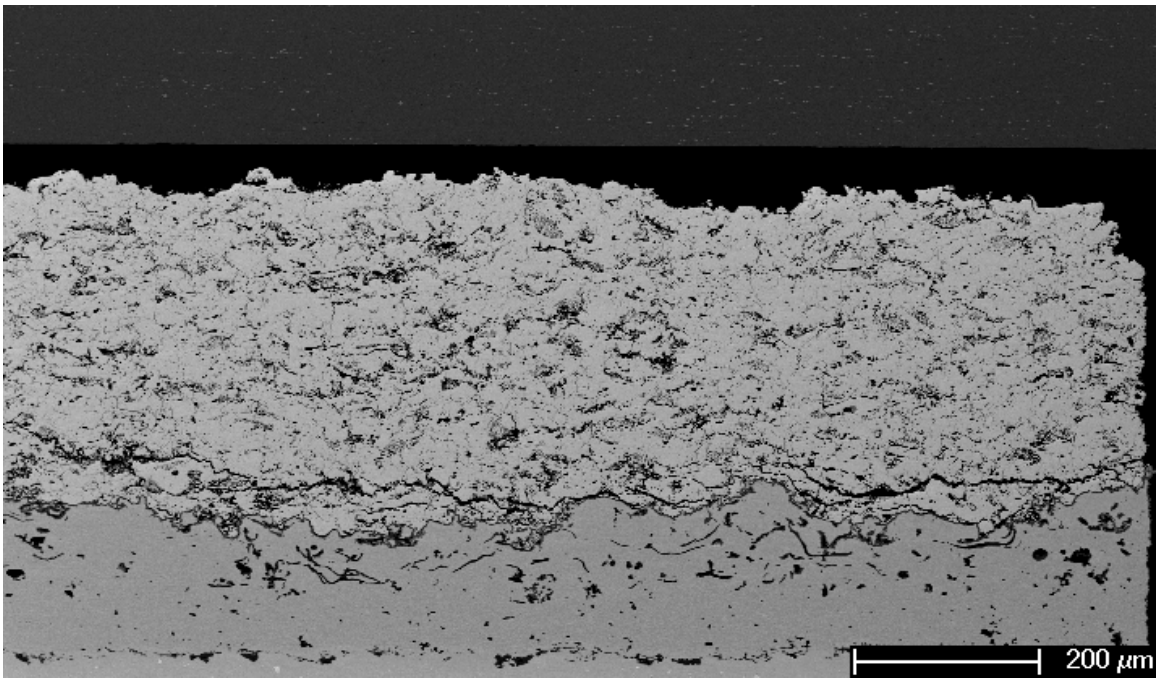

Figure 46 – Edge associated cracking in the 15mil sample.

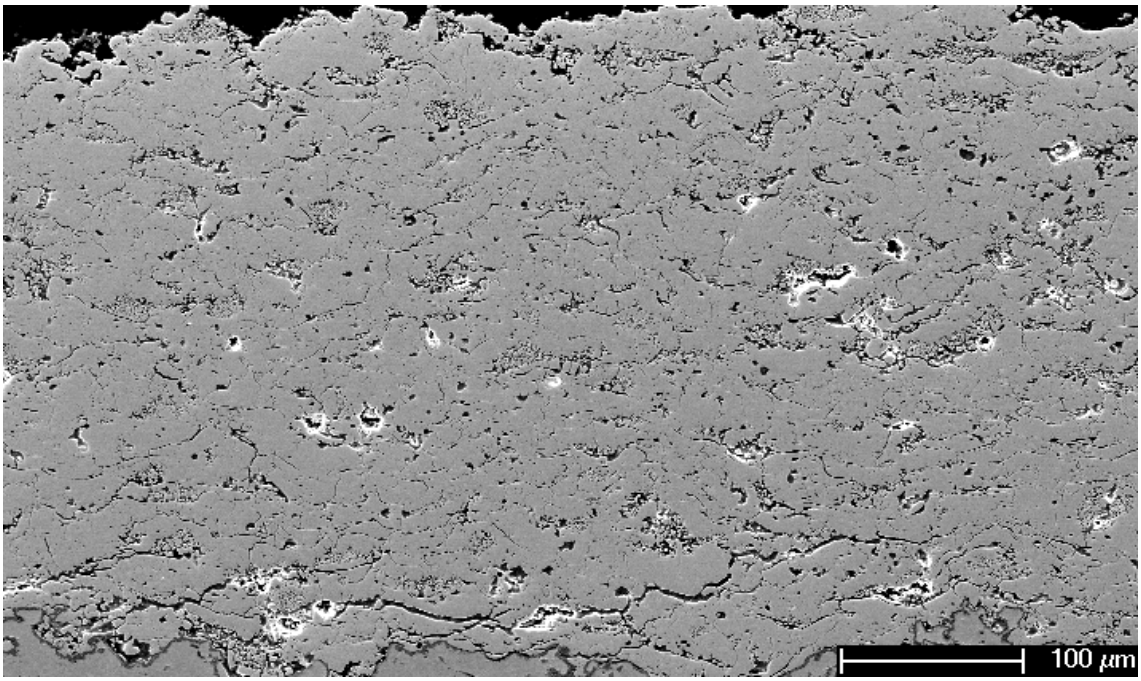

Figure 47 - Internal crack that formed within the 15mil sample during JETS testing.

All three JETS specimens had consistently uniform thermally grown oxides (TGO) along their cross sections with regard to thickness. Also, all three had localized regions where the TGO was excessively thick, which could be due to bond coat curvature or defect concentration resulting in increased influx of oxygen ions through the TGO.

TGO measurements were made using the following procedure. First the specimens were cross-sectioned, polished and then micrographs were taken of the TGO at high magnification (~6400X) with an SEM. For each specimen, five micrographs were taken from different areas along the cross-section of the specimen. These images were then carefully analyzed to compute an average thickness for each individual micrograph. Finally, using these five mean values, a

final average TGO thickness was calculated for each specimen. The results are listed in Table 6 and Figure 48 shows a normal distribution plot of these data. Also, Figure 49 presents a comparison of TGO micrographs taken of each specimen.

Table 6 - JETS and FCT TGO thickness measurements

Average TGO Thickness						
Sample	**TBC**	**Hot Time (hr)**	**TGO Thickness (µm)**	**Std Dev. (µm)**	**Max (µm)**	**Min(µm)**
FCT 10cyc	45mil	7.5	2.96	0.51	3.6	2.4
FCT 20cyc	45mil	15	3.68	0.33	4	3.2
JETS 2000cyc	45mil	11.1	0.83	0.16	1	0.6
JETS 2000cyc	30mil	11.1	1.09	0.23	1.4	0.8
JETS 2000cyc	15mil	11.1	1.8	0.33	2.2	1.4

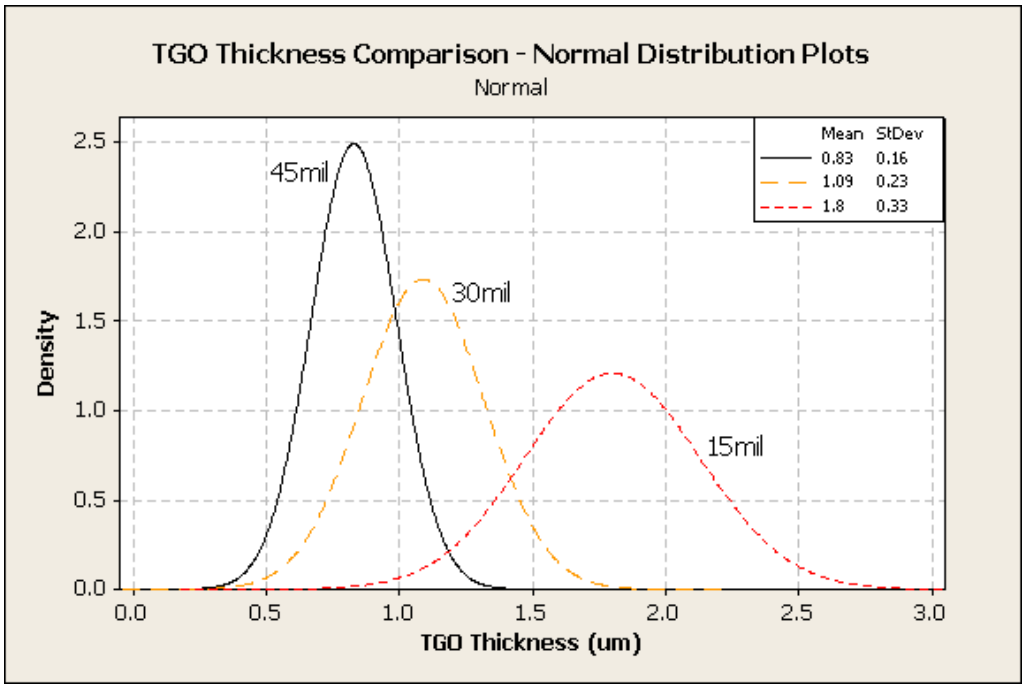

Figure 48- Normal Distribution plot of the TGO Thickness Data.

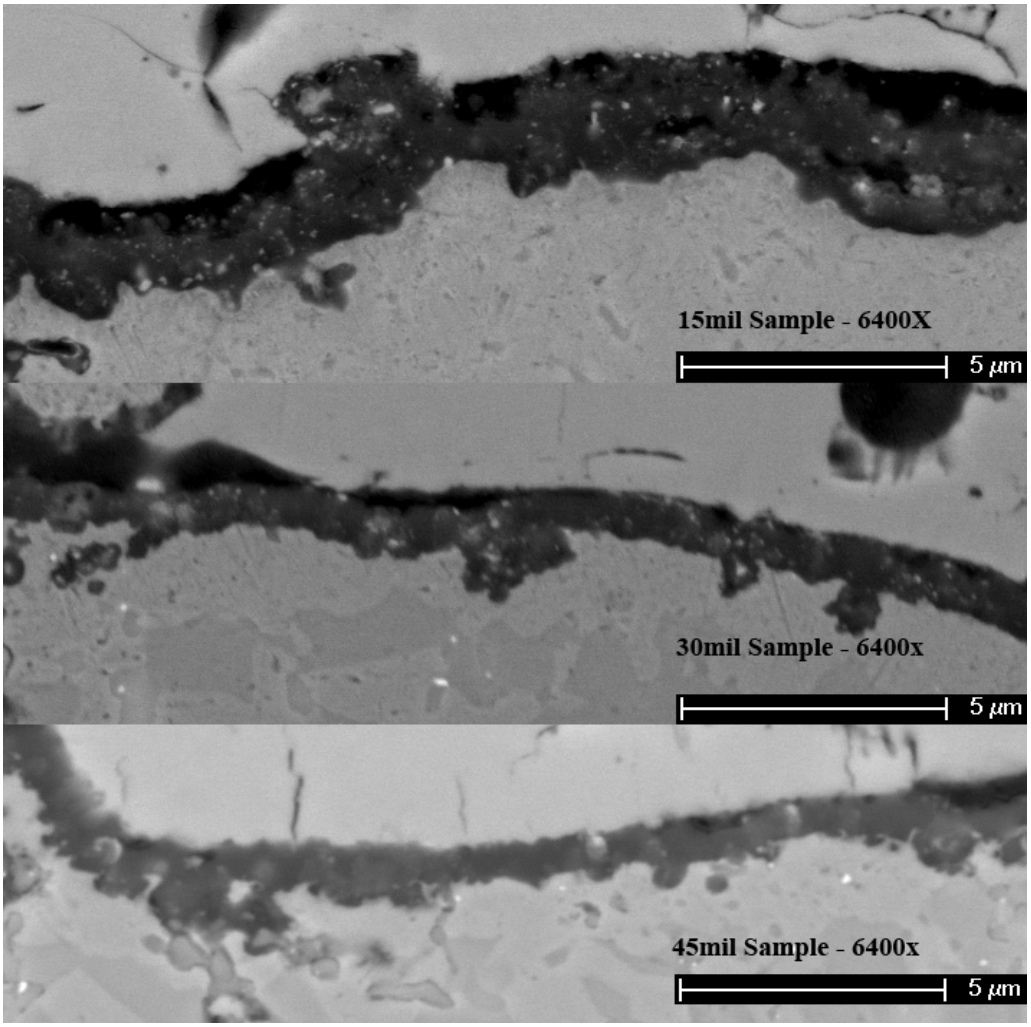

Figure 49 - Micrographs of the TGO from the 3 JETS specimens.

There seems to be a considerable difference in the TGO thickness in the three JETS specimens. This trend is likely the result of the variations in ceramic topcoat thickness, where the thicker topcoats are providing increased thermal shielding for the underlying bond coat which is

subsequently at a lower temperature and yields a slower growing scale. Also, in all three specimens, the TGO contained considerable amounts of yttrium-aluminum-rich particle inclusions.

In comparing experimental results from the two thermal cycling test used in this study one must consider the modes of the tests. In the FCT all specimens are held in a low-density ceramic tray, one edge down and arranged in a square array of rows separated by about 2.5 cm. All the specimens are automatically elevated into the hot zone of the furnace at once, all heated at the same rate and, within 10 minutes, all are within ±5˚C of the setpoint. Thus the superalloy substrate, the bond coat, and the YSZ layer heat at the same rate and are isothermal to each other at any time in the heating and cooling cycle. This results in the maximum thermal expansion mismatch between the layers.

In the JETS test, the specimens are heated only from the YSZ surface side by an oxygen-propylene flame (the heating curve shown in Figure 29). This temperature is measured by non-contact infrared pyrometers imaging the center 6 mm diameter spot on the 25 mm diameter face. The flame is about 12 mm in diameter and is centered on the YSZ face. The button heats more quickly at the center of the button and, as the flame impinges and the hot gases flow to the edges of the button face, the hot spot grows to full diameter. This heat spreading effect occurs in the first 10 seconds, before the entire button face is near uniform temperature. Thus, the heating in the JETS test is, in effect, two-dimensional and dynamic. It forms a temperature gradient from the hot YSZ face center, which spreads in time to the edges like a time-dependent bulls-eye. During the last 5-10 seconds of the heating period the in-plane temperatures are likely uniform across the diameter at any thickness level in the coating/substrate and the front-to-back

temperature gradient has stabilized to that shown in Figure 30a. However, during initial heat-up the expanding bulls-eye thermal pattern likely concentrates expansion stresses at the button center first and at the central area of the YSZ-bond coat interface.

Thus the smooth gradual trend in the extent of edge cracking in the JETS test, in contrast with the FCT testing results, which showed a step-like difference in the lifetime behavior between the thick (45 mil) and the thin (15 and 30 mil) specimens, is the result of the different heating patterns. This observation agrees with a previously conducted study at Praxair Surface Technologies where the capabilities of different testing methods (JETS, FCT, and fluidized bed test) to exploit/differentiate flaws within the TBC system were compared [38]. The conclusion reached in that study indicated the JETS testing was ideal for investigating the durability of the topcoat whereas the FCT was better suited for investigating the interactions between the TGO, bond coat, and topcoat layers. The FCT also affected the durability of the topcoat layer, but to a lesser degree than the JETS test.

It is important to note that these TGO thicknesses for the JETS specimens are considerably thinner than the TGOs for the FCT specimens, even for specimens exposed for similar hot times (see Table 6). The thinner oxide layer can be partially attributed to the relatively rapid and brief heating periods in the JETS cycling, where the specimens are placed under a flame for 20 seconds. The time-temperature profile shown in Figure 29 shows the temperature of the front surfaces of the specimens is constantly changing and the time spent above 1100°C is 20 seconds at most (including heating and cooling periods.) More importantly, the temperature at the bond coat interface is much lower than the temperature measured at the YSZ surface as a result of the TBC establishing a temperature gradient between the two surfaces which in turn slows the growth of the TGO. For these reasons, the JETS test does not appear to

target bond coat properties or the interactions between the TGO-bond coat-topcoat layers. Instead, it primarily tests the durability of the topcoat to successive rapid thermal cycling.

It is significant to note that even when the FCT results in a failure contained completely within the topcoat (e.g. the 45 mil coating in Figure 22) the development of this failure appears to be different than that in the JETS test. Therefore, since the JETS test is somewhat more simulative of turbine operating conditions, it is necessary to establish a "calibration" of the FCT if it is to yield meaningful results for thick APS-TBCs.

4.1.3.3 Extended Duration Furnace Cycling Test (Pseudo-Isothermal)

The three different topcoat thickness specimens, 15, 30, and 45mils, failed after 480, 420, 300 hours of hot time, respectively, when exposed in the pseudo-isothermal test. All three failed by complete TBC spallation. Images of the three fracture surfaces are presented in Figure 50- 52.

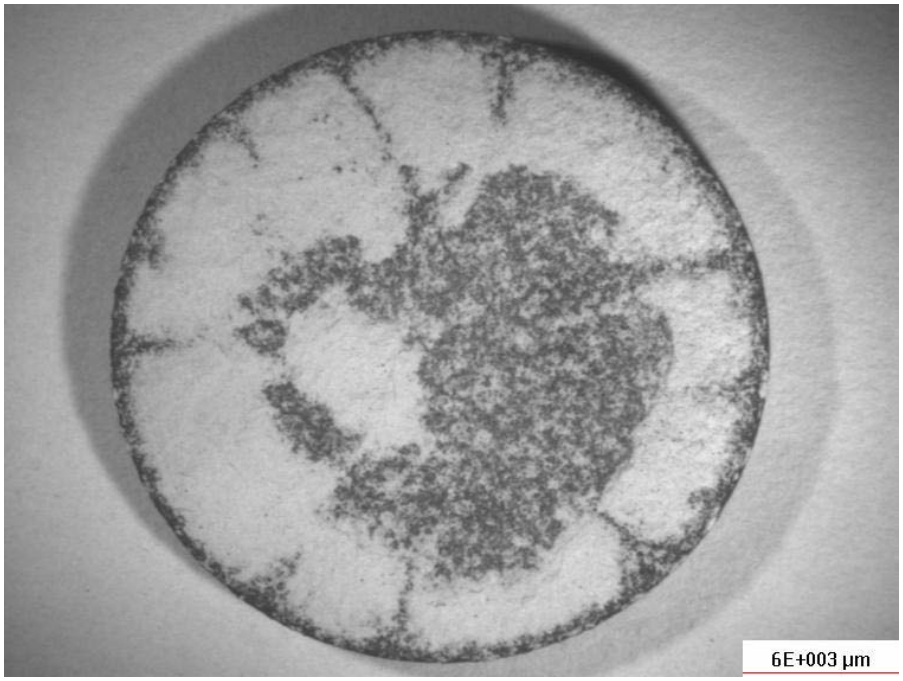

Figure 50 - Fracture surface of the 45 mil specimen exposed in the pseudo-isothermal.

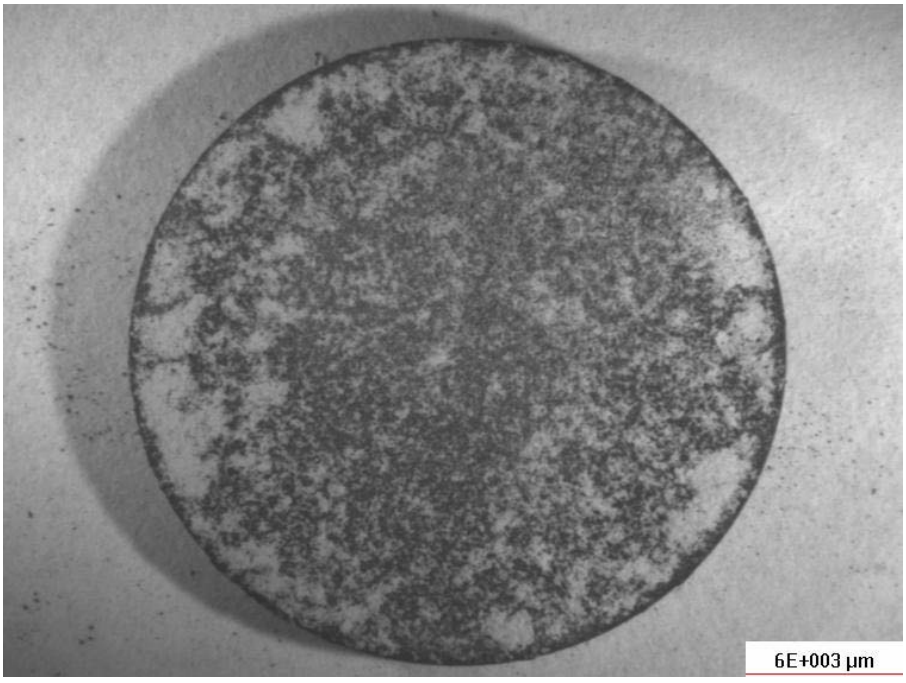

Figure 51 - Fracture surface of the 30 mil specimen exposed in the pseudo-isothermal.

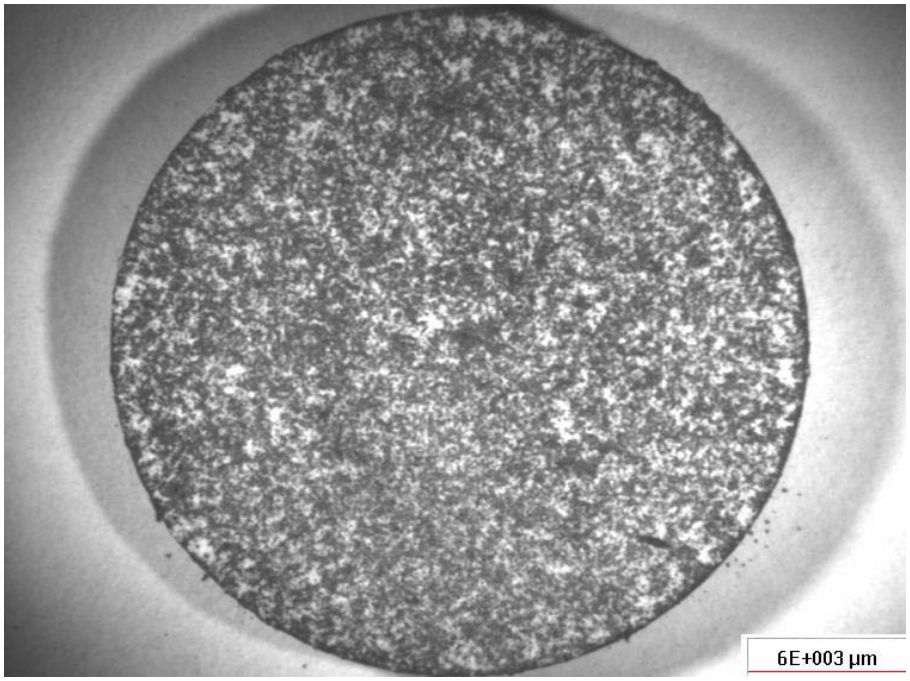

Figure 52 - Fracture surface of the 15 mil specimen exposed in the pseudo-isothermal test.

The amount of remaining YSZ on the surface was measured through image analysis. The technique involved converting low magnification optical micrographs into black and white images where the white pixels represented YSZ and black pixels TGO/bond coat. The relative amounts of white and black pixels could then be compared to yield the percent coverage of YSZ. Estimated values of remaining YSZ are listed in Table 7 for the three specimens.

Table 7- Results of Pseudo Isothermal Testing.

Pseudo-Isothermal Testing @ 1100C w/ 60hr cycles				
TBC Thickness (mils)	**# of Cycles**	**Exposure Time (hr)**	**% TGO&BC**	**% YSZ**
15	8	480	68.2	31.8
30	7	420	58.9	41.1
45	5	300	25	75

As the values in this table and simple visual observation indicate the amount of YSZ remaining on the fracture surface decreases with decreasing TBC thickness. Another key observation with the 30 and 45mil coatings is there seems to be more residual YSZ around the edges than in the center of the specimens.

SEM analysis of the three fracture surfaces indicated the fracture that occurred within the TBC was mixed between intra-splat and inter-splat fracture as Figure 53 depicts.

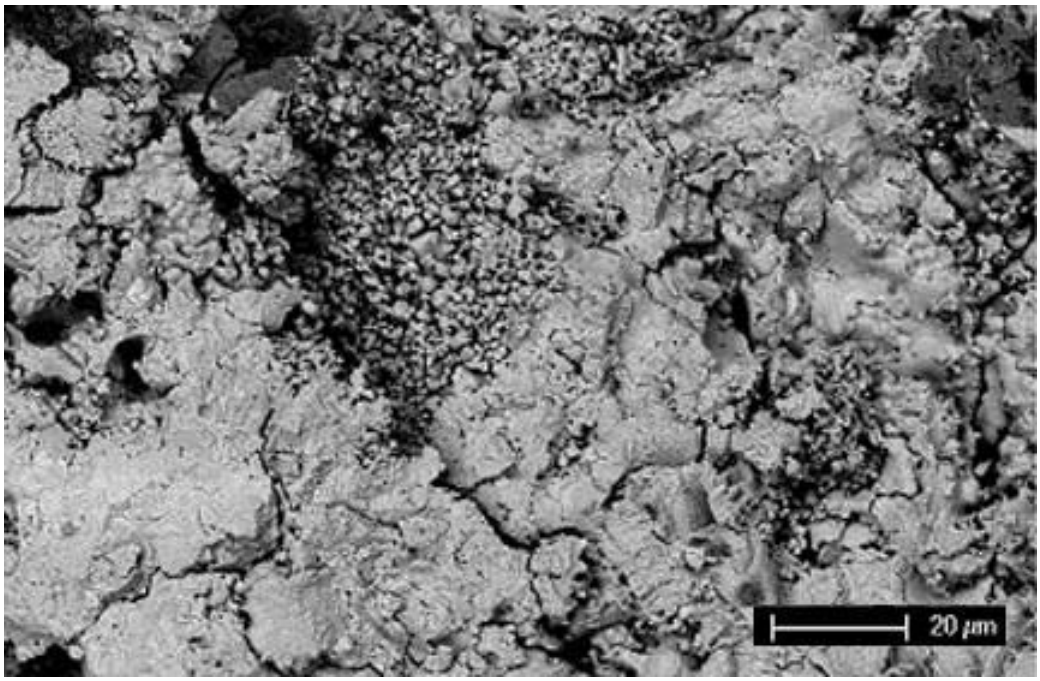

Figure 53 - Typical fracture surface of YSZ TBC.

In this micrograph the smooth regions are where inter-splat fracture occurred and the rough regions are where intra-splat fracture occurred leaving a rough surface. There was also a considerable amount of TGO and bond coat present at the fracture surface in all three specimens. In the 45mil specimen, a significant number of yttrium-aluminum oxide particles were found dispersed in the exposed TGO, particularly in regions where alumina was the primary oxide present at the surface. This is seen in Figure 54, where the bright white particles are the yttrium-aluminum oxide and the dark phase around them is alumina.

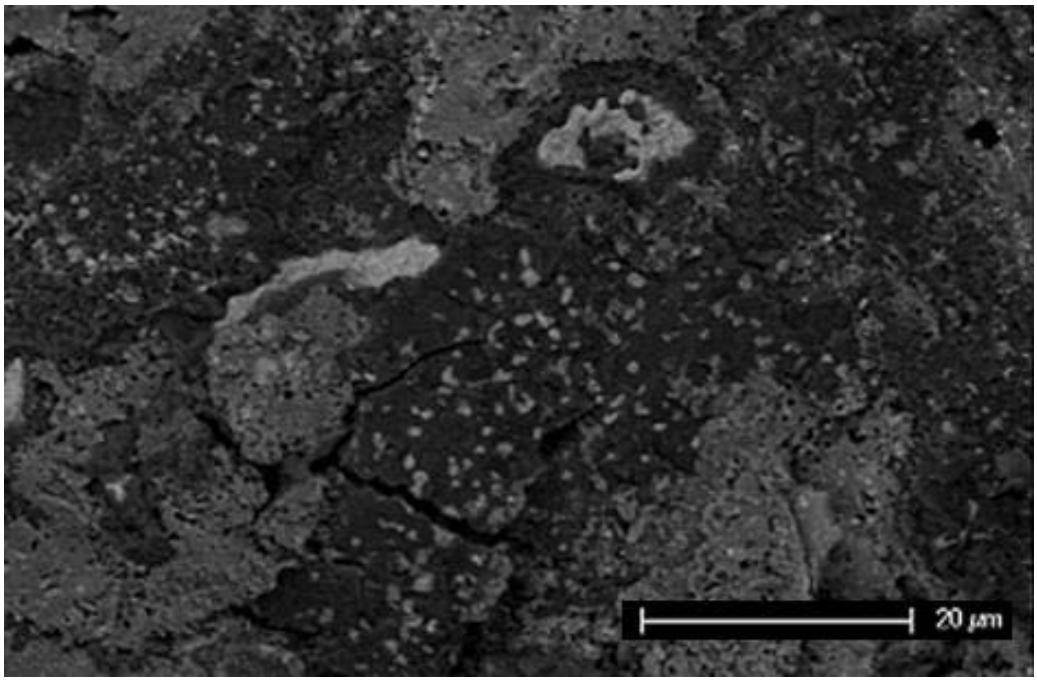

Figure 54 - Small white particles are yttrium-aluminum oxides, perhaps YAG, which are contained in relatively pure alumina.

Areas similar to this were also found in the 30 and 15mil specimens. The oxides present at the surface contained Al, Al-Cr, Al-Cr-Y, and Al-Cr-Ni; however alumina and aluminum-chromium oxides were the most prevalent. In the 30 and 15 mil specimens there was much more TGO and bond coat present than in the 45mil specimen. A final observation is that there were isolated regions on the fracture surface that contained high levels of niobium (7~8 at%), which is a component in the underlying alloy substrate but not the bond coat layer.

Cross-sectional analysis of the 45mil specimen revealed that in the regions where there was TBC still intact, that the underlying TGO was heavily damaged and contained several horizontal cracks. These cracks most likely formed during the cooling process when the coefficient of thermal expansion (CTE) mismatch caused delamination to occur. Then upon

subsequent cycling, new adherent TGOs formed thus building up the cracked layer structure. Also yttrium-aluminum oxide particles were found dispersed in the TGO in the vicinity of these cracks which is seen in Figure 55.

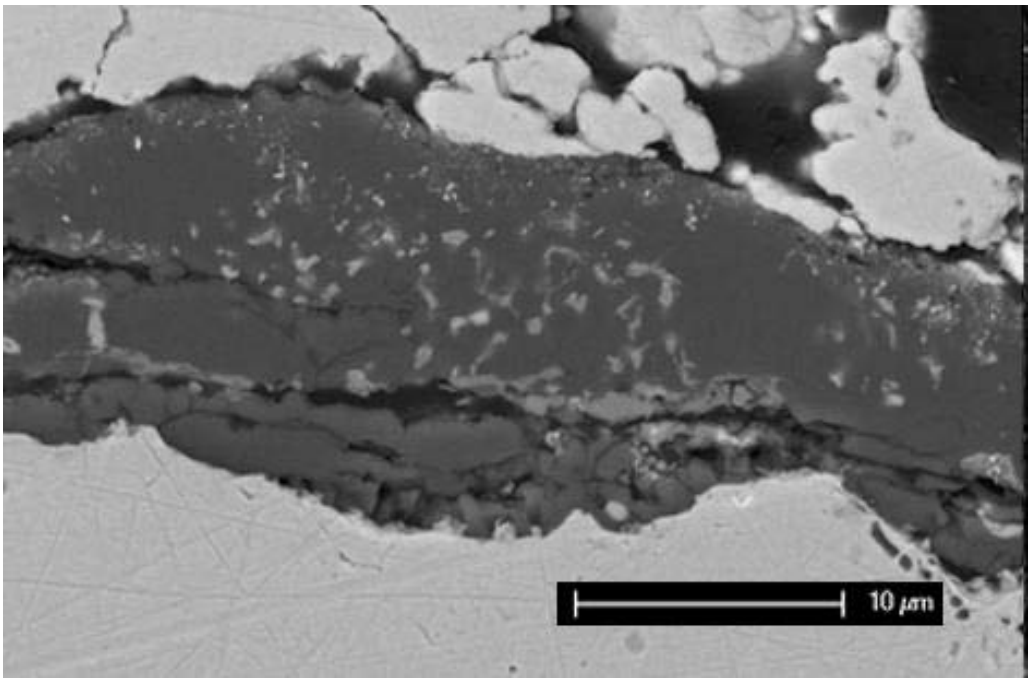

Figure 55 - TGO of 45mil specimen. Notice the horizontal cracks within the TGO and the numerous yttrium-aluminum oxide particles near these cracks.

The cross-sectional analysis of the 30 and 15mil specimens confirmed the observations of the surface analysis in that the fracture path appeared to follow the bond coat-TGO interface. The 15mil coating, fracture appears to follow the most horizontally linear path across the interface whether that meant cutting through the TGO, bond coat, or YSZ as seen in Figure 56.

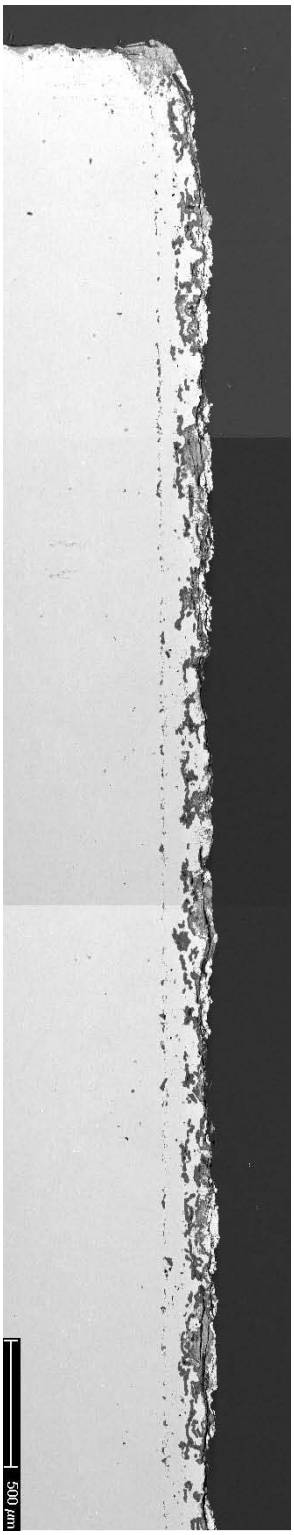

Figure 56 - Composite Cross-section of 15mil specimen.

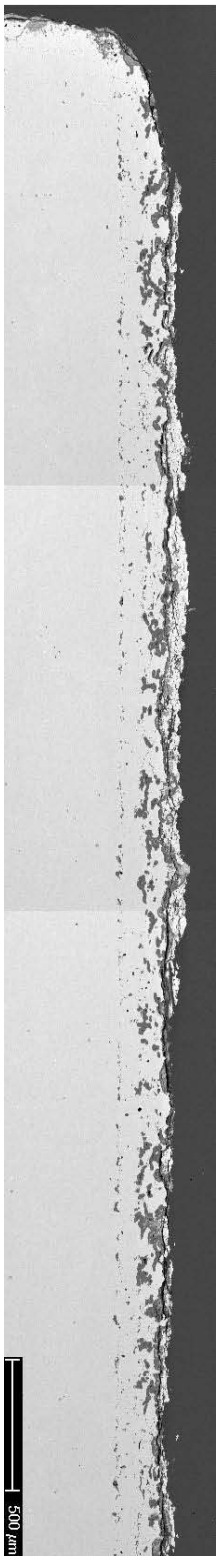

Figure 57 - Composite Cross-section of 30mil specimen.

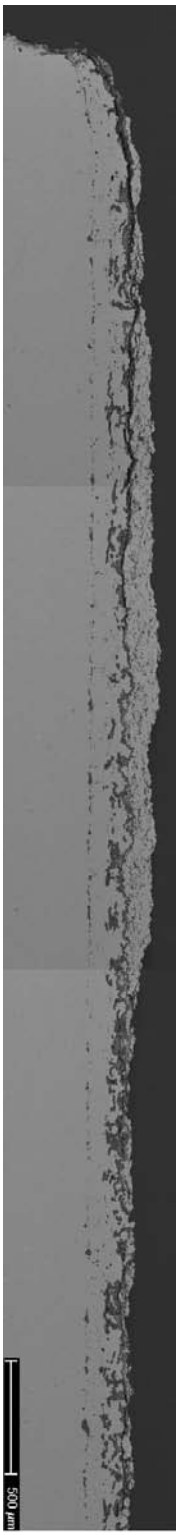

Figure 58 - Composite Cross-section of 45mil specimen.

As a result there seem to be equal amounts of TGO, bond coat, and TBC at the fracture surface. With the thicker coatings, this same type of fracture occurred in the center regions of the specimens but not near the edges. Instead, near the edges in the 45 and 30 mil coatings, the crack path deflected upwards into the TBC and then back downward as it approached the edge of the specimen leaving an outer ridge of TBC on the fracture surface as seen in Figure 57 and Figure 58. The upward deflection of the crack moving towards the perimeter of the specimen may be a result of the extra strain energy due to the increased thickness of the TBCs

4.1.4 Phase I Specimens: Summary

The preparation of TBCs with unconventionally thick topcoats was successfully completed. The high purity YSZ used for these specimens showed a strong resistance to sintering and phase transformations at normal operating temperatures (1100°C-1200°C) and at higher than normal operating temperatures (1300°C-1500°C). This was attributed to the lack of impurities in conventional purity YSZ that aid in diffusional transport between adjacent splats resulting in higher shrinkage and sintering rates.

The results from all three thermal exposure experiments indicated that there is a strong relation between thickness and failure time, where thicker coatings fail in shorter times. Furnace cycling tests also revealed two failure mechanisms. The first being associated with the thick 45mil TBCs where failure was occurring well within the YSZ topcoat and after a relatively short number of cycles (20-40cycles). The second mechanism was associated with the thinner 15mil and 30mil TBCs. With these, failure occurred after an increased number of cycles (80-180cycles) along the topcoat – TGO interface as a result of thermal fatigue and bond coat oxidation.

The thermal exposure experiments also revealed an effect of thermal cycling frequency on the amount of hot time (time spent at 1100°C) to failure. Figure 59 shows the hot time to failure for the three different thermal exposure types.

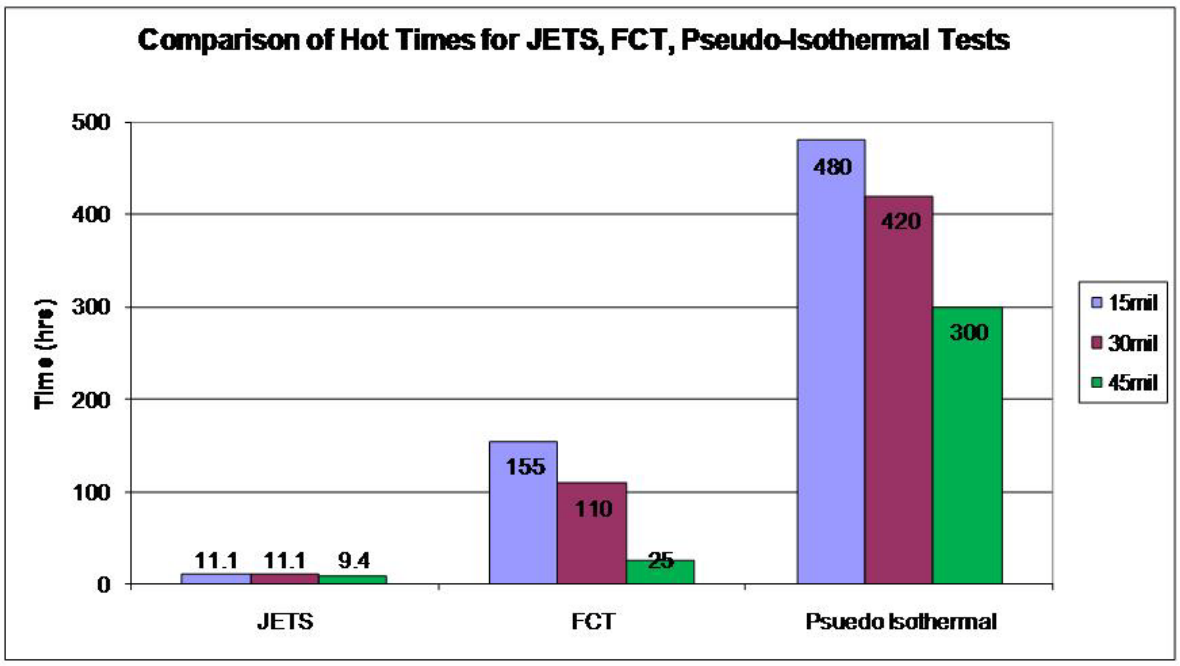

Figure 59 - Effect of thermal exposure frequency on hot time to failure.

According to Figure 59, the hot time to failure increases when moving from the JETS test to the FCT and then to the pseudo isothermal test. The thermal cycling frequency can be thought to be the ratio of heating and cooling time to the isothermal hold time. Since the JETS test has 20 second heating and cooling periods and virtually no isothermal hold time, it has the highest cycling frequency and the pseudo isothermal test, which has 10 minute heating and cooling

periods and 60 hour isothermal holds, has the lowest thermal cycling frequency. This correlation between thermal cycling frequency and hot time to failure was also made by Bolcavage et al [38].

4.2 SECOND GENERATION SPECIMENS

The effects of the significant variables on the FCT lives of the second generation specimens are presented in Figure 60. These effects are described in the following.

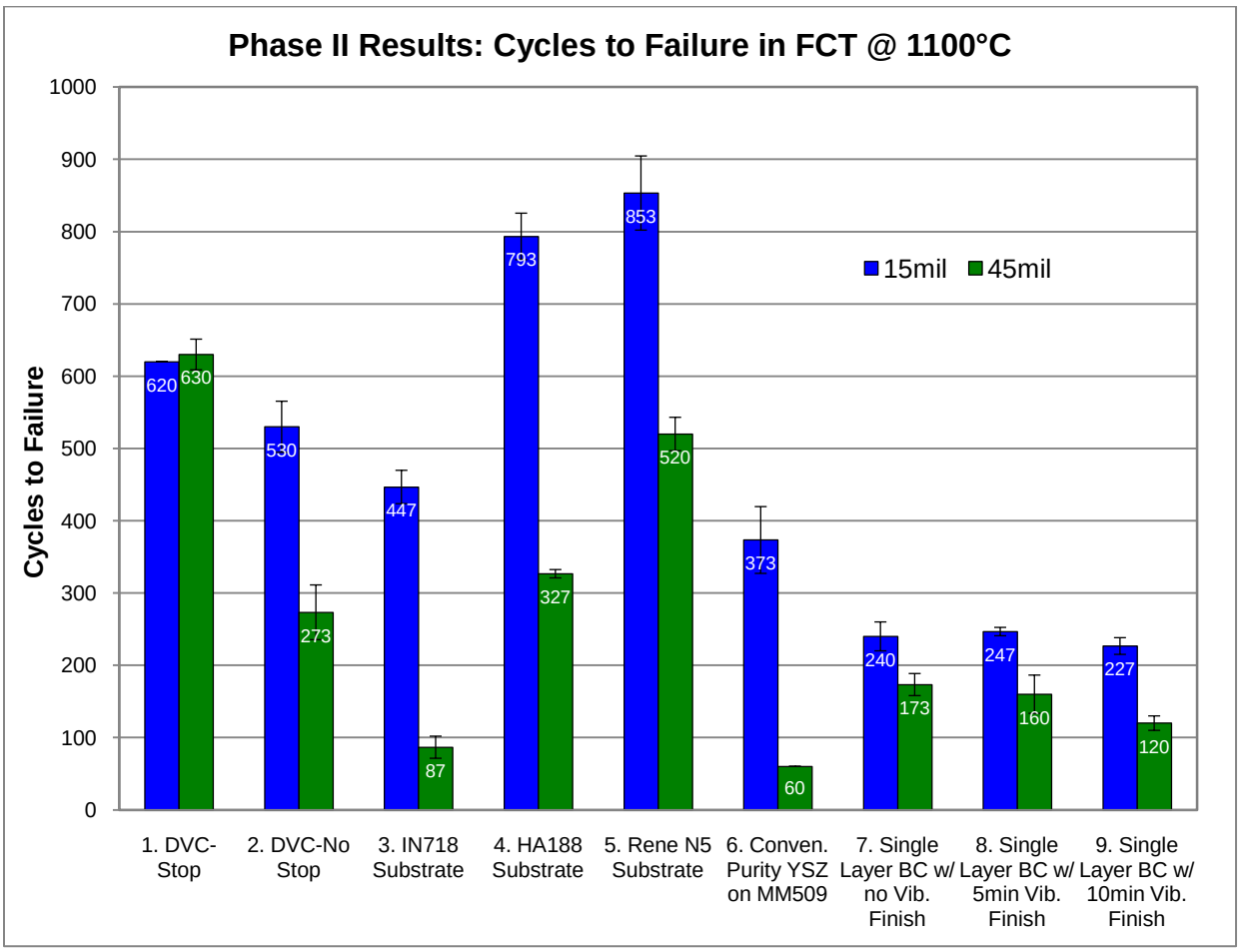

Figure 60 - Effect of different variables on the 1100˚C FCT lives of the second generation specimens.

4.2.1 Effects of Superalloy Substrates

To investigate the effect of superalloy substrate, all coating parameters (topcoat density, topcoat and bond coat composition, bond coat roughness, etc.) were held constant and the substrate material was changed. Two different thickness topcoats were prepared for each substrate as well. The third, fourth and fifth categories in Figure 60 show the FCT results for the substrate effect on lifetime of the TBCs. As shown on the graph, when moving from IN718 to HA188 and then to René N5, the lifetime of the TBCs drastically increased. The 45mil TBC on René N5 outperformed the 15mil TBCs on IN718 and furthermore the 15mil coatings on HA188 and René N5 both had comparable lifetimes to that of a state-of-the-art 150μm EBPVD coating on a platinum aluminide bond coat on René N5 substrate which were reported to have a FCT lifetime of 1000 cycles [7]. From these test results, there seems to be a relatively strong affect of the substrate material on the TBC lifetime.

Figure 61 shows the measured mean coefficient of thermal expansion for the substrate materials used in this study. Inconel 718 has the highest CTE at 1100°C followed by HA188 and then René N5.

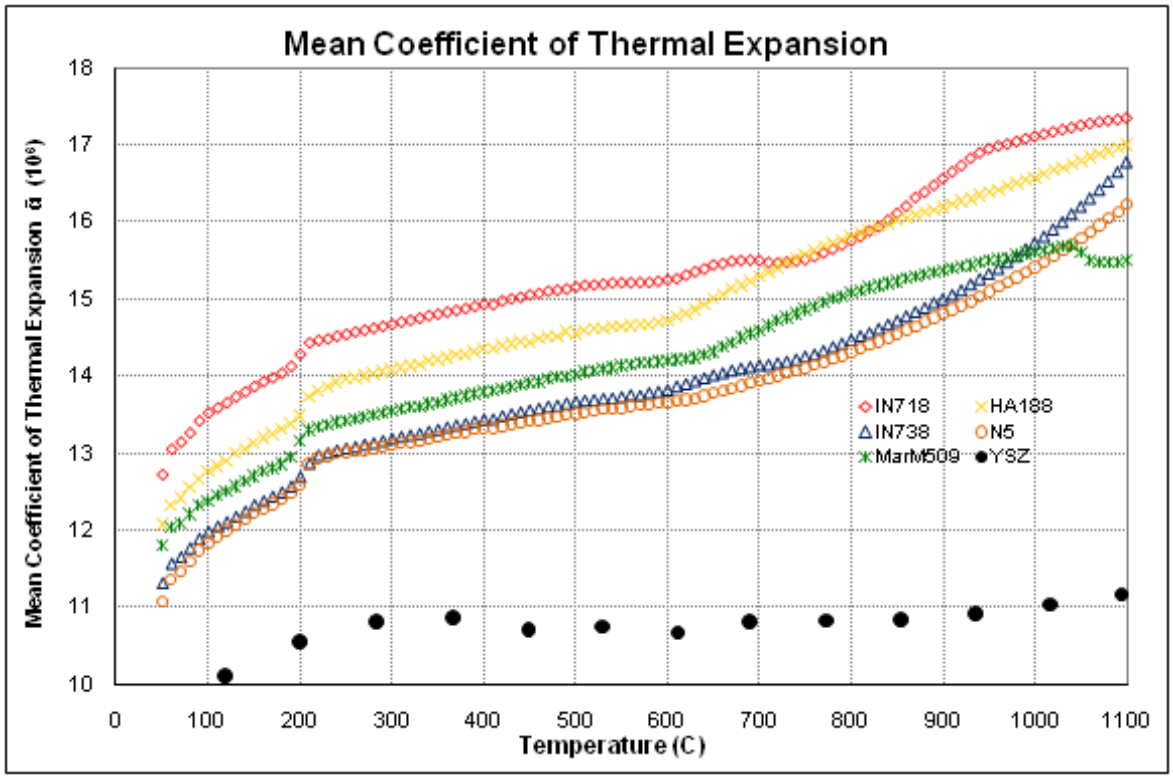

Figure 61 - Experimentally measured coefficient of thermal expansion for the alloys used in this study. Note: IN738 was not used in this study, its CTE was measured for use in future work.

The CTE data above and the FCT data were used to fit a regression equation that relates the number of cycles to failure to the topcoat thickness and the CTE mismatch between the topcoat and the substrate alloy. It is given by Equation 2:

Equation 2

$$N_f = 1300 - 13.651 \times h_{ysz} - 5.732 \times 10^{12} \times (\Delta_{CTE})^2$$

Where h is the thickness of the topcoat in mils (0.001in) and N_f is the number of cycles to failure. It should be noted that the coefficients in this equations are fit parameters and do not have

explicit underlying significance as of the date of this publication. This equation, based on our data, indicates that by minimizing the CTE mismatch and the topcoat thickness, the number of cycles until failure can be maximized. It should be also pointed out that this equation is based on furnace cycling testing done at 1100°C. Attempting to apply this equation to different temperatures or different furnace cycles (i.e. longer isothermal holds, more rapid cooling/heating) will yield unrealistic results.

A more fundamental connection between thermal misfit strains and coating lifetime has been investigated by He et al [39]. In their study they derived a fundamental equation for the lifetime (number of cycles to failure) of TBC systems based on system/material parameters. Equation 3 shows this relationship they developed.

Equation 3

$$N_f = N_0 + \frac{\Gamma_{TBC}}{E_{TBC} L (\Delta\alpha \Delta T)^2 \kappa}$$

Where N_f is the number of cycles to failure, N_0 is a set minimum cycles to failure, Γ_{TBC} is the fracture toughness of the APS TBC, E_{TBC} is the elastic modulus of the TBC, $\Delta\alpha$ is the CTE mismatch between the alloy and the topcoat, ΔT is the temperature difference between the stress free temperature and the isothermal hold temperature, and κ is a coefficient that depends on the assumptions of the TGO growth strains and other bond coat properties. This model does a rigorous derivation of the stresses, strains, and displacements and incorporates many aspects of the dynamic TBC system that are often left out. In particular, bond coat plasticity and deformation and TGO growth strains and displacements are accommodated for in a cyclic manner, where stress/strains grow as the number of cycles increase. A key similarity between

Equation 2and Equation 3 is they both have a given number of cycles the TBC systems can survive (1300 in Equation 2 and N_0 in Equation 3). However, in the case of Equation 2, the limit is an upper limit and with Equation 3, it is a lower limit.

In light of the observation that topcoat thickness has a significant effect on the number of cycles to failure, Equation 3 seems to be lacking a variable to accommodate for this. The authors of this equation caution that this equation should be compared with experimental results once the appropriate properties are determined. Therefore it is plausible that the N_0 term could be incorporating the topcoat thickness somehow, however this may be somewhat speculative. Nonetheless, Equation 3 points out the influence of the CTE mismatch with respects to TBC lifetime.

With the 45mil TBCs on IN718, we again observed, as we did with the Phase I specimens, failure indicative of fracture mechanism one where the cracking and failure occurred solely within the TBC layer. However, when switching from IN718 to HA188 and René N5 substrates, failure mechanism one was suppressed and failure occurred by mechanism two, where cracking and delamination occurred at the thermally grown oxide (TGO) – TBC interface. It is the authors' opinion that by reducing the thermal expansion mismatch between the TBC and the substrate failure mechanism one can be suppressed, increasing the lifetime.

Once failure mechanism one is suppressed and mechanism two dominates, the cause of failure is closely linked to bond coat oxidation and thermal cyclic fatigue. During extended thermal cycling, a substantial amount of interdiffusion will occur between the bond coat and alloy substrate and, depending on the composition of the substrate, can have positive or negative effects. In the case of IN718 which contains 5wt% niobium, the TGO was primarily composed of an alumina and chromia scale except for regions where niobium was detected in the TGO where

(Nb-Ni-Cr-Al)-O spinel oxides were also present. Such niobium rich oxides were found on the underside of the fracture surface of the TBC as seen in Figure 62.

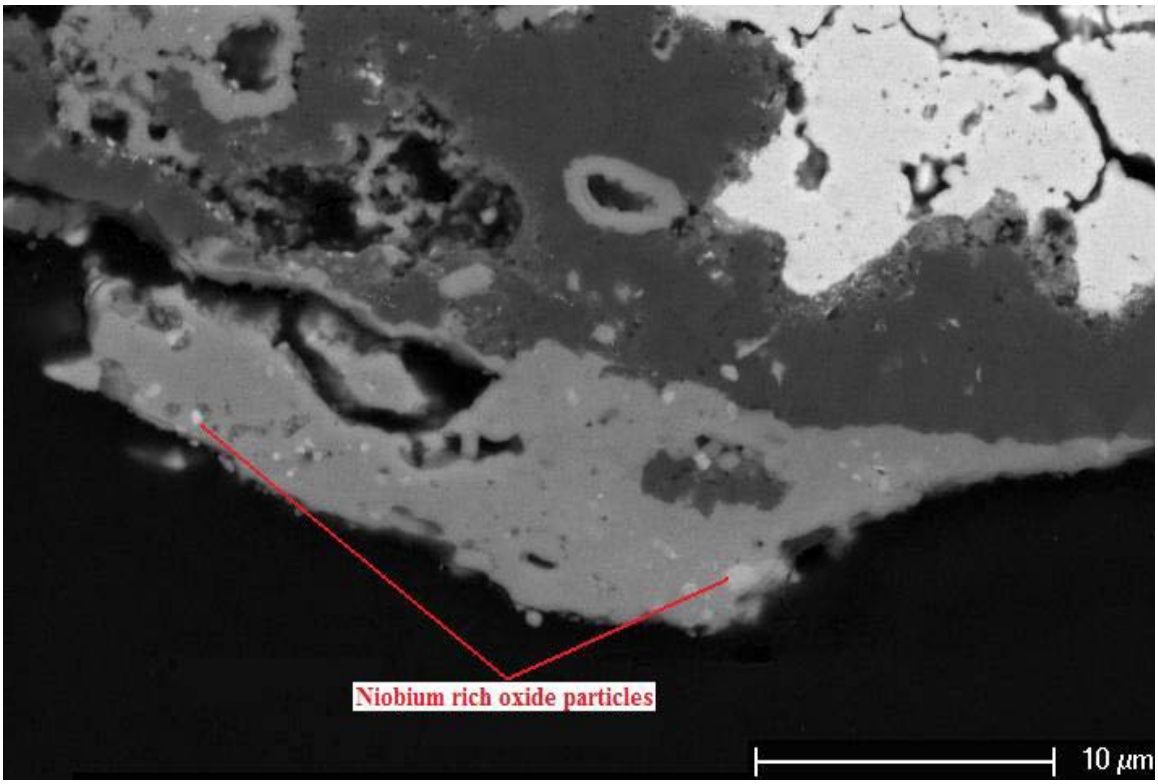

Figure 62 - Bright regions in the gray scale are rich in niobium. Dark phase is alumina and the lighter grey is Ni-Cr spinel.

There were also regions where Ni-Cr-Al spinel oxides were present but niobium was not detected. Regardless of the location, the spinel oxides are unwanted as they have poorer adhesion with the YSZ [40]. Here the substrate is poisoning the TGO and having a negative effect on the lifetime of the system. Similarly, if the substrate has a substantially lower concentration of aluminum than the bond coat, the aluminum in the bond coat will diffuse into the substrate which, in the case of the NiCoCrAlY bond coat, depletes the reservoir of available aluminum in

the β-NiAl phase for TGO formation. As the aluminum is depleted in the bond coat, other spinel oxides begin to form which again are detrimental to the lifetime of the TBC system. However, this may not be a strong effect in the TBCs tested in this section as they contained high amounts of internal pores leading to internal oxidation and rapid β-phase depletion. Overall, with the thin 15mil TBCs and the 45mil TBCs on HA188 and René N5, the failure is due to bond coat oxidation and thermal cyclic fatigue caused by the expansion mismatch in the components in the TBC system.

4.2.2 Effects of YSZ Topcoat Purity

TBCs with conventional purity YSZ were prepared with target thicknesses of 15 and 45mils (45mil coating ended up having a thickness of 60mil). They were prepared on MarM509 substrates with dual layer bond coats. The sixth category in Figure 60 represent the lifetimes of the conventional purity YSZ TBCs. It is difficult to compare the performance of these TBCs with that of the high purity TBCs because no high purity TBCs on MarM509 were prepared. Also, even though the composition of MarM509 and HA188 are similar (both Co-based alloys), their CTEs are substantially different (Figure 61) and having identified the significance of the substrate effect in the previous section, a comparison of the two does not seem valid. However, there were several differences between the high and conventional purity YSZ coating observed during microscopy of the cycled specimens. The conventional purity coatings contained numerous SiO_2- Al_2O_3 particles which were dispersed throughout the TBC as seen in Figure 63.

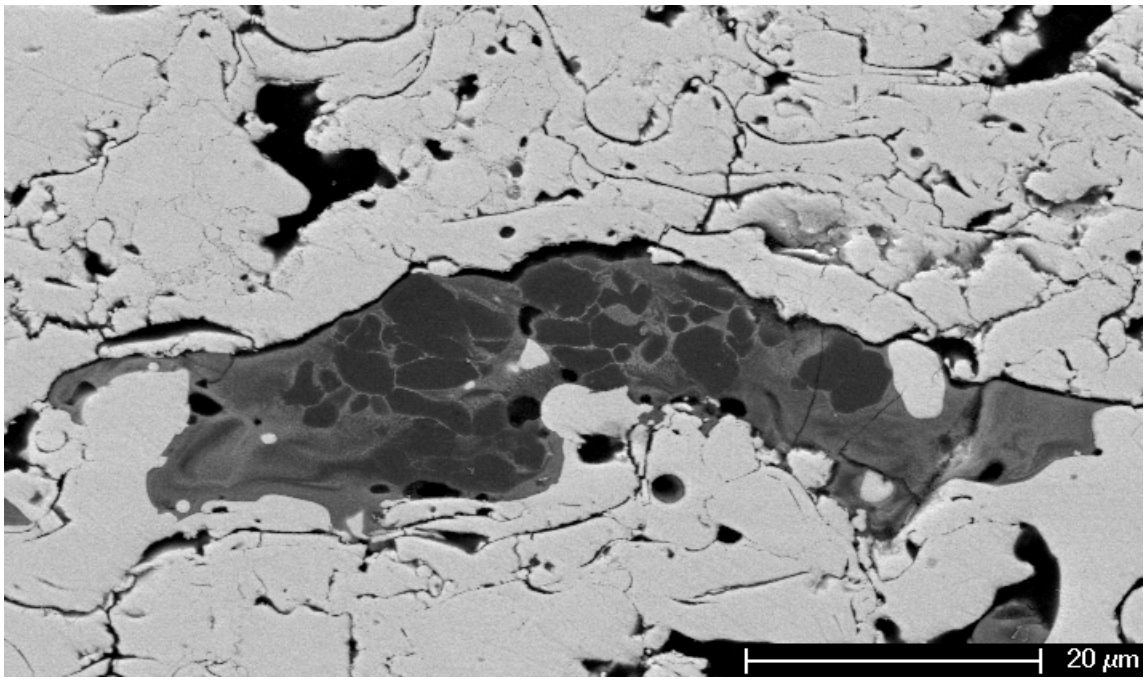

Figure 63 - Micrograph of an impurity in a conventional purity TBC. The dark phase in the center of the image is a Si-Al-Zr rich oxide.

These particles can increase the rate of densification in the TBC which is undesired as sintering increases the strength but decreases the toughness making the coating more susceptible to fracture [19-20]. These particles also have been observed near the topcoat / bond coat interface in the as-processed specimens, Figure 64, and at the fracture surface as in Figure 65 of the thermally cycled specimens. Sintering and densification near this interface can lead to large void formation which can then serve as crack nucleation sites, as shown in Figure 66.

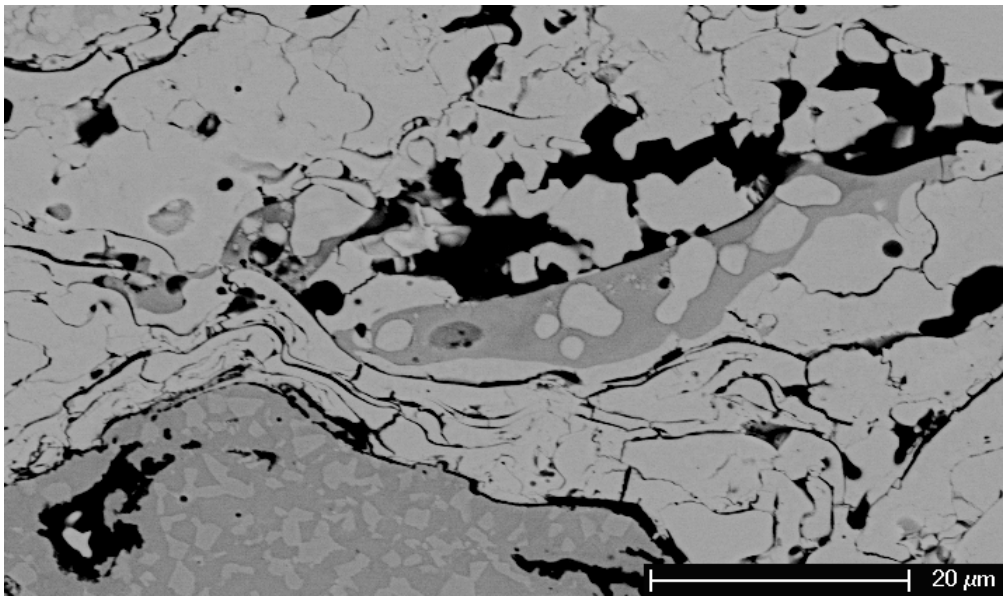

Figure 64 - Conventional purity TBC with impurity particle near bond coat / topcoat interface. Dark phase in YSZ was identified to be rich in Si-Al-Na-O.

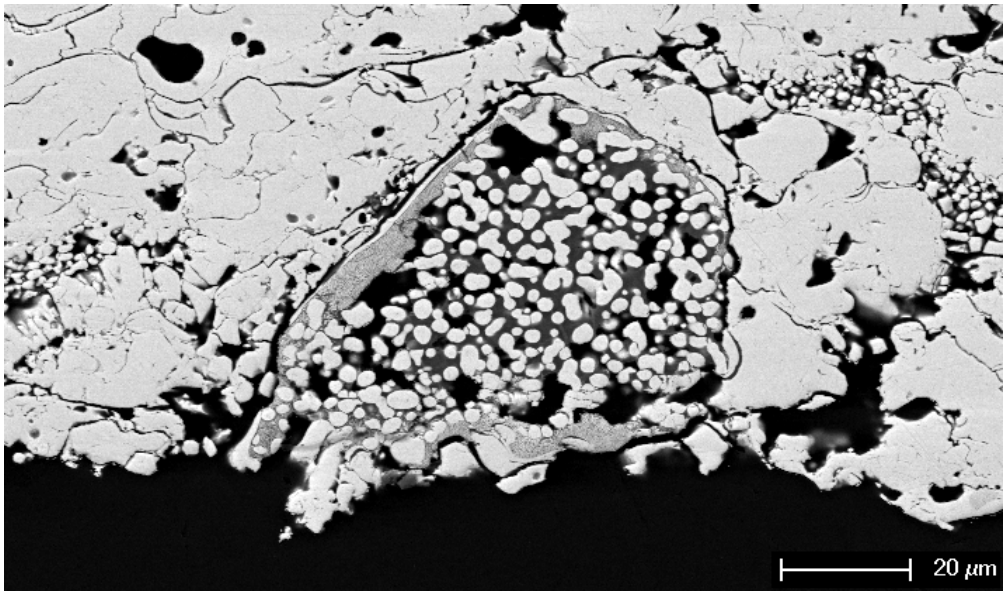

Figure 65 - Conventional purity TBC with impurity particle at fracture surface. Dark phase in YSZ was identified to be rich in Si-Al-Na-O.

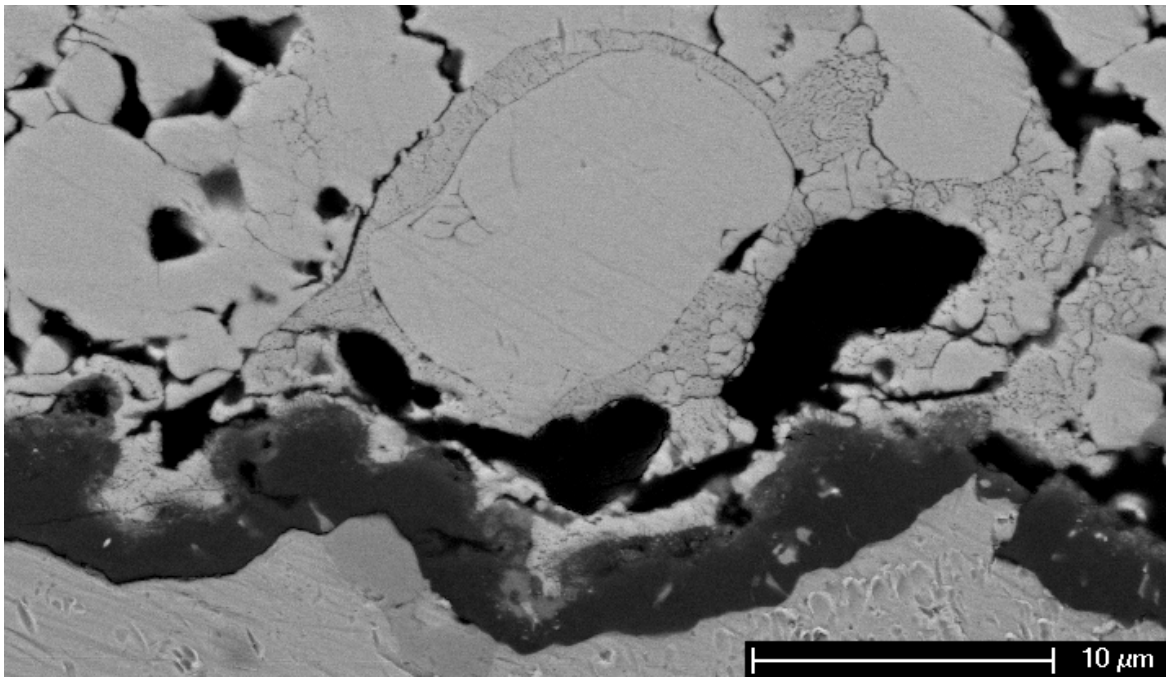

Figure 66 - Conventional purity TBC with impurity particle at topcoat / TGO interface with a large void forming around dark Si-Al-Na rich phase as indicated in the micrograph.

4.2.3 Use of Dense Vertically Cracked (DVC) Inner Layers in the Topcoat

The purpose of dense vertically cracked (DVC) TBCs are to provide strain relief during the heating and cooling periods when thermal strain occurs. These coatings usually have a higher thermal conductivity than the low density coatings because the spraying parameters used to achieve the segmented structure also produce a dense YSZ structure, which subsequently increases the thermal conductivity. To minimize the thermal conductivity and still provide strain relief, coatings were prepared with a DVC inner layer of 7-8mils thickness and an outer layer of low density (85% theoretical) YSZ of either 7-8mils or 37-38mils thickness for an overall topcoat thickness of 15 and 45mils, respectively. Two coating processes were employed to

produce these coatings. In the first process the DVC layer was sprayed, deposition was stopped, the spray parameters, were adjusted and then the rest of the low density coating was sprayed. These coating will be referred to as 'Stop' coatings. The second process involved spraying the DVC layer and then, during the deposition, adjusting the spraying parameters to achieve the low density YSZ structure. These coatings will be referred to as 'Non-Stop' coatings.

The first two categories in Figure 60 show the FCT results for the DVC under layer effect. Unlike the other specimen types, the 45mil DVC Stop coatings performed almost as well as the 15mil coatings performed. Examination of the as-processed specimens revealed a definitive difference in microstructure of the two layers. The lower DVC layer contained denser YSZ with vertical cracks, and some horizontal ones, scattered throughout the layer extending up from the bond coat –topcoat interface. The upper layer was much less dense, and closely matched the low density structure seen in the other Phase I and Phase II coatings. The 15mil DVC Stop coating is shown in Figure 67.

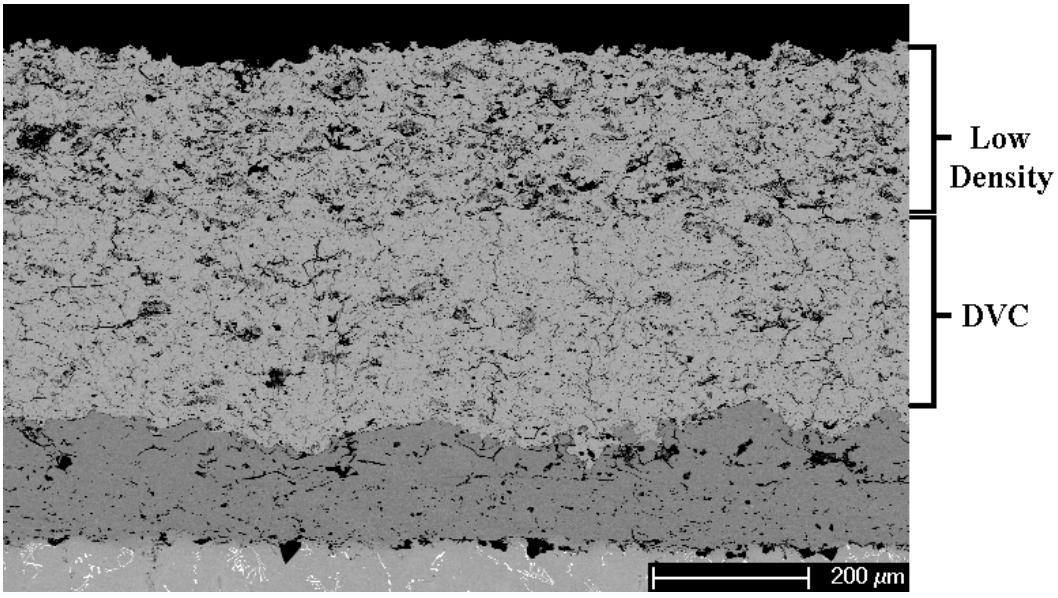

Figure 67 - Micrograph of 15mil DVC Stop under layer TBC.

Notice the abrupt change in porosity when entering the low density portion of the coating. The microstructure of the Non-Stop DVC TBC can be seen in Figure 68.

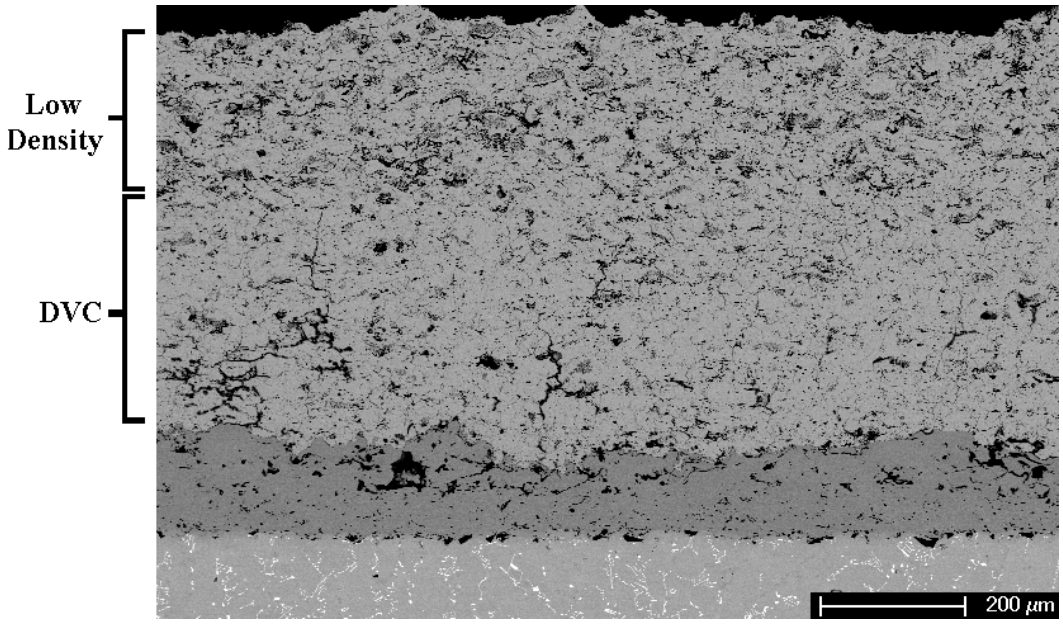

Figure 68 - Micrograph of 15mil DVC Non-Stop under layer TBC without stop.

The vertical cracks are again at the base of the TBC at the bond coat – topcoat interface and extend upward. However there is no abrupt change in porosity as there was with the DVC Stop coating. Rather, the high density YSZ seems to blended into the low density YSZ.

The as-processed 45mil DVC Stop coating contained several horizontal delamination cracks within the cross section of the specimen. The cracks occurred at the interface between the DVC under layer and the low density outer layer as shown in Figure 69.

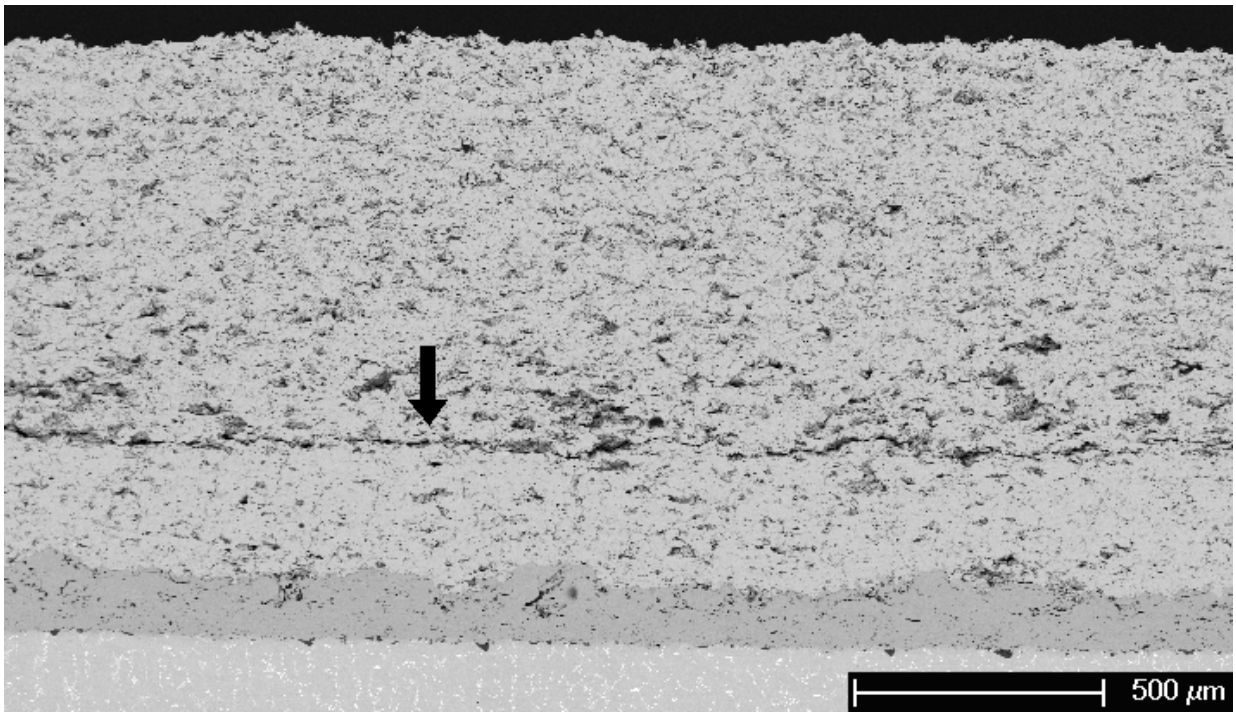

Figure 69 - Interface crack between the DVC layer and the low density outer layer of the 45mil DVC Stop TBC.

The 45mil Stop TBCs was the only group that showed the interfacial cracks. When these specimens were tested in the FCT, around 200 cycles, a small ring of YSZ on the outer edge of the specimens failed and spalled off. Figure 70 shows an optical micrograph of the outer spalled region for both the 15mil and 45mil specimens.

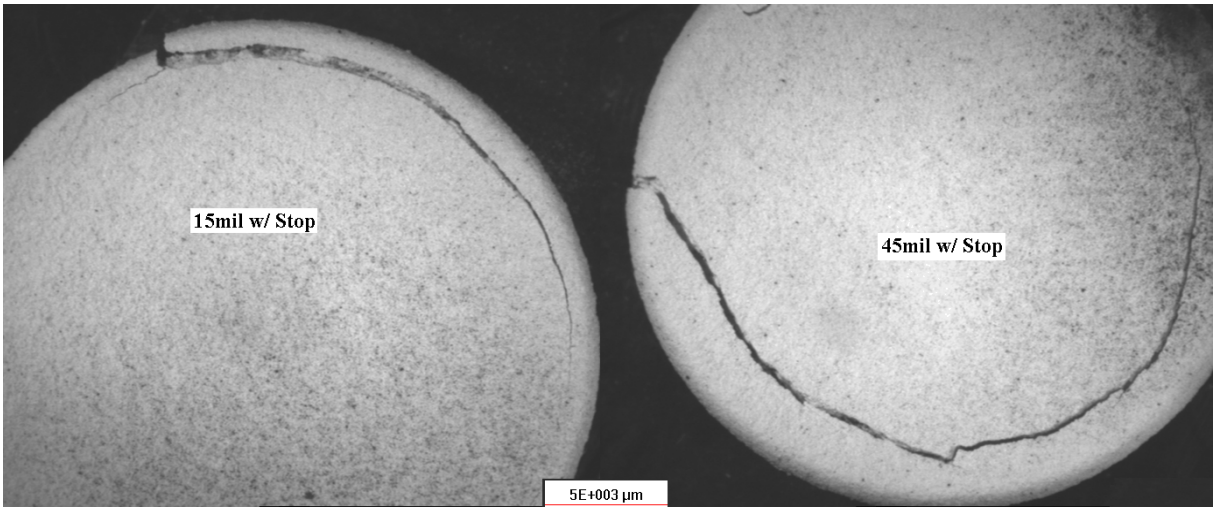

Figure 70 - Micrograph of cracked edges of the 15 and 45mil DVC Stop specimens.

The thickness of this outer ring for the 15 and 45mil coatings was roughly 1mm and 3mm respectively. Both the stop and non-stop coatings exhibited this behavior however, in the DVC Stop coatings, the edge crack extended from the free surface of the topcoat down through the low density layer and then deviated off to the edge of the specimen at the DVC - low density interface. This crack pattern is shown in Figure 71.

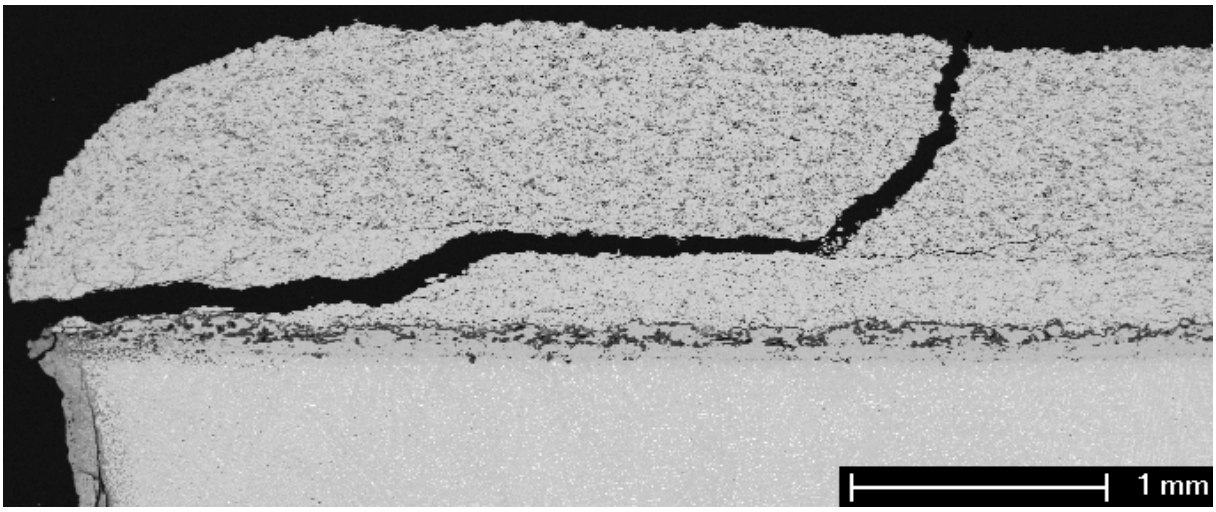

Figure 71 - This micrograph shows the typical edge cracking pattern seen with the 15 and 45mil DVC Stop TBCs. This particular micrograph is the 45mil coating.

The cracks in these coatings probably started at the free edge of the coating and propagated inwards along the TGO/bond coat interface. Eventually these cracks linked up with some of the vertical cracks in the dense lower layer, which changed the crack direction along with some contribution from compressive shear stresses. Then, due to instabilities between the upper and lower segments and existing cracks along this interface, the crack again deviated to the horizontal towards the center of the coating. Finally, compressive shear stresses in the coatings due to thermal expansion mismatch between the YSZ and substrate on cooling caused the crack to again deviate at an upward angle where it finally reached the free surface.

The edge cracks in the 15 and 45mil DVC Non-Stop coatings extended from the topcoat free surface, down through the low density YSZ and DVC regions, and down to the topcoat - bond coat interface and then to the free edge. This cracking pattern is shown in Figure 72.

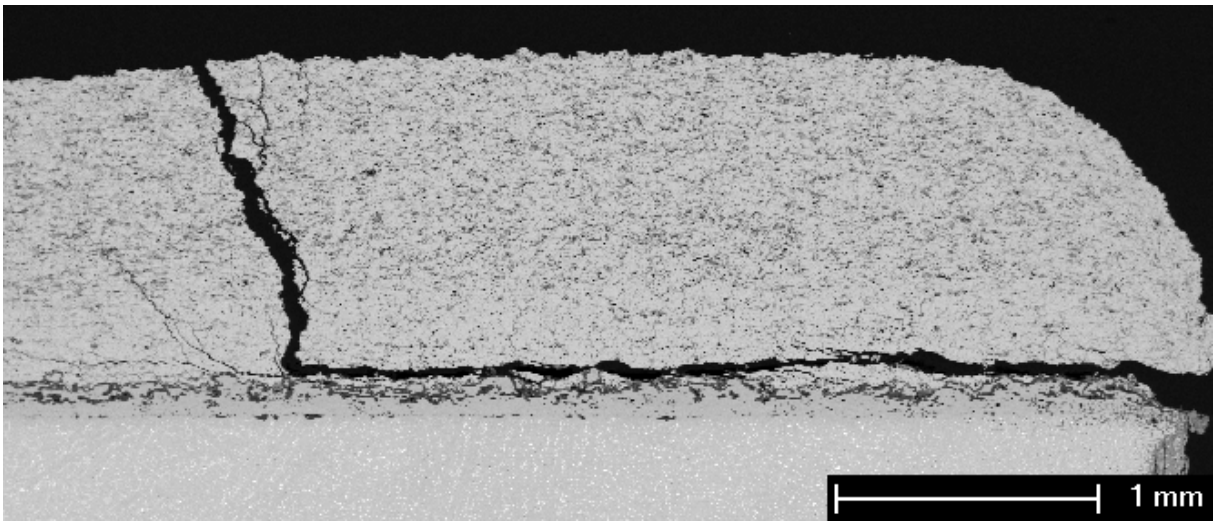

Figure 72 - This micrograph shows the typical edge cracking pattern seen with the 15 and 45mil DVC Non-Stop TBCs. This particular micrograph is the 45mil coating.

Again, these cracks probably initiated at the free surface and propagated towards the center of the specimen and then linked up with some of the vertical cracks in the YSZ which changed the direction of the crack. However, because there was no interface between the DVC layer and the low density layer, the crack most likely did not “feel” this instability and so it continued to the free surface.

After spallation of this outer ring, the samples, both DVC Stop and Non-Stop, did not exhibit any further cracking or spallation during cycling until failure by complete spallation of the entire topcoat. All four coatings completely spalled off leaving a fracture surface covered with exposed TGO and some residual YSZ.

Again, because having identified the substrate effect, it is difficult to compare the performance of these coatings to those with the other low density APS topcoats since there is no high purity low density YSZ topcoat on MarM509. However, one important observation is that

the 45mil coatings performed just as well as the 15mil coatings which is something that has not been observed with any of the other coating systems. This seems to indicate that providing some strain relief in the lower portion of the coating must provide some beneficial relief to the upper portion of the TBC giving it a longer lifetime.

4.2.4 Modification of the Bond Coat Topography

Three different bond coat topographies were investigated in this section. MarM509 substrates were used along with a single layer bond coat, produced by blending small and large particle size bond coat powders and then spraying. Two groups of these specimens were then vibratory finished for 5 and 10 minutes while a third was not vibratory finished at all. Once the bond coat modifications were complete, topcoats were deposited in 15 and 45mil thicknesses.

The last three categories in Figure 60 show the FCT test results for the modified bond coat specimens. All specimens had MarM509 substrates with a single layer NiCoCrAlY bond coat that was argon shrouded plasma sprayed from a blend of 75% fine particle feed and 25% coarse particle feed. Once sprayed, several of the specimens were then sprayed with a topcoat while others were first vibratory finished for five and ten minutes and then given a YSZ topcoat. In total there were three different bond coat finishes which are seen in Figure 73.

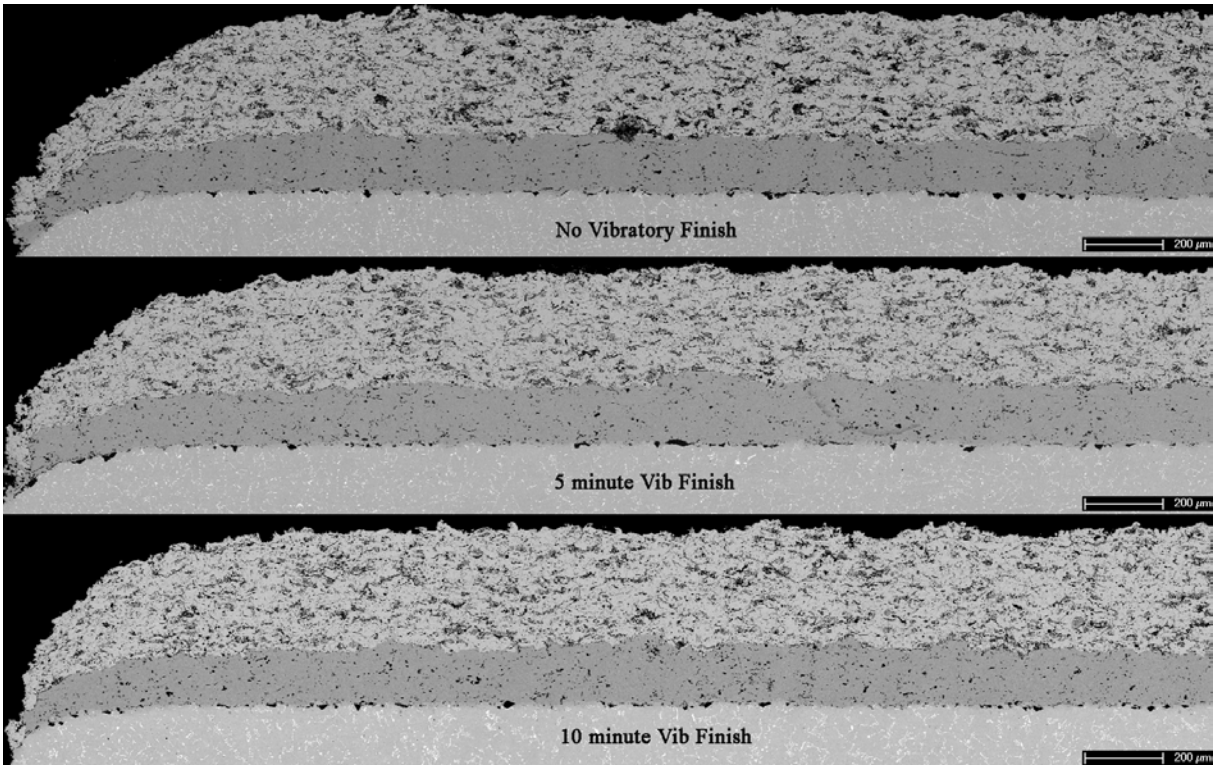

Figure 73 - Cross-sections of: top.) single layer bond coat, middle.) 5 minute vibratory finish bond coat and bottom.) 10 minute vibratory finish bond coat.

Using SEM micrographs and image analysis techniques described in Appendix, the roughness of the bond coats was measured. The R_a values for the roughness of the no modification, the five minute vibratory finish and the ten minute vibratory finish bond coats were R_a=10.7μm, 9.8μm and 8.6μm, respectively. A visual comparison qualitatively confirms these measurements in the sense that the coatings appear very similar with the only noticeable difference being the non-vibratory finished coating still retains a few areas of high roughness where hillocks and asperities still remain.

These finishes did not seem to have a substantial effect on the lifetime behavior as indicated by Figure 60. All specimens had very similar lifetimes with little to no difference in the

number of cycles to failure. It is conventionally thought that a rough bond coat surface is needed for a strong mechanical attachment of the YSZ topcoat [4]. The vibratory finish seemed to remove the rough hillocks on the bond coat surface, however, despite the smoothing effect, there was no substantial impact on the lifetime behavior. The 15mil coatings did have longer lives than the 45mil coatings which is consistent with the performance of the other TBC systems.

Finite element analysis (FEA) simulations in the literature indicate that rougher surfaces in APS TBCs cause larger tensile and compressive residual stress to form at the TGO-bond coat interface [41]. Initially, the residual tensile stresses in the TBC are above the bond coat peaks and the residual compressive stresses are above the bond coat valleys. Cracks are prone to form in the tensile regions but they cannot propagate from peak to peak because of the compressive zones above the valleys. However, as the TGO grows, these stress fields begin to reverse, permitting crack propagation between peaks. By reducing the roughness of the bond coats, the stresses in the topcoat are too reduced which helps prevent crack formation. At the same time though, a smoother bond coat reduces the mechanical bond with the topcoat. Alternatively, other FEA simulations propose that although the rougher interfaces lead to higher initial residual stress levels in the TBCs, the higher initial stress levels in the TBC require larger reversal stresses (a thicker TGO and hence more thermal cycles) to overcome the high initial stress fields which can lead to longer lifetimes [24]. Regardless, the FCT results do not support or negate either theory because the modifications had little to no effect on lifetime. This does not go to say that bond coat topography does not make a difference in the lifetime behavior, it more so indicates that the bond coat modifications employed here did not alter the lifetimes. A more complete study with more drastic bond coat modifications would be needed to make this conclusion.

One benefit of having the smoother single layer bond coats was that the aluminum depletion in the bond coat was much slower than in the more porous dual layer bond coats as Figure 74 depicts.

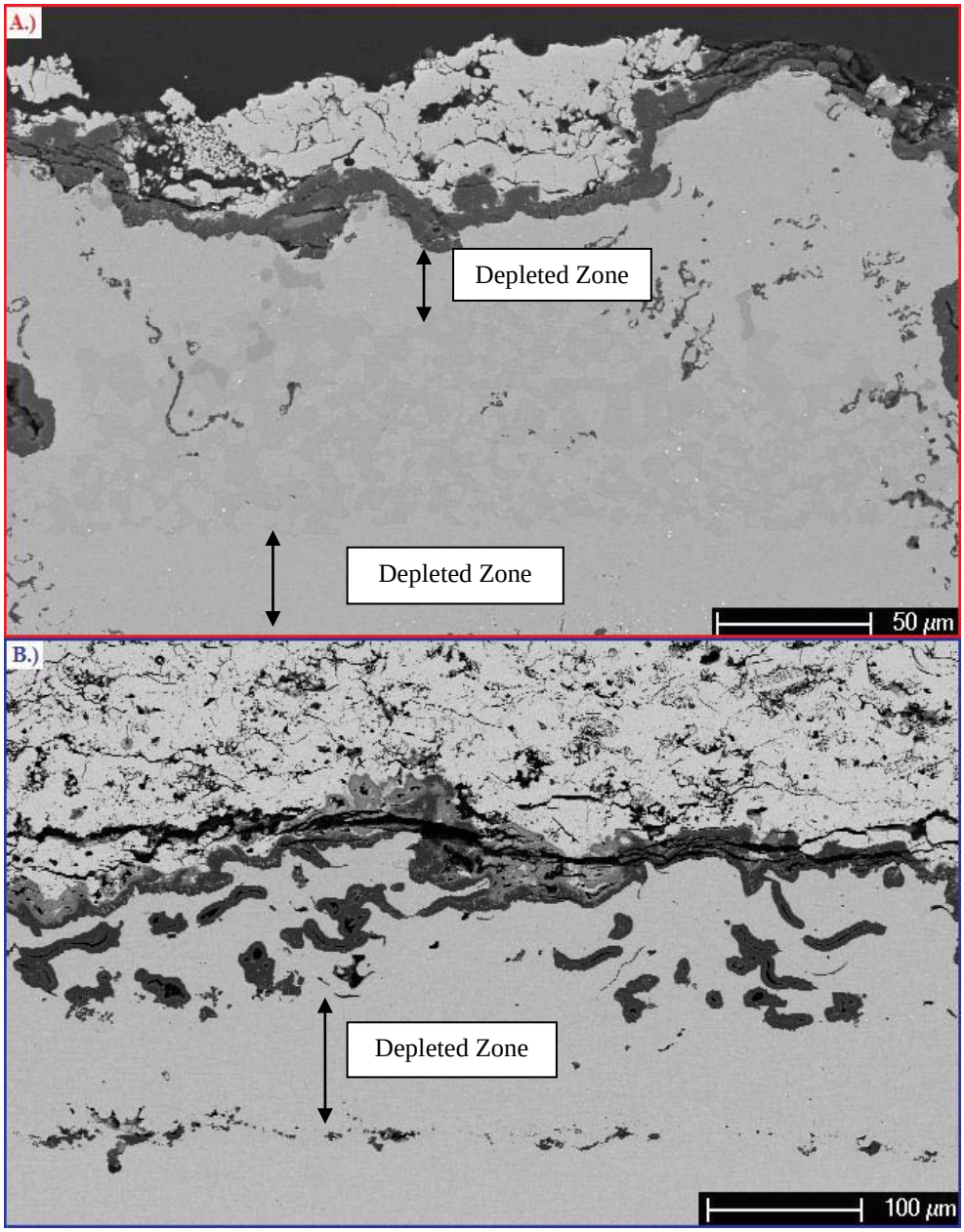

Figure 74 - a.) single layer bond coat on MarM509 after 240cyc with the dark β-phase still present in significant quantities (darker 2nd phase in center region) b.) dual layer bond coat on IN718 after 180cyc with no remaining β-phase present.

Figure 74a also shows how the aluminum can diffuse into the substrate material at an equal (if not faster) rate to which the aluminum is depleted by scale growth. The bottom of Figure 74a is the interface between the bond coat and substrate. Considering this, it can be seen that 50μm of the beta phase is depleted by diffusion into the substrate.

4.2.5 Measurement of Thermal Conductivity

The thermal conductivity of the as-processed coating was measured at temperatures up to 1000°C in 100°C increments. The results are shown in Figure 75. This measured conductivity is well below the typical thermal conductivity of higher density coatings which are around 1.5 W/m-K.

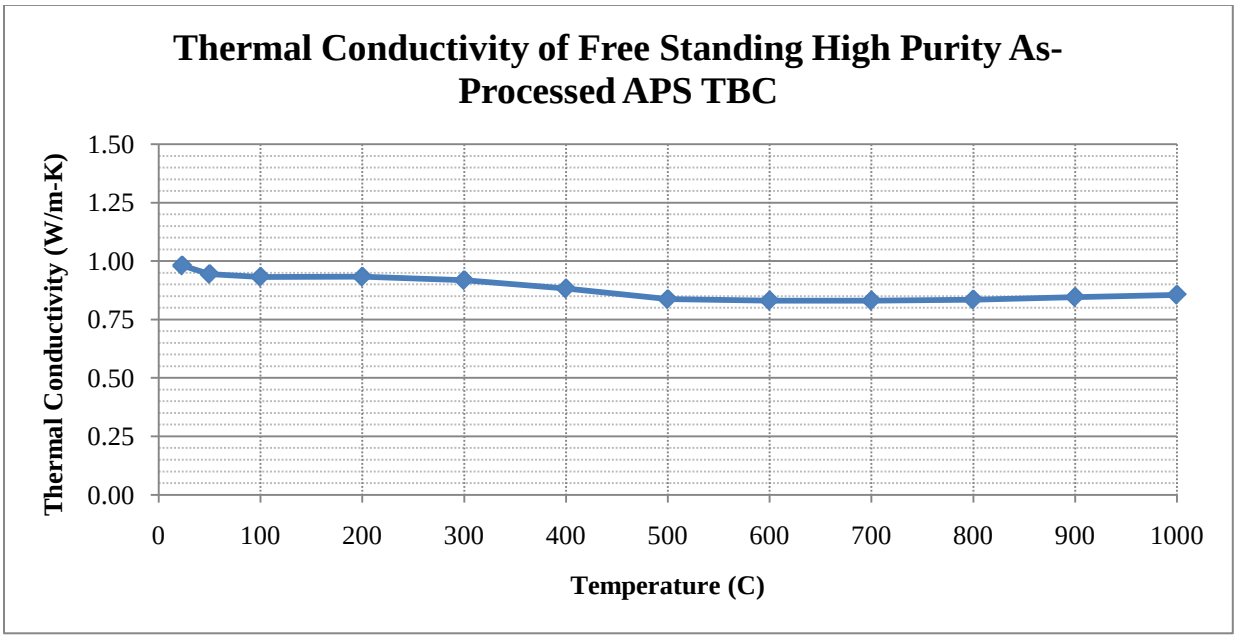

Figure 75 - Plot of the measured thermal conductivity of the as-processed low density APS TBC as a function of temperature.

4.2.6 Yttrium Content Effect

The phase II specimens prepared in 15 and 45mil thicknesses on IN718 substrates lasted over twice as long (average of 450 and 80 cycles to failure respectively) as the 15and 45mil specimens prepared in Phase I of this project (average of 210 and 35 cycles to failure respectively). Cross sectional analysis of the as-processed specimens revealed an abundance of Y-Hf rich particles within the bond coat layer of the phase I TBCs but none in the phase II TBCs as seen in Figure 76. Furthermore, cross sections of the cycled specimens revealed large quantities of Y-rich precipitates in the TGO layer as seen in Figure 77.

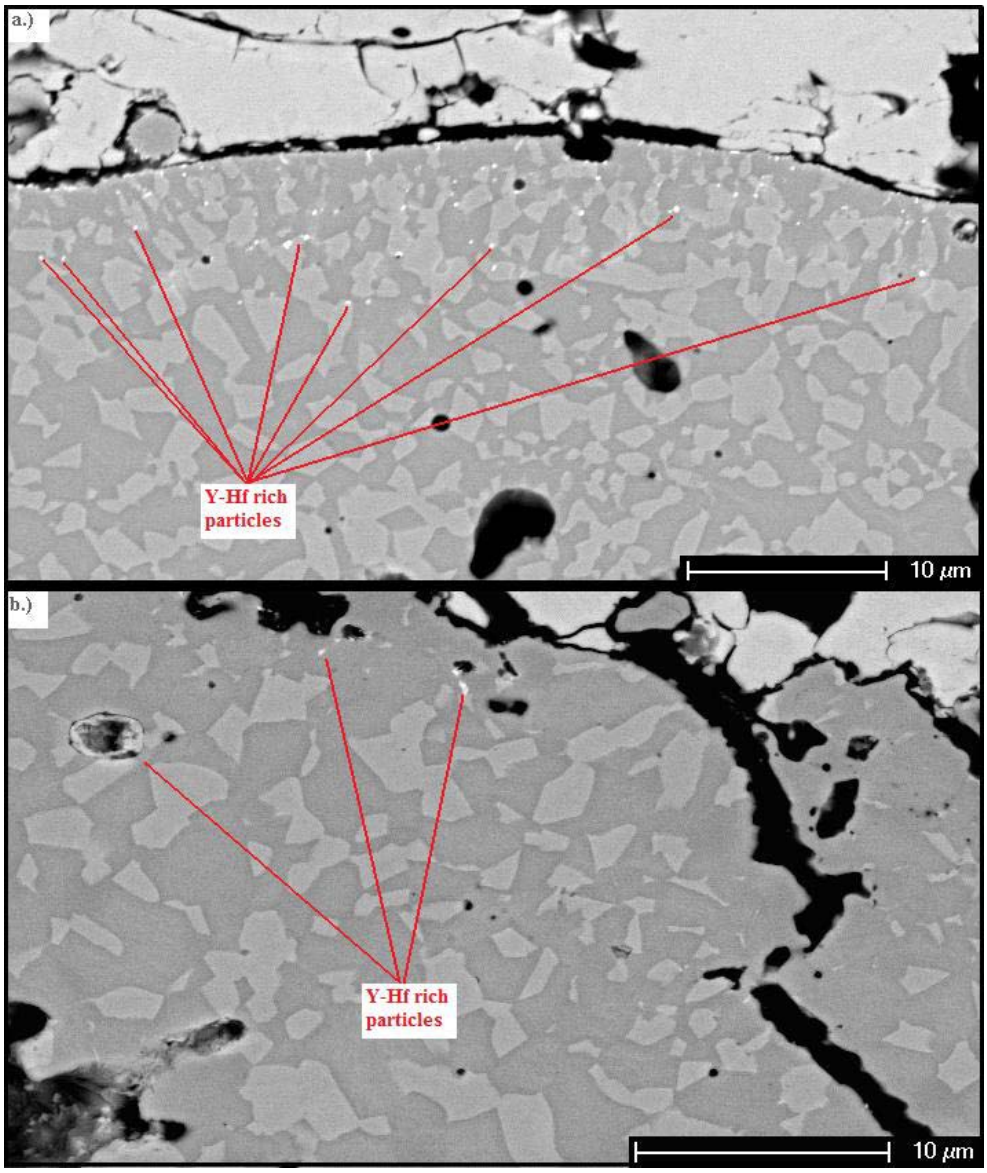

Figure 76 - As-processed cross-section of a.) 15mil TBC on IN718 from Phase I group and b.) 15mil TBC on IN718 from Phase II group. White particles in a.) are Y-Hf rich. Very few of these particles were seen in the Phase II specimens (.b).

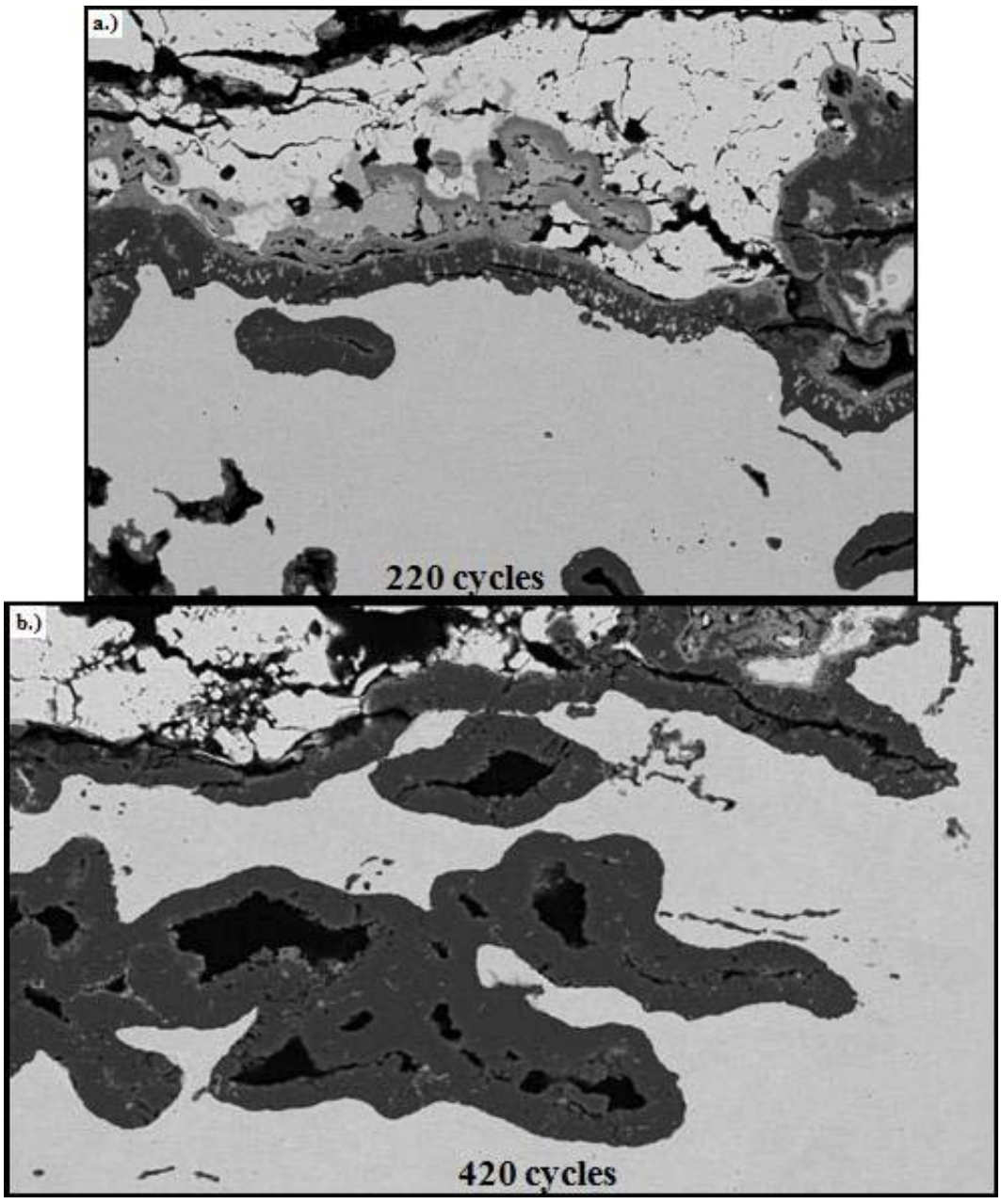

Figure 77 - Cycled a.) Phase I 15mil TBC on IN718 substrate and b.) Phase II 15mil TBC on IN718 substrate. White pegs in TGO layer are rich in yttrium.

These pegs were essentially nonexistent in the Phase II 15mil on IN718. The difference in the structures indicates the bond coat compositions may have been different which would explain

this drastic difference in TGO structure. The specific powder lots used for the Phase I bond coats had ~0.1 wt% more yttrium than the phase two bond coats which is a relatively small difference given the allowable limits are 0.5wt% ±0.25wt% (where Phase I had 0.61wt% and Phase II had 0.52wt %). However, during the spraying process, some of the yttrium can be lost if the yttrium oxidizes and gets trapped in the coating as oxide particles [30]. So, if 0.4wt% is lost during coating process, the Phase I and Phase II bond coats will have yttrium levels of 0.21wt% and 0.12wt% respectively. In the end, the small difference of 0.1wt% can result in the bond coat in Phase I having twice the content of yttrium as the Phase II bond coats. Also, deposition of the bond coat via argon shrouded plasma spraying can result in the non-uniform distribution of yttrium which leads to areas with higher concentrations which can then result in excessive yttrium inclusions in the TGO scale [42]. Depending on the structure of these pegs, they can act as fast diffusion paths for O^{-2} ions through the alumina scale and cause aluminum depletion in the local bond coat area leading to the formation of spinel oxides. As mentioned above, this is an unwanted effect.

Even when there is a uniform distribution of yttrium in the as-sprayed bond coat, these pegs can still develop non-uniformly because of rough bond coat interfaces. Gil et al [43] found that the pegs form preferentially in concave regions of the bond coat interface even when the yttrium is finely dispersed. Previous work by the Meier et al [44] showed that by polishing the coating to a low roughness this effect can be prevented. Polishing or smoothing of the bond coat surface prior to deposition of an APS topcoat is undesirable though. However, it has also been found that reducing the yttrium content of the coating eliminated the peg formation but still

maintained an adherent TGO [44]. Nonetheless, it is clear that more attention needs to be given to the composition and distribution control of the yttrium in bond coats for APS TBCs, as it has a strong affect on the TBC lifetime.

4.2.7 Phase II Summary

A variety of TBC systems were prepared and thermally cycled. The 15 and 45mil TBCs on the different substrate superalloys revealed that the substrate selection had a significant influence on the number of cycles to failure. The explanation for such behavior was linked to the minimization of the CTE mismatch between the substrate and the YSZ topcoat which was supported with the experimentally measured CTE data and lifetime models found in the literature. Another important observation was the suppression of failure mechanism one, which was seen to occur with the thick 45mil TBCs on IN718, when switching the substrate material to HA188 or René N5. This again was linked to the CTE misfit between the layers. As a reference point, the 15mil TBC on René N5, which averaged 850 cycles, performed very closely to a state of the art 150μm EBPVD TBC on a platinum-aluminide bond coat on a René N5 substrate at 1000 cycles.

A direct comparison between the FCT performance of conventional purity and high purity YSZ TBCs could not made in this study, however the conventional purity YSZ TBCs contained numerous particle impurities, which the high purity coatings did not, in and throughout the topcoat. A literature survey indicates these impurities can aid in the sintering process thereby increasing the stiffness and modulus of elasticity of the coatings making it more susceptible to cracking and spallation.

The three bond coat modifications employed in this research did not induce any major differences in the lifetime behavior. However, this is not to imply that bond coat topography does not have any effect on the lifetime, instead it can mean the modifications used here were not severe enough, or different enough to induce a change in the number of cycles to failure.

A key observation with the DVC inner layer specimens, particularly the DVC Stop group, was the 45mil coatings performed just as well as the 15mil coatings. This was the only case of the 45mil coating lasting as long as the 15mil coating indicating the importance of the strain relief cracks at the base of the TBC.

Finally, a comparison of the behavior of the Phase I and Phase II IN718 TBCs revealed the importance of the yttrium content and distribution in the bond coat. The Phase I coatings had numerous yttrium-hafnium rich particles in the bond coat. It is hypothesized these lead to the formation of yttrium-rich stringers in the TGO. The stringers then acted as fast-path diffusion sites causing rapid oxidation and aluminum depletion within the bond coat. Once at a lower enough aluminum content, other oxides form, leading to interfacial instabilities and shorter lifetimes. The Phase II specimens did not have nearly the same quantity of yttrium-hafnium rich particles and therefore grew a denser and more protective scale that leads to longer lifetimes. The literature indicates that a more precise control of the processing conditions can prevent this over doping effect.

5.0 SUMMARY AND CONCLUSIONS

5.1 SUMMARY

Through the research of various APS TBC systems, several factors have been identified which affect the lifetime of the TBC systems. The thickness of the topcoat was a dominant lifetime factor that was observed in every specimen group except for the DVC Stop specimens. The extra thickness provides more thermal protection but at the same time, according to our tests, caused the TBCs to fail after a shorter number of cycles. The DVC under layer did seem to address the thickness factor, probably by adding some strain relief to the lower portion of the TBC, but more testing and a direct comparison with low density high purity topcoats on MarM509 would be needed to confirm this.

The 15, 30 and 45mil TBCs on IN718 in the Phase I group also revealed two different fracture mechanisms. The first mechanism occurred with the thick TBC where spallation occurred in the topcoat (failure mechanism one) and the other with the 15 and 30mil TBCs where spallation occurred along the TGO – topcoat interface by bond coat oxidation (failure mechanism II).

These two failure mechanisms again occurred in the Phase II specimens with the IN718 substrates where the 15mil coating failure by mechanism two and the 45mil failed by mechanism

one. However, the 45mil TBCs on HA188 and René N5 specimens did not fail by mechanism one but instead mechanism two. This observation was accompanied by the fact that the 15 and 45mil TBCs on René N5 and HA188 had much longer lifetimes, comparable to those of state-of-the-art 150μm EBPVD TBCs. This was explained by the CTE mismatch effect where larger CTE mismatches between the substrate and the topcoat lead to short lifetimes. This theory was supported by CTE data measured for the actual alloys used ($CTE_{N5} < CTE_{HA188} < CTE_{IN718}$) in these tests and by Equation 3 from the literature which indicates that by decreasing the CTE mismatch between the substrate and the topcoat the lifetime of the coating can be increased. By minimizing the thermal misfit strains, failure mechanism one seen in the 45mil IN718 specimens was suppressed in the 45mil René N5 and HA188 coatings so that failure mechanism two could dominate.

The high purity YSZ used in these coatings was very resistant to sintering and phase transformation. The as-sprayed coatings had remarkably low thermal conductivities as a result of their low densities and resistance to sintering. A head to head comparison of the high purity and conventional purity YSZ could not be made however the literature indicates that impurities, which were numerous in the conventional purity coatings, are detrimental and unwanted. Furthermore, the sintering experiments that were completed for the high purity YSZ at 1200°C, 1300°C, 1400°C, and 1500°C, when compared with the impurity content versus sintering rate in the literature, indicate there is a benefit to decreasing the silica impurity content below a given content (0.02wt%) contrary to Vaßen et al's findings. An explanation might be that these impurities form a secondary phase between the splats and aid in the transport of material.

The bond coat modifications employed did not have an effect on the number of cycles to failure; however this is mostly a result of the "modifications" not actually modifying the bond

coat topography enough to see a substantial difference in FCT performance. The literature supports such a claim as other studies have shown that bond coat tailoring has had a significant effect on TBC performance.

The yttrium distribution and composition of the bond coat proved to have a significant effect on the scale formation and thus lifetime of the TBC coatings. The Phase I specimens with the numerous yttrium-hafnium rich particles had a thick TGO filled with yttrium stringers that lead to the formation of Ni-Cr-Al spinel oxides, that weakened the TGO-topcoat interface. The Phase II specimens had a thick, dense, adherent alumina TGO that limited the areas for spinel oxides to grow resulting in a strong TGO-topcoat interface and an increased lifetime. These observations along with previous studies in the literature indicate that not only yttrium content but also yttrium distribution is an important factor in TBC lifetime.

5.2 CONCLUSIONS

From this study it is evident the following variables have a substantial influence on TBC lifetime:

- Topcoat thickness
- Substrate superalloy selection (CTE mismatch and composition effects)
- Bond coat yttrium content and distribution

The other variables this study identified but could not explicitly prove they have a substantial influence on TBC lifetime are:

- YSZ topcoat purity
- Bond coat topography

- DVC under layer

These three variables did provide important insight, however, because a low density, high purity YSZ TBC on Mar509 was not prepared, a direct comparison of FCT performance could not be made. Nonetheless, a literature survey does indicate these variables to be important influences on TBC lifetime.

APPENDIX

ROUGHNESS MEASUREMENTS

Roughness measurements done on the bond coat topography specimens were performed via image analysis. A series of 4 to 5 micrographs were taken at high magnification 200x-300x and then carefully joined together to make one large composite micrograph. The interface between the bond coat and topcoat (of the as-processed specimen) was traced out and rendered the color white (pixel value ‘256’ in a 256-bit tiff image file). The grayscale image was then converted to a black and white image with the black white threshold set at 255 so that all pixels except the white ones would turn into black pixels, leaving a white line over a black background as showing in Figure 78.

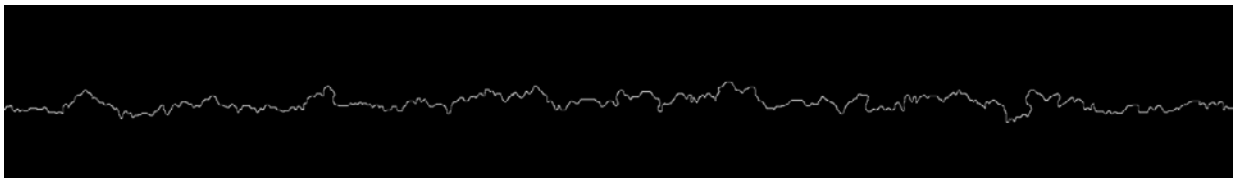

Figure 78 - Black and white image of bond coat/topcoat interface.

The image, which was now a large matrix of 1's and 0's (1=white 0=black), was then loaded into a self-made program Matlab program where several calculations were done. First, an average y coordinate was computed to find the mean "white pixel position." Equation 4 was used for this

Equation 4

$$\overline{\boldsymbol{y}} = \sum_{\boldsymbol{j=1}}^{\boldsymbol{m}} \frac{\sum_{\boldsymbol{i=1}}^{\boldsymbol{n}} \left[\boldsymbol{pixel\_value}_{\boldsymbol{y_i, x_j}} \times \boldsymbol{y_i} \right]}{\sum_{\boldsymbol{i=1}}^{\boldsymbol{n}} \boldsymbol{pixel\_value}_{\boldsymbol{y_i, x_j}}}$$

Then Equation 5 was used to calculate the R_a value with pixels as units. This was then converted into real space using the scale bar with the image.

Equation 5

$$\boldsymbol{R_a} = \frac{\boldsymbol{1}}{\boldsymbol{n}} \sum_{\boldsymbol{i=1}}^{\boldsymbol{n}} |\overline{\boldsymbol{y}} - \boldsymbol{y_i}|$$

The total sample length of the composite micrographs was roughly 1mm and 3 composite micrographs were used for each for a total sampling length of 3mm. This is only a small portion of the specimen cross-section, however described process was very labor intensive. As an accuracy test, the method was used to measure the roughness of a previously measured surface. The roughness of a bond coat measured by Praxair using a stylus method on the as-sprayed bond coat was R_a=11.1μm ± 1.1μm and the image analysis method indicated it to be R_a=12.63μm. Though the image analysis method gave a slightly higher value, it does fall within 1.5 standard deviations.

BIBLIOGRAPHY

1. Neil Birks, G.H.M., Fredrick S. Pettit., *Introduction to the high-temperature oxidation of metals*. Second Edition ed. 2006, New York: Cambridge University Press.

2. Rangaraj, S. and K. Kokini, *Fracture in single-layer zirconia (YSZ)-bond coat alloy (NiCoCrAlY) composite coatings under thermal shock.* Acta Materialia, 2004. **52**(2): p. 455-465.

3. Echsler, H., et al., *Bond coat oxidation and its significance for life expectancy of thermal barrier coating systems.* Materials Science and Technology, 2004. **20**: p. 307-318.

4. Taylor, T.A. *Review of Thermally Sprayed Thermal Barrier Coating*. in *AMS International Surface Engineering Congress*. 2004. Orlando, FL.

5. Fox, A.C. and T.W. Clyne, *Oxygen transport by gas permeation through the zirconia layer in plasma sprayed thermal barrier coatings.* Surface and Coatings Technology, 2004. **184**(2-3): p. 311-321.

6. Guo, H.B., R. Vaßen, and D. Stöver, *Atmospheric plasma sprayed thick thermal barrier coatings with high segmentation crack density.* Surface and Coatings Technology, 2004. **186**(3): p. 353-363.

7. Yanar, N., F. Pettit, and G. Meier, *Failure characteristics during cyclic oxidation of yttria stabilized zirconia thermal barrier coatings deposited via electron beam physical vapor deposition on platinum aluminide and on NiCoCrAlY bond coats with processing modifications for improved performances.* Metallurgical and Materials Transactions A, 2006. **37**(5): p. 1563-1580.

8. Taylor, T.A., *U. S. Patent 5,073,433*. 1991.

9. Kulkarni, A., et al., *Processing effects on porosity-property correlations in plasma sprayed yttria-stabilized zirconia coatings.* Materials Science and Engineering A, 2003. **359**(1-2): p. 100-111.

10. Schwingel, D., et al., *Mechanical and thermophysical properties of thick PYSZ thermal barrier coatings: correlation with microstructure and spraying parameters.* Surface and Coatings Technology, 1998. **108-109**(1-3): p. 99-106.

11. Portinha, A., et al., *Characterization of thermal barrier coatings with a gradient in porosity.* Surface and Coatings Technology, 2005. **195**(2-3): p. 245-251.

12. Portinha, A., et al., *Residual stresses and elastic modulus of thermal barrier coatings graded in porosity.* Surface and Coatings Technology. **188-189**: p. 120-128.

13. Scott, H.G., *Phase relationships in the zirconia-yttria system.* Journal of Materials Science, 1975. **10**(9): p. 1527-1535.

14. Robert A. Miller, J.L.S., Ralph G. Garick, *Phase Stability in Plasma-Sprayed, Partially Stabilized Zirconia-Yttria*, in *Advances in Ceramics - Volume 3 - Science and Technology of Zirconia*, A.H.H.a.L.W. Hobbs, Editor. 1981, The American Ceramic Society, Inc.: Columbus. p. 241-253.

15. Robert A. Miller, R.G.G., James L. Smialek, *Phase Distributions in Plasma-Sprayed Zirconia-Yttria.* Ceramic Bulletin: American Ceramic Society, 1983. **62**(12): p. 1355-1358.

16. Garvie, R.H.J.H.a.R.C., *Sub-Eutectiod Aged Mg-PSZ Alloy with Enhanced Thermal Up-Shock Resistance.* Journal of Materials Science, 1982. **17**(9): p. 2637-43.

17. Paul, S., et al., *Effects of Impurity Content on the Sintering Characteristics of Plasma-Sprayed Zirconia.* Journal of Thermal Spray Technology, 2007. **16**(5): p. 798-803.

18. Tekeli, S., M. Erdogan, and B. Aktas, *Microstructural evolution in 8 mol% Y_2O_3-stabilized cubic zirconia (8YSCZ) with SiO_2 addition.* Materials Science and Engineering A, 2004. **386**(1-2): p. 1-9.

19. Eaton, H.E. and R.C. Novak, *Sintering studies of plasma-sprayed zirconia.* Surface and Coatings Technology, 1987. **32**(1-4): p. 227-236.

20. Vaßen, R., et al., *Influence of impurity content and porosity of plasma-sprayed yttria-stabilized zirconia layers on the sintering behaviour.* Surface and Coatings Technology, 2001. **141**(2-3): p. 135-140.

21. R.A. Miller, W.J.B., J.G. Goedjen, R. Tiwari, D. Mess. *The Effect of Silica on the Cyclic Life of a Zirconia-Yttria Thermal Barrier Coating*. in *7th National Thermal Spray Conference*. 1994. Boston, MA: ASM International.

22. J.G. Goedjen, W.J.B., R.A. Miller. *Sintering of Plasma-Sprayed Sol Gel Zirconia-Yttria as a Function of Silica Conent*. in *8th National Thermal Spray Conference*. 1995. Houston, Texas: ASM International.

23. Rabiei, A. and A.G. Evans, *Failure mechanisms associated with the thermally grown oxide in plasma-sprayed thermal barrier coatings.* Acta Materialia, 2000. **48**(15): p. 3963-3976.

24. Traeger, F., et al., *A life time model for ceramic thermal barrier coatings.* Materials Science and Engineering A, 2003. **358**(1-2): p. 255-265.

25. Smialek, J., *Improved oxidation life of segmented plasma sprayed 8YSZ thermal barrier coatings.* Journal of Thermal Spray Technology, 2004. **13**(1): p. 66-75.

26. Goward, G.W., *Progress in coatings for gas turbine airfoils.* Surface and Coatings Technology, 1998. **108-109**(1-3): p. 73-79.

27. Gil, A., et al., *Y-rich oxide distribution in plasma sprayed MCrAlY-coatings studied by SEM with a cathodoluminescence detector and Raman spectroscopy.* Surface and Coatings Technology, 2009. **204**(4): p. 531-538.

28. Stecura, S., *NASA-TM-78976: Effects of Compositional Changes on the Performance of a Thermal Barrier Coating System*, in *Third Annual Conference on Composites and Advanced Materials*. 1979, NASA Glenn Research Center: Merritt Island, Florida. p. 32.

29. Choquet, P., C. Indrigo, and R. Mevrel, *Microstructure of oxide scales formed on cyclically oxidized M---Cr---Al---Y coatings.* Materials Science and Engineering, 1987. **88**: p. 97-101.

30. Subanovic, M., et al., *Effect of manufacturing related parameters on oxidation properties of MCrAlY-bondcoats.* Materials and Corrosion, 2008. **59**(6): p. 463-470.

31. Pint, B.A., et al., *Substrate and bond coat compositions: factors affecting alumina scale adhesion.* Materials Science and Engineering A, 1998. **245**(2): p. 201-211.

32. Renusch, D., M. Schorr, and M. Schütze, *The role that bond coat depletion of aluminum has on the lifetime of APS-TBC under oxidizing conditions.* Materials and Corrosion, 2008. **59**(7): p. 547-555.

33. Barrett, C.A., R.V. Miner, and D.R. Hull, *The effects of Cr, Al, Ti, Mo, W, Ta, and Cb on the cyclic oxidation behavior of cast Ni-base superalloys at 1100 and 1150°C.* Oxidation of Metals, 1983. **20**(5): p. 255-278.

34. Miller, R.A. and C.E. Lowell, *Failure mechanisms of thermal barrier coatings exposed to elevated temperatures.* Thin Solid Films, 1982. **95**(3): p. 265-273.

35. Stecura, S., *Two-Layer Thermal-Barrier Systems for Ni-Al-Mo Alloy and Effects of Alloy Thermal Expansion on System Life.* American Ceramic Society Bulletin, 1982. **61**(2): p. 256-262.

36. Wu, B.-C., et al., *Degradation Mechanisms of ZrO_2 wt% Y_2O_3 / Ni-22Cr-10Al-1Y Thermal Barrier Coatings.* Journal of the American Ceramic Society, 1989. **72**(2): p. 212-218.

37. T. A. Taylor, N.H., and A. Feuerstein, *Unpublished Research*, G.H. Meier, Editor. 2007: San Diego.

38. Bolcavage A., F.A., Foster J., and Moore P. *Thermal Shock Testing of TBC/Bondcoat Systems*. in *Heat Treat/Surface Engineering Conference*. 2003. Indianapolis, IN: ASM.

39. He, M.Y., J.W. Hutchinson, and A.G. Evans, *Simulation of stresses and delamination in a plasma-sprayed thermal barrier system upon thermal cycling.* Materials Science and Engineering A, 2003. **345**(1-2): p. 172-178.

40. Shillington, E.A.G. and D.R. Clarke, *Spalling failure of a thermal barrier coating associated with aluminum depletion in the bond-coat.* Acta Materialia, 1999. **47**(4): p. 1297-1305.

41. Ali, M.Y., S.Q. Nusier, and G.M. Newaz, *Mechanics of damage initiation and growth in a TBC/superalloy system.* International Journal of Solids and Structures, 2001. **38**(19): p. 3329-3340.

42. Haynes, J.A., et al., *Characterization of Alumina Scales Formed During Isothermal and Cyclic Oxidation of Plasma-Sprayed TBC Systems at 1150°C.* Oxidation of Metals, 1999. **52**(1): p. 31-76.

43. Gil, A., et al., *Effect of surface condition on the oxidation behaviour of MCrAlY coatings.* Surface and Coatings Technology, 2006. **201**(7): p. 3824-3828.

44. Jackson, E.M.M., et al., *Effect of surface preparation on the durability of NiCoCrAlY coatings for oxidation protection and bond coats for thermal barrier coatings.* Materials and Corrosion, 2008. **59**(6): p. 494-500.